Interactions of Peroxynitric Acid and Hydrogen Peroxide with Ice and the Envrionmental Implications

Inauguraldissertation
der Philosophisch-naturwissenschaftlichen Fakultät
der Universität Bern

vorgelegt von
Thomas Ulrich
aus Deutschland

Leiter der Arbeit:

Prof. Dr. Samuel Leutwyler
Departement für Chemie und Biochemie

Interactions of Peroxynitric Acid and Hydrogen Peroxide with Ice and the Envrionmental Implications

Inauguraldissertation
der Philosophisch-naturwissenschaftlichen Fakultät
der Universität Bern

vorgelegt von
Thomas Ulrich
aus Deutschland

Leiter der Arbeit:

Prof. Dr. Samuel Leutwyler
Departement für Chemie und Biochemie

Von der Philosophisch-naturwissenschaftlichen Fakultät angenommen.

Bern, 31. Mai 2013   Der Dekan:

Prof. Dr. Silvio Decurtins

La gravitation de l'esprit nous fait tomber vers le haut.
Simone Weil (1909-43)

Abstract

Peroxynitric acid (HNO_4) and hydrogen peroxide (H_2O_2) are important trace gases with strong links to the oxidative capacity of the troposphere. Their adsorption to ice and snow in the troposphere can lead to a scavenging of both trace gas species from the atmosphere. Also their adsorption on snow packs and ice on the ground affect the atmospheric chemistry of the overlaying boundary layer. In this thesis results of laboratory experiments are presented and discussed, investigating the uptake of HNO_4 and H_2O_2 to ice.

A new gas phase synthesis for HNO_4 is presented. This gas phase synthesis comprises a purification step, consisting of a Ti(IV) denuder and a cooling trap. The synthesis was successfully tested in packed bed flow tub experiments with different nitrogen oxides, resulting in a partitioning from the gas phase towards the ice surface in the order of $HNO_3 > HNO_4 = HNO_2 > NO_2$.

In a subsequent study, the new synthesis was used in coated wall flow tube experiments. For the first time ice adsorption measurements low in impurities were possible and the temperature dependency of the partition constant K_{LinC} from gas phase to ice surface was derived. The temperature dependence follows a relation ship given by $3.74 \times 10^{-12} \times e^{(7098/T)}$ [cm]. The results differ from a previous study, our results show a much lower reversible adsorption process on the ice surface. Uptake of HNO_4 to ice was often compared to that of HNO_3 in literature. Using the lower partition constant derived in this study a different adsorption behavior of HNO_4 as compared to HNO_3 in upper tropospheric cirrus clouds becomes evident. The uptake of HNO_4 to ice particles in those clouds only becomes important lower temperatures. Below 220 K and with very dense clouds present less than 10 % of HNO_4 is adsorbed on the ice particles. Considering snow on the ground, snow packs represent a sink for HNO_4 due to the high specific surface area of ice there.

Literature results of the second trace gas species investigated in this thesis, H_2O_2, differed three orders of magnitude considering partitioning towards the ice surface. The older studies investigated H_2O_2 uptake to ice on short time scales to smooth ice surfaces. The results presented here agree with the higher, more temperature dependent partitioning reported earlier. In addition it is shown in this thesis, that the uptake of H_2O_2 to ice also includes a long term uptake to the ice, which is beyond the surface adsorption process. The long term uptake agrees quantitatively with an older packed bed study. Our results in the coated wall flow tube experiments suggest a diffusion process into the smooth polycrystalline ice. The environmental relevance of this bulk uptake exceeds that of the surface adsorption process when the chemistry above snow packs is concerned.

On a more fundamental approach on the uptake of trace gases to ice, grain boundaries in polycrystalline ice have been proposed as a major reservoir for the bulk uptake of trace gases. In the last part of this thesis the development of a new flow through reactor for grain boundary dependent uptake of trace

gases is presented. With this reactor different types of ices, varying in a grain boundary content by a factor of five, can be produced. With this setup the uptake of trace gases into grain boundaries could be disentangled from the uptake into the ice crystal in follow-up studies. Preliminary results with nitrous acid (HONO) in the reactor are presented.

Contents

List of Figures

List of Tables

Chapter 1

Introduction

The topic of this thesis is the interaction of trace gases with ice surfaces. In the following laboratory studies are presented considering trace gas uptake on ice. The resulting environmental consequences are discussed for each topic. Ice surfaces are ubiquitously present in the environment. In February the land ice and seasonal snow on ther northern hemisphere covers 46 million km^2 and the Antarctic land ice coverage alone is 14 million km^2 (Washburn, 1980). In the atmosphere ice is present in clouds, for example in cirrus clouds in the upper troposphere which consist mostly of ice particles. They can cover up to 40 % area fraction of earth (Popp et al., 2004). Atmospheric trace gases interact with the ice surfaces both in the atmosphere and on the ground. The interactions in the upper troposphere and on the ground are summarized in a simplified version in Figure 1.1. Trace gases can be scavenged by falling snow or adsorb directly on snow or ice on the ground. In the interstitial air of snow packs diffusion can take place. Snow packs can act as a chemical reactor by provdining sites for heterogeneous reactions or photo chemistry.

In this chapter the relevant environments and the tropospheric chemistry are introduced, followed by the scientific context of this study and discussion of the open questions. The introduction ends with a summary of the main goals of this thesis.

1.1 Troposphere

To give the reader the context of this study, the relevance of tropospheric and polar environments for trace gas ice interactions are highlighted. Regarding ice surfaces in the troposphere, ice clouds are of major relevance. It has been proposed that the interactions of the trace gases with ice in cirrus clouds play a role in O_3 depletion in the upper troposphere and lower stratosphere through scavenging O_3 precursors (Jaegle et al., 1998; Roumeau et al., 2000). The ice particles of such clouds scavenge
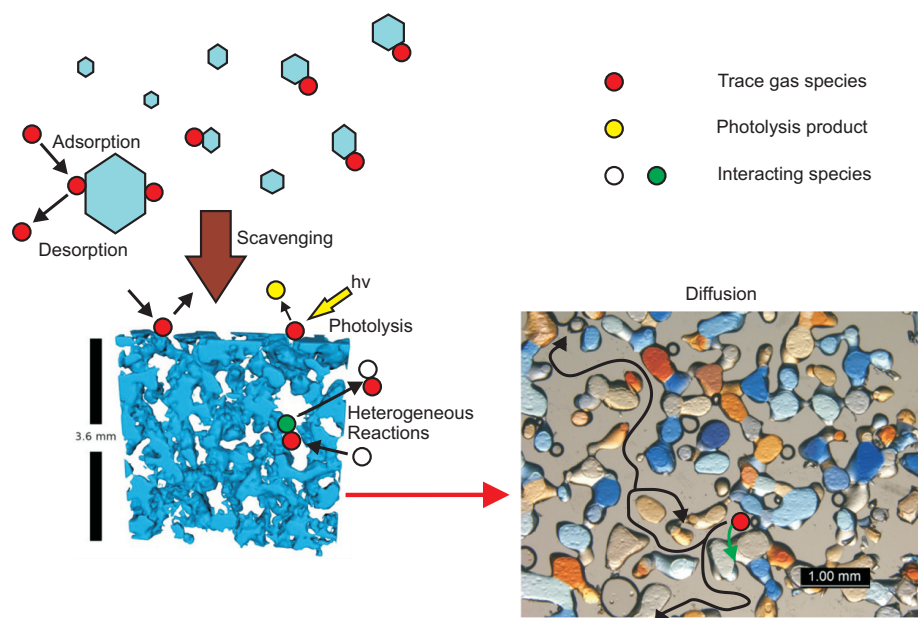
Figure 1.1: Interaction of trace gases with ice particles in the troposphere and subsequent scavenging. In the lower part processes in the snow pack are shown. Left side: Tomography picture (adapted from Pinzer et al., 2010). Right side: Microscopy picture with individual ice grains and grain boundaries (adapted from Riche et al., 2012).

trace gas species with a high affinity to the ice surface and remove them from the atmosphere by deposition. The reduction of ozone, driven by the uptake of precursor trace gases to cirrus clouds has recently been confirmed using atmospheric chemistry-transport models (Marecal et al., 2010; Neu and Prather, 2012).

1.2 Polar environments

A snow pack with its ice surface and interstitial air acts as a multi-phase chemical reactor (Domine and Shepson, 2002; Bartels-Rausch et al., 2013a). Photochemical production of NO_X for example can be enhanced compared to production in the gas-phase in the photic zone of a snow pack. Also glacial ice can be formed from the snow packs after firn to ice transfer, making chemical and physical processes in the snowpack relevant for ice core studies. Climatic change has a big impact on the snow cover of our planet. For example the arctic sea is estimated to be ice free during the summer season from 2030 plus minus 10 years (Wang and Overland, 2012). The lower extend in snow covers leads to less heterogeneous chemisty in snow packs.

The Arctic and Antarctic represent important examples of snow and ice environments in contact with the atmosphere. Both environments are covered with extensive areas of snow or ice, yet the conditions present differ for each of them. The Arctic boundary layer is influenced by the transport of polluted air masses from the northern American and Eurasian regions. Air pollution is of major concern for human health. The world health organization (WHO) stated that in 2002 around 865 000 people died due to bad air quality in their 191 member states (WHO, 2007). The greatest part of this death toll is due to small airborne particulate matter; but also a significant part is due to high ozone (O_3) and NO_X ($= NO + NO_2$) concentrations. The Environmental Protection Agency (EPA) reported air pollution related health costs from 2005 to 2007 of \$ 1 768 833 due to Ozone health effects in California (Romley et al., 2010). Air pollution is primarily important in urban zones, where its sources are ubiquitous. But polluted air masses transported from northern American and northern Eurasian regions towards the Arctic impact the local inhabitants and wild life population (Barrie et al., 1981). As discussed in a later section chemistry in snow packs also impacts reactive nitrogen budgets, which contribute to the local air pollution. The Antarctic is a very prisinte envrionment, but also very high NO_X and O_3 concnterations have been measured above the Antarctic plateau.

1.3 Choice of trace gas species

This study focuses on two atmospheric trace gases: Peroxynitric acid (HNO_4 or HO_2NO_2) and hydrogen peroxide (H_2O_2). HNO_4 is an important trace gas species in the polar environments. In Antarctica for example HNO_4 has been measured in concentrations comparable in magnitude to other important trace gases like HNO_3 and HONO (Slusher et al., 2010) (3×10^{10} molecules / cm^3). Also in the cold upper troposphere HNO_4 has been measured in significant concentrations (Kim et al., 2007) (6×10^8 molecules / cm^3).

H_2O_2 is present in the global atmosphere in significant mixing ratios. Global satellite observations (Allen et al., 2013) measured mixing ratios of 600 ppt – 700 ppt in the low to mid latitudes up to an altitude of 6.5 km. At the higher latitudes mixing ratios of 100 ppt – 300 ppt were measured up to an altitude of 6 km.

In the following the links of HNO_4 and H_2O_2 to some important atmospheric cycles are discussed. The atmospheric reaction circles of NO_X, ,O_3 and VOCs are closely connected (Finlayson, Pitts and Pitts, 1997; Atkinson, 2000). Central to these networks is the oxidative capacity of the atmosphere and with it the OH radical (Atkinson, 2000). The OH radical acts like a cleaning agent of the atmosphere. This cleaning agent degrades volatile organic compounds (VOCs), which are emitted into the atmosphere by both anthropogenic and natural sources. OH attacks the VOCs and oxidizes them; a process which produces many intermediate species. As OH

oxidizes VOCs in a first step; alkyl radicals ($R^\bullet$), alkyl peroxy and alkoxy radicals ($RO + RO_2 = RO_X$) are produced and OH is converted to HO_2 as shown in equation (1.1 - 1.4).

$$VOC + OH \longrightarrow R^\bullet + H_2O \tag{1.1}$$

$$R^\bullet + O_2 \xrightarrow{M} RO_2 \tag{1.2}$$

$$NO + RO_2 \longrightarrow NO_2 + RO \tag{1.3}$$

$$RO + O_2 \longrightarrow RCHO + HO_2 \tag{1.4}$$

Both RO_X and HO_2, are directly linked to a second atmospheric reaction of great importance: They oxidize NO to NO_2, a reaction which recreates OH from HO_2 (1.5) and enhances the production of tropospheric ozone (O_3) by subsequent photolysis of NO_2 to NO (1.6 + 1.7).

$$NO + HO_2 \longrightarrow NO_2 + OH \tag{1.5}$$

$$NO_2 \xrightarrow{h\nu} NO + O(^3P) \tag{1.6}$$

$$O_2 + O(^3P) \xrightarrow{M} O_3 \tag{1.7}$$

It becomes evident now that these reactions are not single pathways; they form complex reaction circles which drive each other. To give the reader an overview, the complex network of gas phase reactions leading to degradation of VOCs, O_3 production and replenishment of OH is depicted in a simplified version in Figure 1.2A.

Both HNO_4 and H_2O_2 are important termination products of the HO_X (OH + HO_2), NO_X and VOC reaction cycles presented; HNO_4 by (1.8) and H_2O_2 by reaction (1.9).

$$HO_2 + NO_2 \xleftrightarrow{M} HNO_4 \tag{1.8}$$

$$HO_2 + HO_2 \longrightarrow H_2O_2 + O_2 \tag{1.9}$$
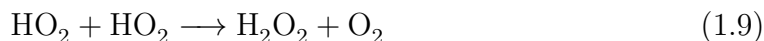
These reactions can interrupt the reaction cycles and by uptake of the termination products to snow and ice they can be removed from the atmosphere as illustrated in Figure 1.2B.

1.4 Ice surfaces as a site for trace gas interactions

The aim of this study is to elucidate uptake processes of trace gas by snow and ice, the focus being laid on the ice surface in the experiments. This gives an approach
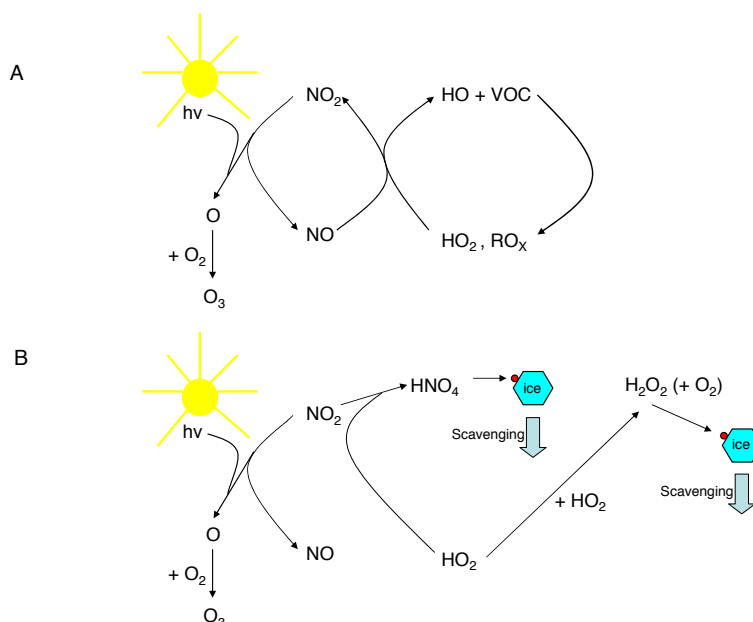
Figure 1.2: NO_X and VOC reaction cycles

to the identification of the physical and chemical aspects of the interaction without the complexity of snow packs with their micro and macro structures.

To understand the physical and chemical processes involving ice surfaces, the properties of the ice surface itself have to be understood. The water molecules in the environmentally relevant ice crystal phase (I_h), are structured in bi-layers ordered in a hexagonal matrix. Ice exists in the environment roughly between 190 K and 273 K. At these temperatures ice has a very high vapor pressure up to 6 mbar near the melting point (Marti and Mauersberger, 1993). This results in a highly dynamic ice surface. For example at 180 K, 100 mono-layers of the ice evaporate and re-condense per second; at 240 K 10 000 mono-layers evaporate and re-condense per second (Abbatt, 2003).

1.4.1 Disordering of the topmost ice surface

Apart from the high dynamics, the ice surface also has very interesting properties, when the topmost layers in the nano-scale are considered. If we imagine the structure of the ice surface without considering additional effects, there would be H-bonds dangling towards the gas phase, providing a very polar surface. The ordered structure of those H bonds is however energetically unfavorable. The result is that the water molecules in the topmost layers of the ice crystal are disordered at
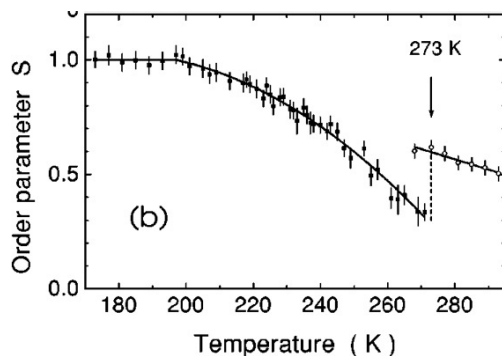
Figure 1.3: Sum-frequency vibrational spectroscopy of the OH bonds on ice (closed squares) and water (open circles). The orientation order parameter S is plotted versus the temperature (from: Wei et al., 2002).

temperatures from around 200 K more prominent towards the melting point (Hobbs, 2010). This disordered ice surface is often termed quasi-liquid layer (QLL) or liquid like layer (LLL). The nature of this disordered layer has been extensively discussed, with in part contradictive interpretations for example considering its thickness (e.g. Bluhm et al., 2002; Henson and Robinson, 2004).

In one study investigating more fundamental properties highlighted here, the authors observed a significant difference of this disordered layer to true liquid water. In sum-frequency vibrational spectroscopy of the OH bonds on the ice crystal the orientational order parameter S has been investigated, (Wei et al., 2002). This orientational order parameter describes the ordering of the free OH-bonds on the surface, where 1 stands for perfect orientational order and 0 for complete disorder. From 200 K on an increasing disorder with increasing temperature has been measured. Yet the results differ compared to liquid water as shown in Figure 1.3.

1.4.2 Ice grains and grain boundaries

Ice consists of single ice grains lying next to each other. Between the ice grains interface areas, so called grain boundaries, exist. Grain boundaries are also present in snow packs, when individual snow grains merge together by snow metamorphism. To give a brief introduction on the importance of grain boundaries relevant for environmental conditions, the properties of the special environments they provide are discussed. The most well known characteristic of grain boundaries is the enhanced diffusivity compared to the bulk of the ice grains. Diffusion of chemical species into solid matrices, like ice at low temperatures, is propagated by defects and vacancies in the matrix (e.g. Hobbs, 2010). Grain boundaries are such areas of defects, as illustrated in Figure 1.3. Due to their structure the diffusion of chemical species is enhanced in grain boundaries. For example the self diffusion of water molecules is
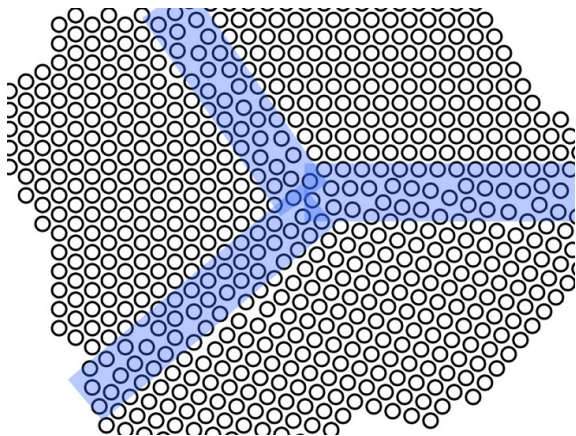
Figure 1.4: Visualization of grain boundaries marked by blue areas in a crystal matrix. Defects of the crystal structure are visible at the grain boundaries. Adapted from G. Lisensky, University of Wisconsin.

about three magnitudes higher in grain boundaries compared to single crystalline ice (Lu et al., 2009). Also for other molecules beside water, for example HCl, higher diffusivities in grain boundaries have been observed (e.g. Domine et al., 1994).

1.4.3 The impact of the surface disorder and grain boundaries on trace gas uptake

Enhanced disordering by impurities

As discussed above the ice surface is disordered on a molecular level at environmental relevant temperatures. Impurities in this disordered layer enhance its water like characteristics (Cho et al., 2002). In laboratory experiments uptake of gas phase HCl (McNeill et al., 2006b) has been shown to induce an enhanced disordered region by ellipsometry at temperatures and gas phase concentrations relevant in the upper troposphere / lower stratosphere. For the less acidic acetic acid no induction of an enhanced disordered region has been observed at similar temperatures by NEXAFS (Krepelova et al., 2013). Such an enhanced disordered layer can lead to higher chemical reactivity (e.g. chlorine activation) or higher partitioning towrads the surface (McNeill et al., 2006b)

Grain boundaries

Grain boundaries have been proposed important reservoirs for trace gas species (Huthwelker et al., 2001; Huthwelker et al., 2006). The higher concentration of impurities in grain boundaries might introduce a similar effect as found in enhanced

Figure 1.5: Vein-network in an ice crystal (Wettlaufer, 1999).

surface disordering into the depth of ice. A theoretical study has shown, that impurities might disorder the grain boundary interfaces, inducing a layer of significant thickness (Benatov and Wettlaufer, 2004). A recent optical scattering study proposed the thickness of such an impurity induced layer to be between 2 nm and 10 nm by theoretical calculations (Thomson et al., 2013).

Veins

A special environment in the ice is created when three grain boundaries meet, to create the so called veins. Figure 1.4 gives an example of the vein network in an ice crystal. Liquid water has been observed in such veins at temperatures near the melting point and in presence of impurities (Wettlaufer, 1999). Impurities like Cl^- and SO_4^{2-} have been shown to be present as ions in solution in such veins (Mulvaney et al., 1988; Mader, 1992). In this condition the veins can act as diffusion channels in the ice (Rempel et al., 2001).

In conclusion, the structure of ice is highly dynamic and complex. For environmentally relevant problems the properties discussed above have to be taken into account.

1.5 Context of this study

1.5.1 Open questions considering HNO_4

In this section the open questions tackled by this thesis are discussed centering around the two species HNO_4 and H_2O_2. HNO_4 is an emerging trace gas species observed in Antarctic field measurements (Slusher et al., 2002). Its interaction with ice has never been investigated under impurity free conditions or relevant concentrations in the laboratory. Hence its impact on the boundary layer processes, which could for example be important in Arctic air pollution, is not yet understood (Law

and Stohl, 2007). In addition recent laboratory studies of trace gas interaction with ice have observed a long term uptake of highly acidic trace gas to the ice (e.g. Ullerstam et al., 2005; McNeill et al., 2007b). The medium acidity of HNO_4 could give new insights into the long term uptake processes.

Development of a gas phase synthesis of HNO_4

Li et al. (1996) studied the uptake of HNO_4 to ice surfaces. For this the authors synthesized HNO_4 in the liquid phase by the method of Kenley et al. (1981). The gas phase products of this synthesis resulted in high concentrations of impurities like HNO_3 and H_2O_2, which interfered with their uptake experiments. One aim of this study was to develop a new synthesis route for HNO_4 with low impurities. A clean synthesis ensures for meaningful results concerning the uptake of HNO_4 on ice.

Atmospheric chemistry-transport models

Atmospheric chemistry-transport models are an important tool to predict gas phase concentrations of chemical species and identify environmentally relevant processes. The uptake of trace gas species to ice in clouds has recently been implemented in such models, but important parameters are still unknown. Marecal et al. (2010) and Neu and Prather (2012) called for the investigation of the HNO_4 partitioning to ice in laboratory studies. Marecal et al. (2010) could not implement HNO_4 in their model due to the missing data. In the model by Neu and Prather (2012) HNO_4 ice interactions have, due to the lack of conclusive laboratory studies, been implemented by assuming the same partitioning towards the ice as HNO_3. Their model runs have shown that HNO_4 could have a significant impact on atmospheric NO_X and O_3 chemistry. O_3 levels are much more sensitive to HNO_4 as compared to HNO_3 and the NO_X – HNO_4 cycling is faster than that of NO_X – HNO_3 (Neu and Prather, 2012). Scavenging of HNO_4 by ice particles and subsequent deposition could thus have a great impact on tropospheric chemistry.

Antarctic and Arctic boundary layer models

Interaction of HNO_4 with snow and ice is of great interest in Arctic and Antarctic environments, since snow and ice are present throughout these polar environments. Concerning the Antarctic, elevated concentrations of NO_X and O_3 are present above the Antarctic plateau (Davis et al., 2008). Davis et al. (2008) proposed that HNO_4 might play a key role in the nitrogen recycling connected to those high NO_X and O_3 values above the Antarctic plateau and called for laboratory studies investigating HNO_4 adsorption on ice in conditions relevant for the plateau, especially regarding HNO_4 hydrolysis after adsorption. On the warmer Antarctic coastal region HNO_4

was found to play a less important role, but its adsorption to ice might still be significant for NO_X chemistry in the colder spring times (Bauguitte et al., 2012).

Considering the Arctic, NO_X and O_3 chemistry is influenced to a greater extent by anthropogenic perturbation (Liang et al., 2011), yet there are still inconsistencies between field measurements and models regarding reactive nitrogen budgets (Law and Stohl, 2007).

Elucidating uptake processes in general

HNO_4 is a trace gas species, which combines a high solubility in water ($H_{298} = 4000$ M/atm) with a medium acidity ($pK_a = 5.85$). Such characteristics can help to elucidate the mechanisms of the trace gas ice interaction. For example the very acidic and highly soluble trace gases HCl (McNeill et al., 2006a; McNeill et al., 2007a) or HNO_3 (Ullerstam et al., 2005) have been found to be taken up by ice surfaces over long time scales, while species like Methanol and Acetone with a lower solubility and no mentionable acidity showed a much lower uptake on shorter timescales (Winkler et al., 2002). It has been discussed that acidic trace gases might alter the surface of the ice, as discussed above. An important driver for such an enhanced disordering could be the acidity of the respective species. As discussed above enhanced disordering has been observed for HCl (McNeill et al., 2006b) but not for the less acidic acetic acid (Krepelova et al., 2013).

On the other hand a high solubility in water is equivalent to the ability of the species to form hydrogen bonds with water molecules. This ability to form hydrogen bonds may also govern the mechanism of interaction with ice surfaces (Sokolov and Abbatt, 2002; Pouvesle et al., 2010). With HNO_4 we now have a species which combines medium acidity with high solubility, which might help to disentangle the mechanism of ice interaction.

1.5.2 Open questions considering H_2O_2

H_2O_2 uptake by ice has been investigated in laboratory experiments (Conklin et al., 1993; Clegg and Abbatt, 2001; Pouvesle et al., 2010). Yet the results in short time scale experiments differed regarding its partitioning towards the ice surface (Clegg and Abbatt, 2001; Pouvesle et al., 2010). The study by Pouvesle et al. (2010) proposed a partitioning towards the ice surface two orders of magnitude higher than the study by Clegg and Abbatt (2001). On long time scales a long term uptake was observed (Conklin et al., 1993). One goal of this study was to shed light on the differing results for surface adsorption and to better understand the long term uptake process.

Partitioning of H_2O_2 to snow and ice

H_2O_2 above snow and ice surfaces is very relevant: It is important as an oxidation agent in snow packs (Bartels-Rausch et al., 2013a) as well as a tracer for the oxidative capacity of the past atmosphere in ice cores studies (e.g. Sigg and Neftel, 1991) and affects light absorption. Its transfer from the atmosphere to firn and ice as well as the reverse process is not well understood (McConnell et al., 1998). Regarding mechanisms of trace gas interaction with ice, it has been proposed that there is a long term uptake into the bulk of the ice (Conklin et al., 1993), but the proposed presence of liquid water in the study referred to, hamper the interpretation of the uptake mechanism. This species was therefore chosen to lend clarity to the differing observations of the partitioning of H_2O_2 to the ice surface (Clegg and Abbatt, 2001; Pouvesle et al., 2010) and give new information about its uptake to the bulk.

H_2O_2 as a chromosphere

H_2O_2 adsorbed onto the ice matrix in terrestrial snow packs has been shown to be an important light absorbing species. Thus it is connected to (1.10).

$$H_2O_2 \xrightarrow{h\nu} OH + OH \tag{1.10}$$

At the sites of Summit, Greenland and Dome Concordia, Antarctica the contribution of H_2O_2 among the light absorbing soluble species (Chromophores) was 20 % at Summit and 15 % at Dome Concordia (Anastasio and Robles, 2007). When considering snow and ice of marine origin the contribution was much lower, below 1 % for the combined H_2O_2 and NO_3^- contribution near Barrow, Alaska (Beine et al., 2012). But at Barrow the contribution of H_2O_2 seems to be lower in general, as terrestrial snow samples only showed a contribution of 2 % for H_2O_2 (Beine et al., 2011). The authors emphasized the importance of inhomogeneous distribution of H_2O_2 in the snow in the terrestrial study. Further knowledge of the distribution of H_2O_2 in ice, regarding surface adsorption and bulk uptake are of interest here and are a subject of this thesis.

1.5.3 Open questions considering grain boundaries

As discussed above the grain boundaries of ice might be an important feature in trace gas uptake. Only few studies have compared ice samples of low and high grain content with regard to trace gas uptake. Uptake of trace gases to grain boundaries has been proposed for example for HONO (Pinzer et al., 2010) and SO_2 (Huthwelker et al., 2001). For methanol and acetone no different magnitude of uptake was found (Bartels-Rausch et al., 2004; Bartels-Rausch et al., 2013b), while for HCl the presence of grain boundaries was proposed as the reason for the two different modes

of adsorption (McNeill et al., 2007b). A difficulty with these studies was that the fraction of grain boundaries on the surface of the ice could not be measured directly. One aim of this thesis was to deal with this issue by building a new flow through reactor to measure the grain boundary dependent uptake of trace gases.

1.6   Main goals of this thesis

When chemical processes with relevance for the environment are investigated, three fields of scientific studies are closely connected: Field measurments, laboratory experiments and modelling studies. In this study the uptake of trace gases to ice surfaces is investigated in laboratory experiments. The main aim is to understand the basic principles of the uptake, which then can be extrapolated to other species. Laboratory studies allow the individual parameters which govern the uptake on ice to be controlled. The main parameters investigated in this study are the temperature, the gas phase concentration of the respective species and the crystallinity of the ice film.

The main aims of this thesis are to answer the following questions:

- What is the partition constant for HNO_4 to ice surfaces in terms of its adsorption on snow and ice on the ground and ice in the atmosphere?

- How does H_2O_2 partition to the ice? Can the surface adsorption be disentangled from the bulk uptake? Can one of the differing results be reproduced?

- How does the uptake of trace gases depend on grain boundaries in ice?

1.7   References

Abbatt, J. P. D.: Interactions of atmospheric trace gases with ice surfaces: Adsorption and reaction, Chemical Reviews, 103, 4783-4800, 10.1021/cr0206418, 2003.

Allen, N. D. C., Abad, G. G., Bernath, P. F., and Boone, C. D.: Satellite observations of the global distribution of hydrogen peroxide (H_2O_2) from ACE, Journal of Quantitative Spectroscopy & Radiative Transfer, 115, 66-77, 10.1016/j.jqsrt.2012.09.-008, 2013.

Anastasio, C., and Robles, T.: Light absorption by soluble chemical species in Arctic and Antarctic snow, Journal of Geophysical Research-Atmospheres, 112, D24304, 10.1029/2007jd008695, 2007.

Atkinson, R.: Atmospheric chemistry of VOCs and NOx, Atmospheric Environment, 34, 2063-2101, 10.1016/s1352-2310(99)00460-4, 2000.

Barrie, L. A., Hoff, R. M., and Daggupaty, S. M.: The Influence of Mid-Latitudinal Pollution Sources on Haze in the Canadian Arctic, Atmospheric Environment, 15, 1407-1419, 10.1016/0004-6981(81)90347-4, 1981.

Bartels-Rausch, T., Guimbaud, C., Gäggeler, H. W., and Ammann, M.: The partitioning of acetone to different types of ice and snow between 198 and 223 K, Geophysical Research Letters, 31, L16110, 10.1029/2004gl020070, 2004.

Bartels-Rausch, T., Jacobi, H.-W., Kahan, T. F., Thomas, J. L., Thomson, E. S., Abbatt, J. P. D., Ammann, M., Blackford, J. R., Bluhm, H., Boxe, C., Domine, F., Frey, M. M., Gladich, I., Guzman, M. I., Heger, D., Huthwelker, T., Klan, P., Kuhs, W. F., Kuo, M. H., Maus, S., Moussa, S. G., McNeill, V. F., Newberg, J. T., Pettersson, J. B. C., Roeselova, M., and Sodeau, J. R.: Relationship between snow microstructure and physical and chemical processes, Atmospheric Chemistry and Physics Discussions, 12, 30409-30541, 2013a.

Bartels-Rausch, T., Wren, S., Schreiber, S., Riche, F., Schneebeli, M., and Ammann, M.: Diffusion of volatile organics through porous snow: Impact of surface adsorption and grain boundaries, submitted to Atmospheric Chemistry and Physics, 2013b.

Bauguitte, S. J. B., Bloss, W. J., Evans, M. J., Salmon, R. A., Anderson, P. S., Jones, A. E., Lee, J. D., Saiz-Lopez, A., Roscoe, H. K., Wolff, E. W., and Plane, J. M. C.: Summertime NO_X measurements during the CHABLIS campaign: Can source and sink estimates unravel observed diurnal cycles?, Atmospheric Chemistry and Physics, 12, 989-1002, 10.5194/acp-12-989-2012, 2012.

Beine, H., Anastasio, C., Esposito, G., Patten, K., Wilkening, E., Domine, F., Voisin, D., Barret, M., Houdier, S., and Hall, S.: Soluble, light-absorbing species

in snow at Barrow, Alaska, Journal of Geophysical Research-Atmospheres, 116, D00r05, 10.1029/2011jd016181, 2011.

Beine, H., Anastasio, C., Domine, F., Douglas, T., Barret, M., France, J., King, M., Hall, S., and Ullmann, K.: Soluble chromophores in marine snow, seawater, sea ice and frost flowers near Barrow, Alaska, Journal of Geophysical Research-Atmospheres, 117, D00r15, 10.1029/2011jd016650, 2012.

Benatov, L., and Wettlaufer, J. S.: Abrupt grain boundary melting in ice, Physical Review E, 70, 06160610.1103/PhysRevE.70.061606, 2004.

Bluhm, H., Ogletree, D. F., Fadley, C. S., Hussain, Z., and Salmeron, N.: The premelting of ice studied with photoelectron spectroscopy, Journal of Physics-Condensed Matter, 14, L227-L233, 10.1088/0953-8984/14/8/108, 2002.

Cho, H., Shepson, P. B., Barrie, L. A., Cowin, J. P., and Zaveri, R.: NMR investigation of the quasi-brine layer in ice/brine mixtures, Journal of Physical Chemistry B, 106, 11226-11232, 10.1021/jp020449+, 2002.

Clegg, S. M., and Abbatt, J. P. D.: Uptake of gas-phase SO_2 and H_2O_2 by ice surfaces: Dependence on partial pressure, temperature, and surface acidity, Journal of Physical Chemistry A, 105, 6630-6636, 10.1021/jp010062r, 2001.

Conklin, M. H., Sigg, A., Neftel, A., and Bales, R. C.: Atmosphere-Snow Transfer-Function for H_2O_2 - Microphysical Considerations, Journal of Geophysical Research-Atmospheres, 98, 18367-18376, 10.1029/93jd01194, 1993.

Davis, D. D., Seelig, J., Huey, G., Crawford, J., Chen, G., Wang, Y., Buhr, M., Helmig, D., Neff, W., Blake, D., Arimoto, R., and Eisele, F.: A reassessment of Antarctic plateau reactive nitrogen based on ANTCI 2003 airborne and ground based measurements, Atmospheric Envrionment, 42, 2831-2848, 10.1016/j.atmosenv-.2007.07.039, 2008.

Domine, F., Thibert, E., Vanlandeghem, F., Silvente, E., and Wagnon, P.: Diffusion and Solubility of HCl in Ice - Preliminary-Results, Geophysical Research Letters, 21, 601-604, 10.1029/94gl00512, 1994.

Domine, F., and Shepson, P. B.: Air-snow interactions and atmospheric chemistry, Science, 297, 1506-1510, 10.1126/science.1074610, 2002.

Finlayson-Pitts, B. J., and Pitts, J. N.: Tropospheric air pollution: Ozone, airborne toxics, polycyclic aromatic hydrocarbons, and particles, Science, 276, 1045-1052, 10.1126/science.276.5315.1045, 1997.

Fischer, H., Wahlen, M., Smith, J., Mastroianni, D., and Deck, B.: Ice core records of atmospheric CO_2 around the last three glacial terminations, Science, 283, 1712-1714, 10.1126/science.283.5408.1712, 1999.

Henson, B. F., and Robinson, J. M.: Dependence of quasi-liquid thickness on the liquid activity: A bulk thermodynamic theory of the interface, Physical Review Letters, 92, 246107, 10.1103/PhysRevLett.92.246107, 2004.

Hobbs, P. V.: Ice Physics, Oxford University Press, New York, 2010.

Huthwelker, T., Lamb, D., Baker, M., Swanson, B., and Peter, T.: Uptake of SO_2 by polycrystalline water ice, Journal of Colloid and Interface Science, 238, 147-159, 10.1006/jcis.2001.7507, 2001.

Huthwelker, T., Ammann, M., and Peter, T.: The uptake of acidic gases on ice, Chemical Reviews, 106, 1375-1444, 10.1021/cr020506v, 2006.

Jaegle, L., Jacob, D. J., Brune, W. H., Tan, D., Faloona, I. C., Weinheimer, A. J., Ridley, B. A., Campos, T. L., and Sachse, G. W.: Sources of HO_X and production of ozone in the upper troposphere over the United States, Geophysical Research Letters, 25, 1709-1712, 10.1029/98gl00041, 1998.

Kenley, R. A., Trevor, P. L., and Lan, B. Y.: Preparation and thermal-decomposition of pernitric acid (HOONO2) in aqueous-media, Journal of the American Chemical Society, 103, 2203-2206, 10.1021/ja00399a012, 1981.

Kim, S., Huey, L. G., Stickel, R. E., Tanner, D. J., Crawford, J. H., Olson, J. R., Chen, G., Brune, W. H., Ren, X., Lesher, R., Wooldridge, P. J., Bertram, T. H., Perring, A., Cohen, R. C., Lefer, B. L., Shetter, R. E., Avery, M., Diskin, G., and Sokolik, I.: Measurement of HO_2NO_2 in the free troposphere during the intercontinental chemical transport experiment - North America 2004, Journal of Geophysical Reasearch-Atmospheres, 112, 10.1029/2006JD007676, 2007.

Krepelova, A., Bartels-Rausch, T., Brown, M. A., Bluhm, H., and Ammann, M.: Adsorption of Acetic Acid on Ice Studied by Ambient-Pressure XPS and Partial-Electron-Yield NEXAFS Spectroscopy at 230-240 K, Journal of Physical Chemistry A, 117, 401-409, 10.1021/jp3102332, 2013.

Law, K. S., and Stohl, A.: Arctic air pollution: Origins and impacts, Science, 315, 1537-1540, 10.1126/science.1137695, 2007.

Li, Z. J., Friedl, R. R., Moore, S. B., and Sander, S. P.: Interaction of peroxynitric acid with solid H2O ice, Journal of Geophysical Reasearch-Atmospheres, 101, 6795-6802, 10.1029/96JD00065, 1996.

Liang, Q., Rodriguez, J. M., Douglass, A. R., Crawford, J. H., Olson, J. R., Apel, E., Bian, H., Blake, D. R., Brune, W., Chin, M., Colarco, P. R., da Silva, A., Diskin, G. S., Duncan, B. N., Huey, L. G., Knapp, D. J., Montzka, D. D., Nielsen, J. E., Pawson, S., Riemer, D. D., Weinheimer, A. J., and Wisthaler, A.: Reactive nitrogen, ozone and ozone production in the Arctic troposphere and the

impact of stratosphere-troposphere exchange, Atmospheric Chemistry and Physics, 11, 13181-13199, 10.5194/acp-11-13181-2011, 2011.

Lu, H., McCartney, S. A., and Sadtchenko, V.: H/D exchange kinetics in pure and HCl doped polycrystalline ice at temperatures near its melting point: Structure, chemical transport, and phase transitions at grain boundaries, Journal of Chemical Physics, 130, 054501, 10.1063/1.3039077, 2009.

Mader, H. M.: The Thermal-Behavior of the Water-Vein System in Polycrystalline Ice, Journal of Glaciology, 38, 359-374, 1992.

Marecal, V., Pirre, M., Riviere, E. D., Pouvesle, N., Crowley, J. N., Freitas, S. R., and Longo, K. M.: Modelling the reversible uptake of chemical species in the gas phase by ice particles formed in a convective cloud, Atmospheric Chemistry and Physics, 10, 4977-5000, 10.5194/acp-10-4977-2010, 2010.

Marti, J., and Mauersberger, K.: A Survey and New Measurements of Ice Vapor-Pressure at Temperatures between 170 and 250k, Geophysical Research Letters, 20, 363-366, 10.1029/93gl00105, 1993.

McConnell, J. R., Bales, R. C., Stewart, R. W., Thompson, A. M., Albert, M. R., and Ramos, R.: Physically based modelling of atmosphere-to-snow-to-firn transfer of H_2O_2 at South Pole, Journal of Geophysical Research-Atmospheres, 103, 10561-10570, 10.1029/98jd00460, 1998.

McNeill, V. F., Loerting, T., Geiger, F. M., Trout, B. L., and Molina, M. J.: Hydrogen chloride-induced surface disordering on ice, Proceedings of the National Academy of Sciences of the United States of America, 103, 9422-9427, 10.1073/pnas.0-603494103, 2006b.

McNeill, V. F., Geiger, F. M., Loerting, T., Trout, B. L., Molina, L. T., and Molina, M. J.: Interaction of hydrogen chloride with ice surfaces: The effects of grain size, surface roughness, and surface disorder, Journal of Physical Chemistry A, 111, 6274-6284, 10.1021/jp068914g, 2007b.

Moussa, S., Kuo, M. H., and McNeill, V. F.: Nitric acid-induced surface disordering on ice, submitted to Physical Chemistry Chemical Physics, 2013.

Mulvaney, R., Wolff, E. W., and Oates, K.: Sulfuric-Acid at Grain-Boundaries in Antarctic Ice, Nature, 331, 247-249, 10.1038/331247a0, 1988.

Neu, J. L., and Prather, M. J.: Toward a more physical representation of precipitation scavenging in global chemistry models: Cloud overlap and ice physics and their impact on tropospheric ozone, Atmospheric Chemistry and Physics, 12, 3289-3310, 10.5194/acp-12-3289-2012, 2012.

Pinzer, B. R., Kerbrat, M., Huthwelker, T., Gäggeler, H. W., Schneebeli, M., and Ammann, M.: Diffusion of NOx and HONO in snow: A laboratory study, Journal of Geophysical Research-Atmospheres, 115, D03304, 10.1029/2009jd012459, 2010.

Popp, P. J., Gao, R. S., Marcy, T. P., Fahey, D. W., Hudson, P. K., Thompson, T. L., Karcher, B., Ridley, B. A., Weinheimer, A. J., Knapp, D. J., Montzka, D. D., Baumgardner, D., Garrett, T. J., Weinstock, E. M., Smith, J. B., Sayres, D. S., Pittman, J. V., Dhaniyala, S., Bui, T. P., and Mahoney, M. J.: Nitric acid uptake on subtropical cirrus cloud particles, Journal of Geophysical Research-Atmospheres, 109, 10.1029/2003JD004255, 2004.

Pouvesle, N., Kippenberger, M., Schuster, G., and Crowley, J. N.: The interaction of H_2O_2 with ice surfaces between 203 and 233 K, Physical Chemistry Chemical Physics, 12, 15544-15550, 10.1039/c0cp01656j, 2010.

Rempel, A. W., Waddington, E. D., Wettlaufer, J. S., and Worster, M. G.: Possible displacement of the climate signal in ancient ice by premelting and anomalous diffusion, Nature, 411, 568-571, 10.1038/35079043, 2001.

Riche, F., Schneebeli, M., and Tschanz, S. A.: Design-based stereology to quantify structural properties of artificial and natural snow using thin sections, Cold Regions Science and Technology, 79-80, 67-74, 10.1016/j.coldregions.2012.03.008, 2012.

Romley, J. A., Hackbarth, A., and Goldman, D. P.: The Impact of Air Quality on Hospital Spending, RAND Corporation, Santa Monica, CA, 2010.

Roumeau, S., Bremaud, P., Riviere, E., Baldy, S., and Baray, J. L.: Tropical cirrus clouds: Apossible sink for ozone, Geophysical Research Letters, 27, 2233-2236, 10.1029/1999gl010898, 2000.

Sigg, A., and Neftel, A.: Evidence for a 50-Percent Increase in H_2O_2 over the Past 200 Years from a Greenland Ice Core, Nature, 351, 557-559, 10.1038/351557a0, 1991.

Slusher, D. L., Huey, L. G., Tanner, D. J., Chen, G., Davis, D. D., Buhr, M., Nowak, J. B., Eisele, F. L., Kosciuch, E., Mauldin, R. L., Lefer, B. L., Shetter, R. E., and Dibb, J. E.: Measurements of pernitric acid at the South Pole during ISCAT 2000, Geophys. Res. Lett., 29, 10.1029/2002GL015703, 2002.

Slusher, D. L., Neff, W. D., Kim, S., Huey, L. G., Wang, Y., Zeng, T., Tanner, D. J., Blake, D. R., Beyersdorf, A., Lefer, B. L., Crawford, J. H., Eisele, F. L., Mauldin, R. L., Kosciuch, E., Buhr, M. P., Wallace, H. W., and Davis, D. D.: Atmospheric chemistry results from the ANTCI 2005 Antarctic plateau airborne study, Journal of Geophysical Reasearch-Atmospheres, 115, 10.1029/2009JD012605, 2010.

Sokolov, O., and Abbatt, J. P. D.: Adsorption to ice of n-alcohols (ethanol to 1-hexanol), acetic acid, and hexanal, Journal of Physical Chemistry A, 106, 775-782, 10.1021/jp013291m, 2002.

Thomson, E. S., Hansen-Goos, H., Wettlaufer, J. S., and Wilen, L. A.: Grain boundary melting in ice, Journal of Chemical Physics, 138, 124707; doi: 10.1063/1.47-974682012, 2013.

Ullerstam, M., Thornberry, T., and Abbatt, J. P. D.: Uptake of gas-phase nitric acid to ice at low partial pressures: Evidence for unsaturated surface coverage, Faraday Discuss., 130, 211-226, 10.1039/b417418f, 2005.

Wang, M., and Overland, J. E.: A sea ice free summer Arctic within 30 years: An update from CMIP5 models, Geophysical Research Letters, 39, L18501, 10.1029/20-12gl052868, 2012.

Washburn, A.L.: Permafrost features as evidence of climatic change. Earth Sciences Review 15, pp. 327-402 1980.

Wei, X., Miranda, P. B., Zhang, C., and Shen, Y. R.: Sum-frequency spectroscopic studies of ice interfaces, Physical Review B, 66, 085401, 10.1103/PhysRevB.66.085401, 2002.

Wettlaufer, J. S.: Ice surfaces: Macroscopic effects of microscopic structure, Philosophical Transactions of the Royal Society A:a-Mathematical, Physical and Engineering Sciences, 357, 3403-3425, 10.1098/rsta.1999.0500, 1999.

WHO: Estimated deaths & DALYs attributable to selected environmental risk factors, by WHO Member State, 2002, World Health Organisation, Department of Public Health & Environnment, 2007.

Winkler, A. K., Holmes, N. S., and Crowley, J. N.: Interaction of methanol, acetone and formaldehyde with ice surfaces between 198 and 223 K, Phys. Chem. Chem. Phys., 4, 5270-5275, 2002.

Chapter 2

A novel synthesis of the N-13 labelled atmospheric trace gas peroxynitric acid

Thorsten Bartels-Rausch[1,0], Thomas Ulrich[1,2], Thomas Huthwelker[1], and Markus Ammann[1]

---

[1]Paul Scherrer Institut, Laboratory of Radiochemistry and Environmental Chemistry, 5232 Villigen PSI, Switzerland

[2]Universität Bern, Department of Chemistry and Biochemistry, 3008 Bern, Switzerland

[0]Author for correspondence (Email: thorsten.bartels-rausch@psi.ch)

2.1 Abstract

Radioactively labeled trace gases have been successfully used to study heterogeneous chemistry of atmospheric relevance. Here we present a new synthesis of gas-phase peroxynitric acid labeled with ^{13}N (H^{13}NO$_4$) to study the interaction of HNO$_4$ with ice and snow surfaces. A yield of about 30% for HNO$_4$ was determined. The main by-products were HNO$_3$ and HNO$_2$. Exposure of an ice packed bed flow tube to these species revealed that the interaction with the surface scale in the order HNO$_3$ > HNO$_4$ = HO$_2$NO$_2$.

2.2 Introduction

The interaction of atmospheric trace gases with the Earth's snow cover or ice surfaces is of high environmental relevance (Abbatt, 2003; Huthwelker et al., 2006). The atmospheric trace gas that we focus on in this work is the nitrogen oxide peroxynitric acid (HNO$_4$). Nitrogen oxides have been of particular interest in atmospheric science, because their gas-phase concentration directly influences the ozone levels and the oxidative capacity of the atmosphere.

For example, in the lower atmosphere, HNO$_3$ adsorbs to and is thus scavenged by ice clouds (Popp et al., 2007). Similarly, on the ground, trace gas uptake by snow may significantly alter the concentration both in the air above snow-covers and in the snow itself (Domin and Shepson, 2002; Grannas et al., 2007). Nitrous acid (HNO$_2$) partitions less to ice or snow, but its interactions with the ice are still strong enough to significantly slow down its diffusion through surface snow (Kerbrat et al., 2010; Pinzer et al., 2010). This longer residence time in the snow pack, as compared to non-interacting species such as NO$_2$, makes its photolytic dissociation and thus its role as source of the strong oxidant OH more probable. Recently, Slusher et al. concluded that the uptake of HNO$_4$ by snow is of similar magnitude than observed for HNO$_3$ (Slusher et al., 2002). The finding that deposition to snow is a major loss process for gas-phase HNO$_4$ above Antarctic surface snow was based on steady-state calculations and comparison to field measurements. Taken its significant fraction of total nitrogen oxides in cold regions of the atmosphere such as in Antarctica and the upper troposphere (Jaegl et al., 2001; Slusher et al., 2001), its uptake would significantly impact the budget of gas-phase nitrogen oxides. Also, as HNO$_4$ has a significant photo-dissociation cross section (Staikova et al., 2002), its deposition should be taken into account when discussing the vivid photochemistry of nitrogen oxides in snow-packs (Grannas et al., 2007). Sound conclusions are however hampered by missing data from well-controlled laboratory experiments on the interaction of HNO$_4$ with ice or any other environmental surface.

^{13}N with a half-life of 10 min has been used in the past to label nitrogen oxides

to be used as tracer in chemical experiments with relevance to Earth's atmosphere (Ammann, 2001). The main aim of this work was to develop a new synthesis route for ^{13}N labeled HNO_4 in the gas phase by an association reaction of $^{13}NO_2$ with HO_2. ^{13}N isotopes are obtained from the PROTRAC facility at the Paul Scherrer Institute. In the first part of the work, we describe the yield of the product (HNO_4) and of other nitrogen oxide by-products by means of a chemical ionization mass spectrometer and of a chemiluminescence detector. This work was done with an excess of $H^{14}NO_4$. As neither method can differentiate ^{13}N from other nitrogen isotopes, the production of ^{13}N labeled nitrogen oxides was verified using a packed bed flow tube for separation and radioactive decays for detection in a second step. This method has been called thermochromatography before (Eichler and Zvara, 1982). In this work, ice was chosen as stationary phase, because the separation of HNO_3, HNO_2, NO_2, and of NO in an ice packed bed flow tube has been shown before (Bartels-Rausch et al., 2002) and additionally, first information on the partitioning of HNO_4 between ice and air can be gained.

2.3 Experimental

Figure 2.1 shows a scheme of the experimental set-up consisting of the production of ^{13}N in a gas target and of the synthesis of HNO_4 (Fig. 2.1A). Included is also a scheme of the packed bed flow tube that was used to verify the production of $H^{13}NO_4$ (Fig. 2.1B) and of the analytical set-up to characterize the HNO_4 synthesis (Fig 2.1C). The tubing of the flow system consisted of perfluoro-alkoxy copolymer (PFA) 4 mm i.d.. Gas flows were controlled by mass flow controllers (Brooks Instruments) or by mass flow regulators (Vögtlin Instruments) both of which have a 1 % full-scale accuracy.

2.3.1 Production of ^{13}N

The production of ^{13}N isotopes *via* the reaction $^{16}O(p,\alpha)^{13}N$ has been described in detail before (Ammann, 2001). In brief, a flow of 10 % O_2 (99,9995 %, AirLiquid) in He (99,9999 %, Messer) passed through a gas target at 1 L min^{-1} flow velocity and at 2 bar pressure that was continuously irradiated with an 11 MeV proton beam - provided by the accelerator facilities at Paul Scherrer Institute, Switzerland. The primary ^{13}N molecules and radicals were reduced to NO over a molybdenum catalyst at 653 K, immediately after the target cell. The resulting gas was continuously transported to the laboratory through a 580 m long capillary. The radiation chemistry in the target cell also led to the production of non-labelled nitrogen oxides at around 2×10^{11} molecules cm^{-3} from nitrogen impurities in the carrier gas supplies.
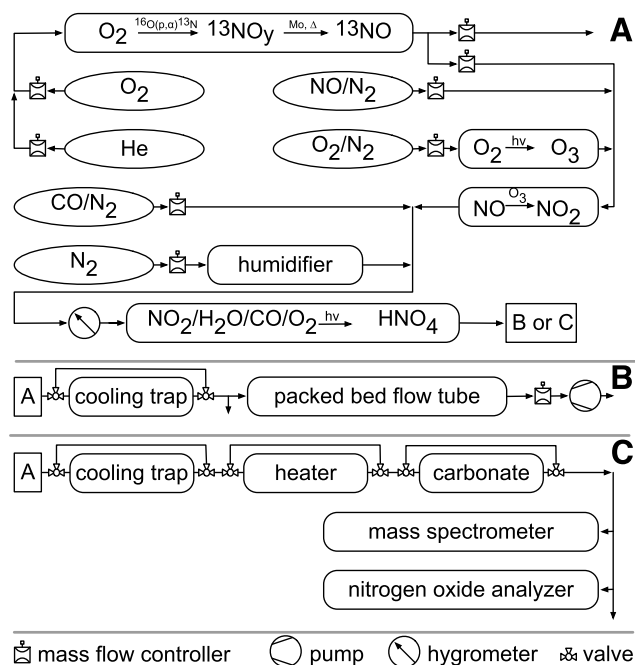
Figure 2.1: Scheme of the experimental set-up. Figure 2.1A shows the production of ^{13}N isotopes and the synthesis of HNO$_4$ molecules. The synthesis was coupled to either a packed bed flow tube for detection of radioactively labeled nitrogen oxides (2.1B), or to analytical devices for detection and characterization of also non-labeled molecules (2.1C).

2.3.2   Synthesis of HNO$_4$

^{13}N labelled and/or non-labelled HNO$_4$ was continuously synthesised in the gas phase by reaction of NO$_2$ with HO$_2$. For this, a H$_2$O/O$_2$/CO/NO$_2$ mixture in a N$_2$ (Carbagas, 99.999 %) gas flow passing an 8 mm i.d. quartz tube was irradiated by an Excimer UV lamp (Heraeus) emitting light at a wavelength of 172 nm. Typical mixing ratios of the gas phase species at atmospheric pressure were 3.5×10^{18} molecules cm^{-3} H$_2$O, 2.3×10^{16} molecules cm^{-3} CO, 1.3×10^{16} molecules cm^{-3} O$_2$, and 9.4×10^{12} molecules cm^{-3} NO$_2$. Ultrapure water (0.054 μS, Millipore) was dosed by passing the gas flow through a home-built, temperature regulated humidifier consisting of a heated Teflon tube immersed in water. The gases were mixed from certified gas bottles of synthetic air (Carbagas, 20 % O$_2$ in N$_2$ (99.999 %), of CO (Carbagas, 10 % CO in N$_2$ (99.999 %)), and of NO (Carbagas, 10 ppm NO in N$_2$ (99.999 %)) as source for NO$_2$, see below.

NO$_2$ was quantitatively synthesized by mixing a gas flow containing NO, from the PROTRAC target and/or from the certified gas bottle, and O$_3$ in a reactor of 2

L volume. O_3 was produced by irradiation of a flow of dry synthetic air with a Hg pen-ray lamp at 185 nm. The irradiation time and the flow of O_2 were adjusted to achieve a small excess of O_3 for full conversion of NO to NO_2, but not more than 2 $\times$ 10^{12} molecules cm^{-3} excess to prevent further oxidation of the NO_2.

2.3.3 Detection of HNO_4 and by-products

A chemical ionization mass spectrometer was used to monitor HNO_4 in the gas phase. The mass spectrometer has been described elsewhere (Guimbaud et al., 2003), the detection scheme was adapted from Slusher (Slusher et al., 2001). The strength of this mass spectrometer method is that – without further use of specific chemical traps – several nitrogen oxides can be detected simultaneously based on specific cluster ions (Huey, 2007). These clusters were produced by reaction with SF_6^- in a home-made ionization chamber situated in front of the mass spectrometer entrance orifice. In detail, a flow of 600 mL min^{-1} of the gas flow exiting the HNO_4 synthesis was mixed with a flow of 1205 mL min^{-1} N_2 and SF_6^- at 11 mbar total pressure. The SF_6^- ions were produced by passing SF_6 (Carbagas, 1 % SF_6 in Ar (99.999%)) in N_2 through a ^{210}Po-ionizer (NRD, p-2031). To enhance the formation of ions, a negative voltage of -136 V was applied to the ionizer and the inner walls of the ionisation chamber. Charged clusters entered the mass spectrometer from the ionization chamber via an orifice at -10 V.

The following clusters have been described and were also observed in this work: $(HF)^-NO_4$ with mass 98 from reaction of HNO_4 with SF_6^- (Slusher et al., 2001), $(HF)^-NO_3$ with mass 82 from HNO_3 (Huey, 2007), $(HF)^-NO_2$ with mass 66 for HNO_2 (Longfellow et al., 1998), NO_2^- with mass 46 for NO_2 (Huey, 2007). A complication of mass spectrometry is that several different species might produce identical fragments. HNO_4, for example, has been described to break apart upon reaction with SF_6^- leading also to the formation of $(HF)^-NO_2$ clusters that are typically used to monitor HNO_2 (Slusher et al., 2001). To quantify this effect the gas flow containing the nitrogen oxides was heated to 373 K for quantitative destruction of HNO_4 to form NO_2. HNO_4 is thermally instable (Zabel, 1995) and the exposure to 373 K at our experimental flow conditions led to a quantitative decomposition of HNO_4 as verified by observation of the mass spectrometer's signal at a mass to charge ratio (m/z) of 98. To heat the gas flow 2 m of the PFA tube were wrapped around an aluminium support and covered by temperature-regulated heating wire (Wisag AG, Switzerland). It was found that the $(HF)^-NO_2$ signal decreased by about 10 %. From this we conclude that the $(HF)^-NO_2$ fragment at m/z = 66 has also a non-negligible contribution from HNO_4 at our detection conditions. We further found that m/z = 66 also rose in absence of nitrogen oxides, as soon as O_3 was added. This correlation of O_3 and the signal at m/z = 66 was observed earlier (Abbatt et al., 2010), and is assigned to $O_3^-(H_2O)$ clusters of mass 66. To correct for this, and derive the fraction

of the signal that is not caused by O$_3$, O$_3$ was also monitored at mass 48 (O$_3^-$). The ratio of m/z = 48 to m/z = 66 was determined in the absence of nitrogen oxides and used to compute the intensity of m/z = 66 due to O$_3$ during the synthesis. This later signal was than subtracted from the raw signal at m/z = 66 to give an estimate of the m/z = 66 traces originating from HNO$_2$. No interferences were observed for m/z = 82 or m/z = 46. Overall, with this measurement method, HNO$_4$, HNO$_3$, and NO$_2$ can be monitored with high selectivity, while HNO$_2$ measurements are less reliable. The mass spectrometer data allow direct analysis of relative trends in the individual nitrogen oxide's abundance with changing synthesis settings. For a quantitative analysis the mass spectrometer needs to be calibrated.

Quantification of the nitrogen oxides in the reactor and calibration of the mass spectrometer was done by means of a chemiluminescence NO monitor equipped with a molybdenum converter (Monitor Labs 9841). This converter reduces nitrogen oxides to NO and its use thus allows detecting the sum of all nitrogen oxides present in a sample (NO$_y$), by-passing it selectively quantifies NO. Please note that the presence of CO interferes with the NO measurements, so that NO cannot be quantified in this study. NO$_y$ measurements via the converter were not affected by the presence of CO, presumably because the molybdenum converter eliminates CO. To further differentiate individual nitrogen oxides selective chemical traps were used. The performance of the traps was verified by observing the individual traces in the mass spectrometer. HNO$_3$ is not detected by this NO monitor, because it is removed from the gas flow prior to entering the molybdenum converter by steel components of the instrument. Its concentration can be given by drop in the instrument's signal intensity when the synthesis is started. Scrubbing HNO$_4$ and HNO$_2$ from the gas phase in a carbonate trap and measuring the remaining nitrogen oxide content in the gas phase quantifies NO$_2$. The carbonate trap was made from firebrick granulate that was soaked with 1.5 % aqueous Na$_2$CO$_3$ (Fluka, p.a.) solution, dried, and placed in a 100 × 6 mm glass tube. The ends of the glass tube were filled with glass wool to keep the covered firebrick in its position. Due to their acidity, carbonate traps HNO$_4$, and HNO$_2$; but neither NO$_2$ nor NO. HNO$_4$ was quantified by heating the gas flow to 373 K, by which HNO$_4$ is converted to NO$_2$, before it enters the carbonate trap. The measured gas-phase concentration corresponds then to HNO$_4$ and NO$_2$. From this measurement, also HNO$_2$ can be derived as fraction of nitrogen oxides that is removed by the carbonate trap. All this requires careful calibration of the nitrogen oxide analyzer that was done with certified bottles of NO (Carbagas, 10 ppm NO in N$_2$ (99.999%)).

2.3.4 Packed Bed Flow tube

The main feature of the packed bed flow tube is a negative temperature gradient along a bed of packed ice spheres – 500 μm in diameter each – as described previously

(Bartels-Rausch et al., 2002). One end, where the gas flow enters the packed bed flow tube was cooled with a circulating cooling liquid regulated at 250 K. The other end where the gas flow exits the apparatus, was immersed in liquid nitrogen. The temperature inside the flow tube was measured with a Pt-100 thermo element (MTS, Switzerland) prior to the measurements.

To start an experiment, a packed bed flow tube was placed in the apparatus und exposed to the temperature gradient for 30 min to allow the temperature equilibrium to be reached at any place in the ice flow tube. Then, the carrier gas containing the[13]N- and ^{14}N-nitrogen oxides was fed into the packed bed flow tube. After 30 min the experiment was stopped, and the flow tube was removed, sealed and immersed in an open bath of liquid nitrogen to stop any further migration of species. In some experiments, the gas flow passed a cooling trap prior to entering the packed bed flow tube to freeze out components from the carrier gas flow with a high partitioning tendency to surfaces. Different geometries and thus surface to volume ratios were used depending on the demands on the capacity. Typically, a quartz tube, 50 mm i.d. and 200 mm in length was filled with quartz spheres, to enhance the surface area, and cooled to 268 K by ethanol cooling liquid circulating around its wall. The cooling trap was operated at least one hour prior to experiments.

The distribution of the ^{13}N-nitrogen oxides on the ice surface along the flow tube is the primary observable of the experiment and was measured by means of a co-incident γ-counter. The coincident γ-counter consisted of two Bismuth-Germanate-detectors; 3 cm in diameter, mounted face to face with a gap of 35 mm. Lead shields were used to reduce the detection width to a slit of 5 mm distance. Coincident γ-counting leads to optimum counting efficiency and low background counting rates (1 count s[-1] or less), because annihilation of positrons following the β^+-decay of ^{13}N results in two γ-rays in opposite direction to each other.

For each experiment, a new packed bed flow tube was prepared as described earlier (Bartels-Rausch et al., 2002; Kerbrat et al., 2010): Spraying of ultra pure water into liquid nitrogen rapidly froze small ice droplets. After a minimum of 2 days of annealing at 253 K, the ice spheres were sieved with calibrated sieves (Retsch, Germany) to grain sizes between 400 μm and 600 μm, filled into a PFA tube (8 mm inner diameter, 360 mm length), and stored again for at least 12 h at -20 C. This preparation was done in a walk-in cold room, during transport to the laboratory, the ice columns were cooled with cooling elements in an insulated box. Based on the mass of the ice filling and the mean diameter of the spheres a mean ice surface area of the packed bed of 20 cm per cm length and a packing density of 70 % can be calculated.

2.4   Results and Discussion

Irradiation at 172 nm of a $H_2O/NO_2/O_2$ mixture leads to the production of OH and
HO_2 radicals by photolysis of water (Eqs. 2.1-2.2), both of which react with NO_2
to form HNO_3 (Eq. 2.3) and HNO_4 (Eq. 2.4), respectively. Central to the synthesis
of HNO_4 with high yields is to shift the OH to HO_2 ratio towards an excess of HO_2
and thus amplify HNO_4 yields. Figure 2.2 shows that this can be achieved in the
presence of CO as scavenger. CO reacts fast with OH but not with HO_2 (Eqs. 2.2
and 2.5)(Schultz et al., 1995).

$$H_2O \xrightarrow{h\nu} OH + H \tag{2.1}$$

$$H + O_2 \xrightarrow{M} HO_2 \tag{2.2}$$

$$NO_2 + OH \xrightarrow{M} HNO_3 \tag{2.3}$$

$$NO_2 + HO_2 \xrightarrow{M} HNO_4 \tag{2.4}$$

$$CO + OH \longrightarrow CO_2 + H \tag{2.5}$$

Figure 2.2 displays the gas phase concentrations of HNO_4, HNO_3, HNO_2, and
NO_2 in the reactor with time as measured with the mass spectrometer during irradi-
ation in absence (Fig 2.2, -30 min - 0 min) and in the presence of NO_2 (Fig 2.2, 0 min
- 90 min). It can be clearly seen that, at a high concentration of 2×10^{16} molecules
cm^{-3} CO, HNO_4 is the main product with a concentration in the reactor of 3×10^{12}
molecules cm^{-3}. HNO_3 and HNO_2 are also detected but at lower concentrations of
2×10^{12} molecules cm^{-3} and 1×10^{12} molecules cm^{-3}, respectively. HNO_3 is most
likely formed via reaction 2.3. HNO_2 can potentially be formed by reaction of NO
with OH, where NO comes from reaction of NO_2 with O- or with H-radicals. H-
radicals are an intermediate product of the reaction 2.1 and 2.5, O-radicals originate
from photolysis of O_3.

Also shown is a significant decrease of 76 % HNO_3 in gas-phase reaching the
mass spectrometer when the flow is feed through a cooling trap at 268 K (Fig 2.2,
60 min - 90 min). This loss can be explained by the high tendency of HNO_3 to
stick to surfaces even at high temperatures. The mass spectrometer traces of HNO_4
and of HNO_2 did also show a response to the cooling trap. But these are caused by
variations in humidity in the chemical ionization mass spectrometer by adsorption
of water in the cooling trap and not by changes in the concentration of HNO_4 or
HNO_2, respectively. This conclusion is supported by independent measurements of
the total nitrogen oxide concentration in the gas flow with the chemiluminescence
detector the performance of which is unaffected by gas-phase humidity. The signal
from this nitrogen oxide analyzer that is sensitive to NO, NO_2, HNO_2, and HNO_4,
but not to HNO_3, did not show any reduction when the gas passed the cooling
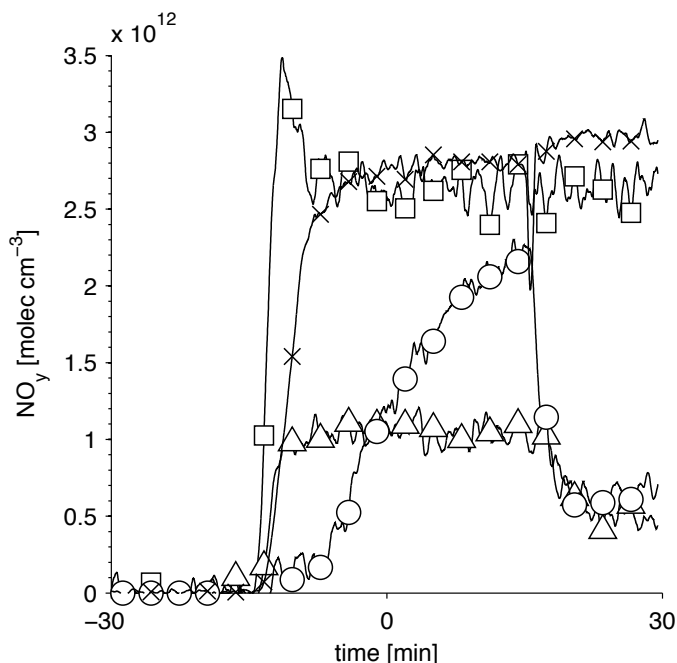
Figure 2.2: Products of the HNO_4 synthesis with time at 8.7×10^{12} molecules cm^{-3} initial NO_2. The line plot shows the calibrated traces as measured with the mass spectrometer of HNO_4 (line with crosses), HNO_3 (circles), HNO_2 (triangles), and NO_2 (squares). On the relative time axis 0 denotes the time when the NO_2 flow was switched on to start the synthesis of HNO_4. 60 min later the gas flow was passed over a cooling trap at 268 K situated just after the reactor.

trap. Additionally, it is well known that the concentration of water in the chemical ionization chamber can significantly affect the formation and yield of ion production (Huey, 2007). For example, water might exchange with HF in (HF)$^-$NO$_4$ clusters of m/z = 98 leading to (H$_2$O)$^-$NO$_4$ clusters of m/z = 96. A slight decrease in relative humidity, when the gas flow is fed over the cooling trap, might thus explain the higher abundance of m/z = 98 and the decrease in observed intensity of the m/z = 96 cluster (data not shown). Similarly, the cluster (HF)$^-$NO$_2$ with m/z = 66 might be sensitive to humidity. Additionally, and likely more important, to derive the concentration of HNO$_2$ based on the measured trace with m/z = 66, the portion of the mass spectrometer signal originating from the O$_3$$^-H_2$O cluster (also at m/z = 66) was subtracted (see experimental). As the later cluster heavily depends on the water content, this analysis becomes questionable when humidity is not stable during an experiment. As the intensity of the cluster (H$_2$O)$^-$NO$_3$ did not change during passage through the cooling trap, we conclude that the cluster (HF)$^-$NO$_3$ does respond to changes in humidity under our experimental conditions and consequently,

the drop in signal intensity observed at m/z = 82 can be fully attributed to loss of HNO$_3$ from the gas phase. Note that the temperature of the cooling trap was always above the dew point of water in the carrier gas to prevent riming.

In summary, in presence of CO in large excess, HNO$_4$, HNO$_3$, HNO$_2$, and NO$_2$ have been identified as products by mass spectrometer measurements. Calibration of the mass spectrometer traces by and comparison to measurements with a chemiluminescence analyzer showed that HNO$_4$ is the main product, but that substantial amounts of HNO$_3$ and HNO$_2$ are present. HNO$_3$ can be significantly reduced by use of a cooling trap at 268 K, whereas HNO$_4$ and HNO$_2$ pass this trap unhindered.

More information on the effect of CO on the product distribution of the photolysis can be seen in Fig. 2.3 showing the concentration of nitrogen oxides with increasing CO content in the gas phase. In the absence of CO, about 90 % of the initial NO$_2$ is oxidized, forming primarily HNO$_3$. This synthesis route to HNO$_3$ is well established and HNO$_3$ yields of up to 90 % can be reached at higher humidity (Ammann, 2001). This approach has been used as HNO$_3$ source in a number of earlier experiments (Guimbaud et al., 2002; Vlasenko et al., 2009). The level of HNO$_3$ drops rapidly to below 20 % with increasing concentration of CO in the reactor and, simultaneously, the HNO$_4$ share increases from below 5 % to over 30 %. The major leap in HNO$_4$ yields is observed at CO concentrations of 1.0×10^{16} molecules cm^{-3}, further increase in CO seems to lead to no significant increases in HNO$_4$ yields, presumably because the self-reaction of HO$_2$ to form H$_2$O$_2$ becomes more important. H$_2$O$_2$ has not been quantified in this study due to a lack of a method to calibrate the mass spectrometer signal. A high count rate of m/z = 140 was observed and can be attributed to H$_2$O$_2$ at our experimental conditions. Bardwell et al. have observed and explained this mass as product of a multi-step reaction from HO$_2$ and SF$_6^-$ previously (Bardwell et al., 2003). We have excluded the presence of HO$_2$ in the sample gas immediately before the sample inlet by adding NO$_2$ to the gas flow after the reactor. In the presence of HO$_2$, HNO$_4$ should have been formed, which was not observed. We thus argue that the fragment of m/z = 140 also originates from H$_2$O$_2$. HNO$_2$ shows no response to varying CO concentrations with a constant yield of about 10 %. NO$_2$ concentration increases slightly from about 20 % to 40 % with increasing CO.

The observed trends for HNO$_4$ and HNO$_3$ with increasing CO as determined with the specific traps and the nitrogen oxide analyzer (Fig. 2.3) are supported by the mass spectrometer measurements. The very selective, but relative, raw mass spectrometer signals of both species at various CO concentrations show the same trend. In contrast, the mass spectrometer data of NO$_2$ indicate the highest yields in the absence of CO followed by a plateau with increasing CO levels, which is quite different from the increasing NO$_2$ levels with rising CO concentration as measured with the nitrogen oxide analyzer. An explanation might be that NO turns up as further by-product at high CO concentrations. NO does not interfere with the NO$_2$ signal of the mass spectrometer, but contributes to the NO$_2$ budget as determined

with the carbonate trap and chemiluminescence analyzer. The same might hold for some organic nitrates that can potentially also be formed in the reactor during the photolysis in the presence of CO.

To increase readability, Figs. 2.2 and 2.3 do not show any error bars. Uncertainties of the mass spectrometer measurements, based on the standard deviation of 3 repeated experiments at 2.3×10^{16} molecules cm^{-3} CO, are 42 % of the mean signal, 18 %, 14 %, and 4 % for NO$_2$, HNO$_2$, HNO$_3$, and HNO$_4$. NO$_2$ is generally difficult to measure by chemical ionization mass spectrometry, because its reaction with SF$_6^-$ is slow which makes this measurement method for NO$_2$ insensitive and uncertain (Huey et al., 1995). The reproducibility of HNO$_2$ measurements is quite low, because of the intense data handling necessary to correct the raw signals for interferences. Measurements of HNO$_3$ by the chemical ionisation mass spectrometer are very sensitive and accurate, but HNO$_3$ might be lost at tubing walls during transport to the mass spectrometer resulting in a lower reproducibility of the amount that actually enters the mass spectrometer. HNO$_4$ measurements show an excellent reproducibility.

The main uncertainty of the chemiluminescence measurements originates most likely from fluctuations of the chemical trap performance. Standard deviations of 16 %, 19 %, 6 %, and 22 % for NO$_2$, HNO$_2$, HNO$_3$, and HNO$_4$ were determined.

To summarize, addition of CO to the gas phase leads to a significant increase of HNO$_4$ as product with a maximum yield of about 30 % of the initial NO$_2$. The fraction of HNO$_3$ decreases significantly with higher CO levels, from the main product in the absence of CO to a share smaller than the HNO$_4$ content at CO levels higher than 1.0×10^{16} molecules cm^{-3}. HNO$_2$, on the other hand, shows a rather invariant yield with higher CO levels and accounts for about 1/3 of the HNO$_4$ concentration. The use of a cold-trap at 268 K further reduces the HNO$_3$ mixing ratio in the gas flow.

2.5   Chromatography of ^{13}N - nitrogen oxides

Based on the above, the following settings were chosen for the production of ^{13}N labelled HNO$_4$ during the packed bed flow tube experiments: 2.3×10^{16} molecules cm^{-3} CO, 1.3×10^{16} molecules cm^{-3} O$_2$, 9.4×10^{12} molecules cm^{-3} NO$_2$, 3.5×10^{18} molecules cm^{-3} H$_2$O. With these settings about 2.6×10^{12} molecules cm^{-3} HNO$_4$, 2.2×10^{12} molecules cm^{-3} HNO$_3$, 1.4×10^{12} molecules cm^{-3} HNO$_2$, and 3.2×10^{12} molecules cm^{-3} NO$_2$ exited the reactor.

The resulting distribution of this mixture along the packed bed flow tube, as shown in Fig. 2.4A, reveals three distinct zones of increased radioactive decays centred around temperatures of 267 K with a 95 per cent confidence interval of 252 K - 282K, 184 K (170 - 198 K), and of 126 K (116 - 136 K). The confidence interval
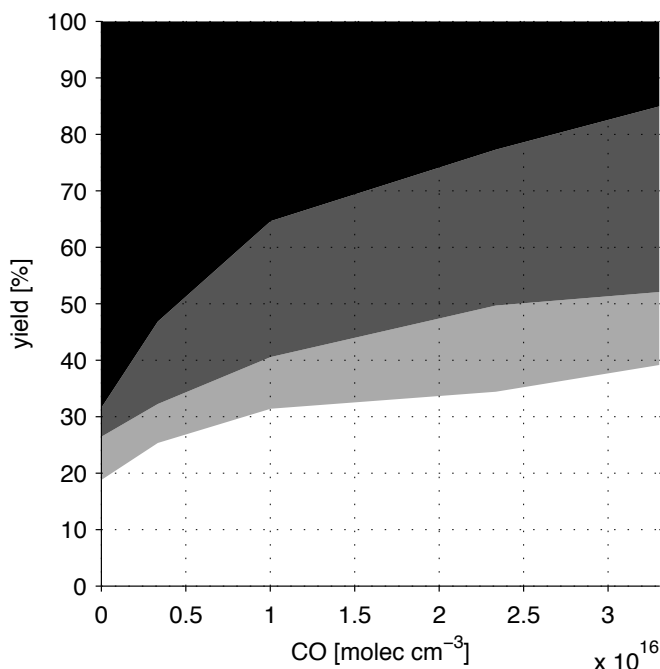
Figure 2.3: Products of the HNO$_4$ synthesis with increasing CO concentration. The area graph displays the proportion of each nitrogen oxide as quantified by chemical traps and by the chemiluminescence detector relative to the amount of total nitrogen oxides: NO$_2$ (white), HNO$_2$ (light gray), HNO$_4$ (dark gray), HNO$_3$ (black).

reflects uncertainties in determining the centre position of the zone by a Gaussian fit to the data and uncertainties in temperature determination at that position by linear regressions.

The evolution of these peaks is a direct consequence of the partitioning of each species between the gas phase passing through the flow tube and the surface of the packed bed (Eichler and Zvara, 1982). As this interaction is both strongly temperature dependent and species-specific, mixtures of trace gases are separated during their migration along the packed bed process reflecting their individual partitioning behaviour (Bartels-Rausch et al., 2002). Thus from the results presented in Fig. 2.4, indicates that the gas flow contains 3 types of nitrogen oxides species, with weak, intermediate and strong partitioning to the ice phase, respectively.

When the gas flow is passed via a cooling trap at 268 K prior to entering the packed bed flow tube, the radioactive decays at the beginning of the packed bed do not exceed the background level and only two peaks are evident at 189 K (175 - 204 K) and at 135 K (126 - 144 K). The first peak appears at an identical position and temperature as the corresponding peak in Fig. 2.4A. The second peak is shifted to a shorter distance and slightly higher temperature, but as the confidence intervals
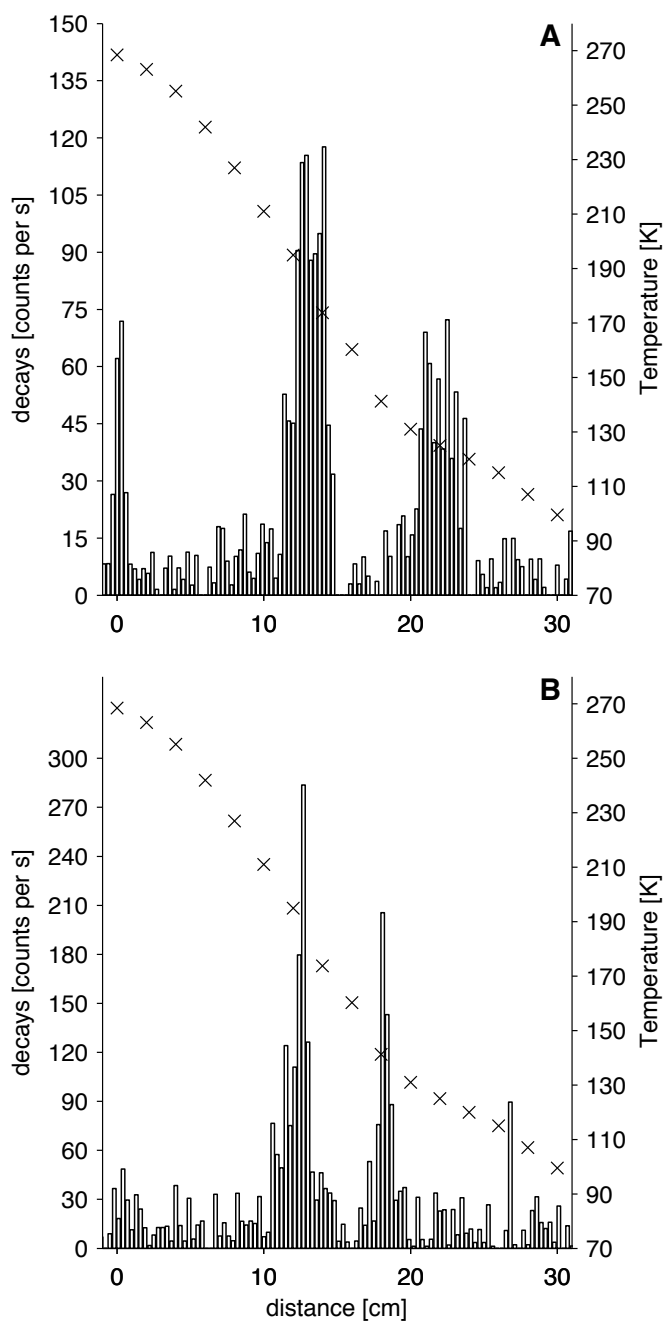
Figure 2.4: The distribution of radioactive decays from ^{13}N-labelled nitrogen oxides along packed bed flow tubes. Zero denotes the beginning of the ice bed. Also shown are the temperature profiles inside the flow tube (crosses). **A**. The gas flow from the synthesis was directly passed over the packed bed flow tube for 30 min. **B**. The gas flow passed a cooling trap at 268 K prior to the packed bed flow tube.

overlap this difference is statistically not significant.

The vanished peak at 267 K can clearly be assigned to HNO$_3$ based on measurements with the mass spectrometer that showed that HNO$_3$ is the only species scrubbed by this cold trap. The strong interaction with ice, or dominant partitioning to the surface at relatively high temperatures, is also supported by recent IUPAC recommendations on the partitioning of HNO$_3$ between ice and air, which predict a high surface concentration of 2×10^3 molecules cm^{-2} in equilibrium for each gas-phase molecule cm^{-3} at 267 K (Ammann et al., 2008). The partitioning of NO$_2$ and HNO$_2$ to ice is much weaker compared to HNO$_3$: Significant adsorption of NO$_2$ to ice has not been observed at temperatures above 195 K (Leu, 1988; Saastad et al., 1993). HNO$_2$ partitioning to ice surfaces occurs at higher temperature (above 170 K) (Fenter and Rossi, 1996; Chu et al., 2000; Kerbrat et al., 2010). Consequently, we can assign HNO$_2$ deposition to the second zone at 184 K and NO$_2$ to the third zone at 126 K. Again, the current IUPAC recommendations for HNO$_2$ support this conclusion with 1×10^4 molecules cm^{-2} HNO$_2$ on the surface per molecule cm^{-3} in the gas-phase at 184 K.

This assessment of HNO$_3$, HNO$_2$, and NO$_2$ is supported by our earlier experiments where we have used selective traps to identify the deposition zones of nitrogen oxides along a negative temperature gradient in a packed bed flow tube (Bartels-Rausch et al., 2002). During those earlier experiments settings such as flow velocity (75 cm^3 min^{-1} and 360 cm^3 min^{-1}) and ice surface area in the packed bed flow tube (4 and 10.9 cm^2 cm^{-1}) were similar but not identical to those in our current investigation. However, systematic variation of these settings during our earlier work was found not to result in modified retention behaviour. Direct comparison of the deposition properties seems thus well suited. NO$_2$ was found to migrate to a position with a temperature of 132 K with a 95 % confidence interval of 18 single experiments of $\pm$ 14 K, which is in excellent agreement with 5 recent experiments, for which a mean of 130 K ($\pm$ 9 K) can be determined. HNO$_2$ was found to migrate to temperatures at 186 K ($\pm$ 20 K for 8 experiments), which overlaps with the intermediate peak as presented in Fig. 2.4 at 191 K ($\pm$ 17 K for 5 experiments).

Li et al. have observed that HNO$_4$ is released from ice surfaces at temperatures above 210 K, whereas HNO$_3$ was only released at higher temperatures of 246 K or above (Li et al., 1996). These results imply for our experimental set-up that HNO$_4$ deposits at lower temperatures than HNO$_3$, i.e. at the same position as HNO$_2$ in the second peak (Fig. 2.4A). This conclusion is supported by comparing the peak areas as measure for the amount of nitrogen oxides deposited to the concentration of nitrogen oxides in the carrier gas as determined by chemiluminescence measurements. For this, the Gauss fits to the distribution of radioactive decays along the packed bed flow tube were integrated. The areas of peak 1: peak 2: peak 3 scale with the ratio 0.5:1.7:1. Taking that pure NO$_2$ deposits in peak 3 and pure HNO$_3$ in peak 1 we can compare this to the ratio of NO$_2$: HNO$_3$ of 0.7 as determined

by quantification of the nitrogen oxide budget by the chemiluminescence analyzer (Fig. 2.3). This agreement is excellent, taking into account that a fraction of HNO_3 is lost during its way to the packed bed flow tube by surface adsorption on the tubing walls. The mass balance analysis of nitrogen oxides further reveals that neither HNO_2, nor HNO_4 alone, can explain the observed high intensity of peak 2. The ratio of HNO_2 to NO_2 is only 0.4 and the ratio of HNO_4 to NO_2 is 0.8; both ratios are less than the ratio of the area of peak 2 to peak 3 of 1.7. Thus it is most likely that both species together deposit in peak 2.

The uptake to ice surfaces heavily depends on the amount of total uptake to the surface, as at high surface concentrations, adsorbate - adsorbate interactions evolve. For our experiments, a surface concentration of HNO_4 on the ice of 1 - 4 $\times$ 10^{14} molecules cm^{-2} can be calculated. For this calculation, a typical length of the deposition zone of 5 cm, HNO_4 gas phase concentration entering the packed bed flow tube of 1 - 5 $\times$ 10^{12} molecules cm^{-3} with a flow of 300 mL min^{-1} for 30 min, were used. The resulting surface concentration is significantly lower than during the early study by Li et al. in which a formal monolayer, here defined as 1×10^{15} molecules cm^{-2}, was exceeded (Li et al., 1996).

We conclude that the interaction of HNO_4 with ice surfaces is significantly weaker than observed for HNO_3, it rather resembles the interaction of HNO_2 with ice. One might thus expect that the partitioning coefficient at the temperature of peak 2 for HNO_4 is similar to the recommendations for HNO_2, and we propose the same partitioning coefficient K_{LinC} of 7.6 $\times$ 10^{-5} cm^{-1} also for HNO_4 at 189 K. The partitioning coefficient K_{LinC} is defined as concentration of adsorbed species per surface area divided by concentration of gas-phase species per volume in equilibrium and is frequently used for parameterization of surface uptake in atmospheric chemistry models.

2.6 Conclusion and Outlook

A new synthesis route to $H^{13}NO_4$ was developed based on the gas-phase reaction of $^{13}NO_2 + HO_2$. At high concentrations of CO, HNO_4 is the main product with a yield of 30 %. HNO_3 and HNO_2 are the most important nitrogen oxide by-products. HNO_3 can be scrubbed from the gas flow in a cold trap at 268 K. Exposure of this mixture to a temperature gradient along a packed ice bed leads to separation of HNO_3 from HNO_2, HNO_4, and from NO_2. This migration behaviour reveals that the interaction of HNO_4 with ice surfaces is similar to that of HNO_2 - ice but much weaker than the HNO_3 - ice interaction. Thus, the surface partitioning coefficient (K_{LinC}) that quantitatively describes the uptake to the ice surface lies in the order of 7.6 $\times$ 10^{-5} cm^{-1} also for HNO_4 at 189 K. This implies that the uptake of HNO_4 by surface snow in Antarctica or ice crystals in the Upper Troposphere,

where temperatures of 190 K can be reached, is a very potential loss process.

Precise measurement of the surface partitioning and especially its temperature dependence is urgently recommended. For this isothermal chromatographic methods are well suited (Chu et al., 2000; Kerbrat et al., 2010). The advantage of isothermal methods is that the highly temperature-depended partitioning coefficient is the observable of such experiments, and can be directly measured at the temperatures of interest. The strength of the gradient method is rather that it directly reflects the relative intensity of trace-gas ice interactions for mixtures exposed to the ice surface.

Scrubbing of HNO$_2$ and HNO$_3$ from the gas flow is required as the concentration of HNO$_2$ in the synthesis presented here is too high for isothermal experiments.

2.7   Acknowledgements

2.8 References

Abbatt, J.: Interactions of Atmospheric Trace Gases with Ice Surfaces: Adsorption and Reaction, Chemical Reviews, 103, 4783-4800, 2003.

Abbatt, J., Oldridge, N., Symington, A., Chukalovskiy, V., McWhinney, R. D., Sjostedt, S., and Cox, R. A.: Release of Gas-Phase Halogens by Photolytic Generation of OH in Frozen Halide/Nitrate Solutions: An Active Halogen Formation Mechanism?, The Journal of Physical Chemistry A, 114, 6527-6533, doi: 10.1021/jp102072t, 2010.

Ammann, M.: Using 13N as tracer in heterogeneous atmospheric chemistry experiments, Radiochimica Acta, 89, 831-838, 2001.

Ammann, M., Atkinson, R., Cox, R., Crowley, J., Hynes, R., Jenkin, M., Rossi, M., Troe, J., Wallington, T., and Subcommittee, I.: Evaluated kinetic and photochemical data for atmospheric chemistry: Heterogeneous reactions on ice, http://www.iupac-kinetic.ch.cam.ac.uk/index.html, 2008.

Bardwell, M., Bacak, A., Raventos, M., Percival, C., Sanchez-Reyna, G., and Shallcross, D.: Kinetics of the HO_2+NO reaction: A temperature and pressure dependence study using chemical ionisation mass spectrometry, Physical Chemistry Chemical Physics, 5, 2381-2385, 10.1039/b300842h, 2003.

Bartels-Rausch, T., Eichler, B., Zimmermann, P., Gäggeler, H. W., and Ammann, M.: The adsorption enthalpy of nitrogen oxides on crystalline ice, Atmospheric Chemistry and Physics, 2, 235-247, 2002.

Chu, L., Diao, G., and Chu, L.: Heterogeneous interaction and reaction of HONO on ice films between 173 and 230 K, Journal of Physical Chemistry A, 104, 3150-3158, 2000.

Domine, F., and Shepson, P.: Air-snow interactions and atmospheric chemistry, Science, 297, 1506-1510, 0.1126/science.1074610, 2002.

Eichler, B., and Zvara, I.: Evaluation of the Enthalpy of Adsorption from Thermochromatographical Data, Radiochim Acta, 30, 233-238, 1982.

Fenter, F., and Rossi, M.: Heterogeneous kinetics of HONO on H_2SO_4 solutions and on ice: Activation of HCl, Journal of Physical Chemistry, 100, 13765-13775, 1996.

Grannas, A. M., Jones, A. E., Dibb, J., Ammann, M., Anastasio, C., Beine, H., Bergin, M., Bottenheim, J., Boxe, C. S., Carver, G., Chen, G., Crawford, J. H., Domin, F., Frey, M. M., Guzman, M. I., Heard, D. E., Helmig, D., Hoffmann, M. R., Honrath, R., Huey, L. G., Hutterli, M., Jacobi, H.-W., Kln, P., Lefer, B., McConnell, J., Plane, J., Sander, R., Savarino, J., Shepson, P. B., Simpson, W.

R., Sodeau, J. R., Von Glasow, R., Weller, R., Wolff, E. W., and Zhu, T.: An overview of snow photochemistry: evidence, mechanisms and impacts, Atmospheric Chemistry and Physics, 7, 4329-4373, 2007.

Guimbaud, C., Arens, F., Gutzwiller, L., Gäggeler, H. W., and Ammann, M.: Uptake of HNO$_3$ to deliquescent sea-salt particles: a study using the short-lived radioactive isotope tracer N-13, Atmospheric Chemistry and Physics, 2, 249-257, 2002.

Guimbaud, C., Bartels-Rausch, T., and Ammann, M.: An atmospheric pressure chemical ionization mass spectrometer (APCI-MS) combined with a chromatographic technique to measure the adsorption enthalpy of acetone on ice, Intternational Jurnal of Mass Spectrometry, 226, 279-290, 10.1016/S1387-3806(03)00019-8, 2003.

Huey, L., Hanson, D., and Howard, C.: Reactions of SF$_6^-$ and I$^-$ with Atmospheric Trace Gases, J. Phys. Chem., 99, 5001-5008, 1995.

Huey, L. G.: Measurement of trace atmospheric species by chemical ionization mass spectrometry: Speciation of reactive nitrogen and future directions, Mass Spectrom Rev, 26, 166-184, 10.1002/mas.20118, 2007.

Huthwelker, T., Ammann, M., and Peter, T.: The uptake of acidic gases on ice, Chemical Reviews, 106, 1375-1444, 2006.

Jaegle, L., Jacob, D., Brune, W., and Wennberg, P.: Chemistry of HO$_X$ radicals in the upper troposphere, Atmosperhic Envrionment, 35, 469-489, doi: DOI: 10.1016/S1352-2310(00)00376-9, 2001.

Kerbrat, M., Huthwelker, T., Gäggeler, H., and Ammann, M.: Interaction of Nitrous Acid with Polycrystalline Ice: Adsorption on the Surface and Diffusion into the Bulk, Journal of Physical Chemistry C, doi: 10.1021/jp909535c, 2010.

Leu, M.: Heterogeneous Reactions of N$_2$O$_5$ with H$_2$O and HCl on Ice Surfaces - Implications for Antarctic Ozone Depletion, Geophysical Research Letters, 15, 851-854, 1988.

Li, Z., Friedl, R., Moore, S., and Sander, S.: Interaction of peroxynitric acid with solid H$_2$O ice, Journal of Geophysical Research, 101, 6795-6802, 1996.

Longfellow, C., Imamura, T., Ravishankara, A., and Hanson, D.: HONO solubility and heterogeneous reactivity on sulfuric acid surfaces, Journal of Physical Chemistry A, 102, 3323-3332, 1998.

Pinzer, B., Kerbrat, M., Huthwelker, T., Gggeler, H., Schneebeli, M., and Ammann, M.: Diffusion of NO$_X$ and HONO in snow: A laboratory study, Journal of Geophysical Research, 115, D03304, 2010.

Popp, P. J., Marcy, T. P., Watts, L. A., Gao, R. S., Fahey, D. W., Weinstock, E. M., Smith, J. B., Herman, R. L., Troy, R. F., Webster, C. R., Christensen, L. E., Baumgardner, D. G., Voigt, C., Kaercher, B., Wilson, J. C., Mahoney, M. J., Jensen, E. J., and Bui, T. P.: Condensed-phase nitric acid in a tropical subvisible cirrus cloud, Geophysical Research Letters, 34, L24812, 10.1029/2007GL031832, 2007.

Saastad, O., Ellermann, T., and Nielsen, C.: On the adsorption of NO and NO_2 on cold H_2O/H_2SO_4 surfaces, Journal of Geophysical Research, 20, 1191-1193, 1993.

Schultz, M., Heitlinger, M., Mihelcic, D. and Volzthomas, A.: Calibration source for peroxy-radicals with built in actinometry using H_2O and O_2 photolysis at 185 nm, Journal of Geophysical Research, 100, 18811-18816, 1995.

Slusher, D., Pitteri, S., Haman, B., Tanner, D., and Huey, L.: A chemical ionization technique for measurement of pernitric acid in the upper troposphere and the polar boundary layer, Geophysical Research Letters, 28, 3875-3878, 2001.

Slusher, D., Huey, L., Tanner, D., Chen, G., Davis, D., Buhr, M., Nowak, J., Eisele, F., Kosciuch, E., Mauldin, R., Lefer, B., Shetter, R., and Dibb, J.: Measurements of pernitric acid at the South Pole during ISCAT 2000, Geophysical Research Letters, 29, 2002.

Staikova, M., Donaldson, A., and Francisco, J.: Overtone-induced reactions on the HO_2NO_2 potential surface, Journal of Physical Chemistry A, 106, 3023-3028, 10.1021/jp0143746, 2002.

Vlasenko, A., Huthwelker, T., Gäggeler, H. W., and Ammann, M.: Kinetics of the heterogeneous reaction of nitric acid with mineral dust particles: an aerosol flow-tube study, Physical Chemistry Chemical Physics, 11, 7921-7930, 10.1039/b904290n, 2009.

Zabel, F.: Unimolecular decomposition of peroxynitrates, Z Phys Chem, 188, 119-142, 1995.

Chapter 3

The adsorption of peroxynitric acid on ice between 230 K and 253 K

T. Ulrich[1,2], M. Ammann[1], S. Leutwyler[2] and T. Bartels-Rausch[1,0]

[1]Paul Scherrer Institut, Laboratory of Radiochemistry and Environmental Chemistry, 5232 Villigen PSI, Switzerland

[2]Universität Bern, Department of Chemistry and Biochemistry, 3008 Bern, Switzerland

[0]Author for correspondence (Email: thorsten.bartels-rausch@psi.ch)

3.1   Abstract

Peroxynitric acid uptake to ice and snow has been proposed to be a major loss process from the atmosphere with impacts on the atmospheric oxidation capacity. Here we present results from a laboratory study on the interaction of peroxynitric acid with water ice at low concentration. Experiments were performed in a coated wall flow tube at atmospheric pressure and in the environmentally relevant temperature range of 230 K to 253 K. The interaction was found to be fully reversible and decomposition was not observed. Analysis based on the Langmuir adsorption model showed that the partitioning of peroxynitric acid to ice is orders of magnitude lower than of nitric acid and similar to nitrous acid partitioning behavior. The partition coefficient (K_{LinC}) and its temperature dependency can be described by $3.74 \times 10^{-12} \times e^{(7098/\mathrm{T})}$ [cm]. Atmospheric implications are discussed and show that the uptake to cirrus clouds or to snow-packs in polar areas is an important sink for peroxynitric acid in the environment.

3.2   Introduction

The nitrogen oxide peroxynitric acid (HO_2NO_2) is an atmospheric trace gas that interlinks both HO_x (= OH + HO_2) and NO_x (= NO + NO_2) chemistry. Connected with those trace gas families are the rate of ozone (O_3) production and also the oxidative capacity of the atmosphere. Due to the thermal equilibrium of HO_2NO_2 with HO_2 and NO_2 (Gierczak et al., 2005), HO_2NO_2 makes up a significant fraction of the total nitrogen oxide budget mainly in the colder parts of the environment. For example, field measurements have shown gas phase concentrations of up to 3×10^{10} molecules cm^{-3} in Antarctica (Slusher et al., 2002; Slusher et al., 2010) and 6×10^8 molecules cm^{-3} in the upper troposphere (Kim et al., 2007). Field data further indicate a strong chemical coupling of HO_2NO_2 and NO (Davis et al., 2008; Slusher et al., 2010) and formation and deposition of HO_2NO_2 has been suggested to contribute to the reduction of OH at increasing NO levels (Grannas et al., 2007).

The fate of HO_2NO_2 in the atmosphere is not well enough known to be captured in atmospheric-chemistry models, which generally overestimate its gas-phase concentration (Slusher et al., 2002; Kim et al., 2007). Diurnal profiles of HO_2NO_2, observed at South Pole, could only be reproduced when deposition to snow was postulated as sink (Slusher et al., 2002). In the upper troposphere a HO_2NO_2 sink is also missing from the model descriptions. Currently the observed altitude profiles cannot be reproduced (Kim et al., 2007). The authors suggested uptake to ice particles in cirrus clouds as one of several potential sink processes. The choice to include a strong deposition of HO_2NO_2 to snowpacks or ice clouds is generally motivated by an earlier laboratory study that showed a significant uptake of HO_2NO_2

to ice surfaces persisting over longer times (Li et al., 1996). This result can however not be applied to atmosphere – ice interactions at environmental conditions for two reasons. First, the HO_2NO_2 concentration during the uptake experiments was up to 2×10^{13} molecules cm^{-3}. Such high levels of acidic trace gases may induce formation of hydrates and significantly alter the interaction of trace gases with the surface (Ullerstam et al., 2005; Huthwelker et al., 2006). Secondly, Li et al. (1996) identified HNO_3 as major nitrogen oxide contamination in the gas-phase with levels of up to 9 % of HO_2NO_2, which corresponds to concentrations of up to 2×10^{12} molecules cm^{-3}. In literally all of their experiments, Li et al. (1996) probed the interaction of HO_2NO_2 with nitric acid hydrates and not with water ice, which is not stable at such high HNO_3 levels (Thibert and Domin, 1998).

The main aim of this study was thus to investigate the uptake of HO_2NO_2 to ice at a low concentration of HO_2NO_2 and its by-products, where ice films are stable. A new cleaning procedure that removes by-products of the HO_2NO_2 synthesis is presented. Further, the uptake of HO_2NO_2 to ice is compared with that of other trace gases and discussed based on their solubility and acidity.

3.3 Methods

Figure 3.1 shows the setup of the experiments. First HO_2NO_2 was synthesized in the gas phase. Then the gas flow containing HO_2NO_2 was purified from by-products. Finally the interaction of HO_2NO_2 with a water-ice film was studied in a coated wall flow tube (CWFT) at atmospheric pressure coupled to a chemical ionization mass spectrometer (CIMS). HO_2NO_2 and its by-products were quantified with a commercial NO_X analyzer, a commercial HONO analyzer, and a commercial H_2O_2 analyzer. In the following the experimental set-up is briefly described. Details on the synthesis of HO_2NO_2 and on the procedure to study the trace gas - ice interaction are given in the Results and Discussion.

3.3.1 Synthesis of HO_2NO_2

The synthesis has been described previously (Bartels-Rausch et al., 2011). First NO_2 is quantitatively synthesized in a reactor of 2 L (RV 1, Fig. 3.1) by mixing a flow of 83 ml min^{-1} NO in N_2 with a flow of 700 ml min^{-1} N_2 and with a small flow of 6 ml min^{-1} O_3 in synthetic air. O_3 is produced by irradiating dry synthetic air with 172 nm light (PhotRct 1, Fig. 3.1). The flow containing NO_2 is then further diluted with 700 ml min^{-1} humidified N_2, mixed with 10 ml min^{-1} CO in N_2, and irradiated in the photolysis reactor (PhotRct 2, Fig. 3.1). Irradiation of a $NO_2/H_2O/CO/O_2/N_2$ mixture at 172 nm yields HO_2NO_2 (Bartels-Rausch et al., 2011), see Results and Discussion for details. About half of the experiments were done at a lower CO flow
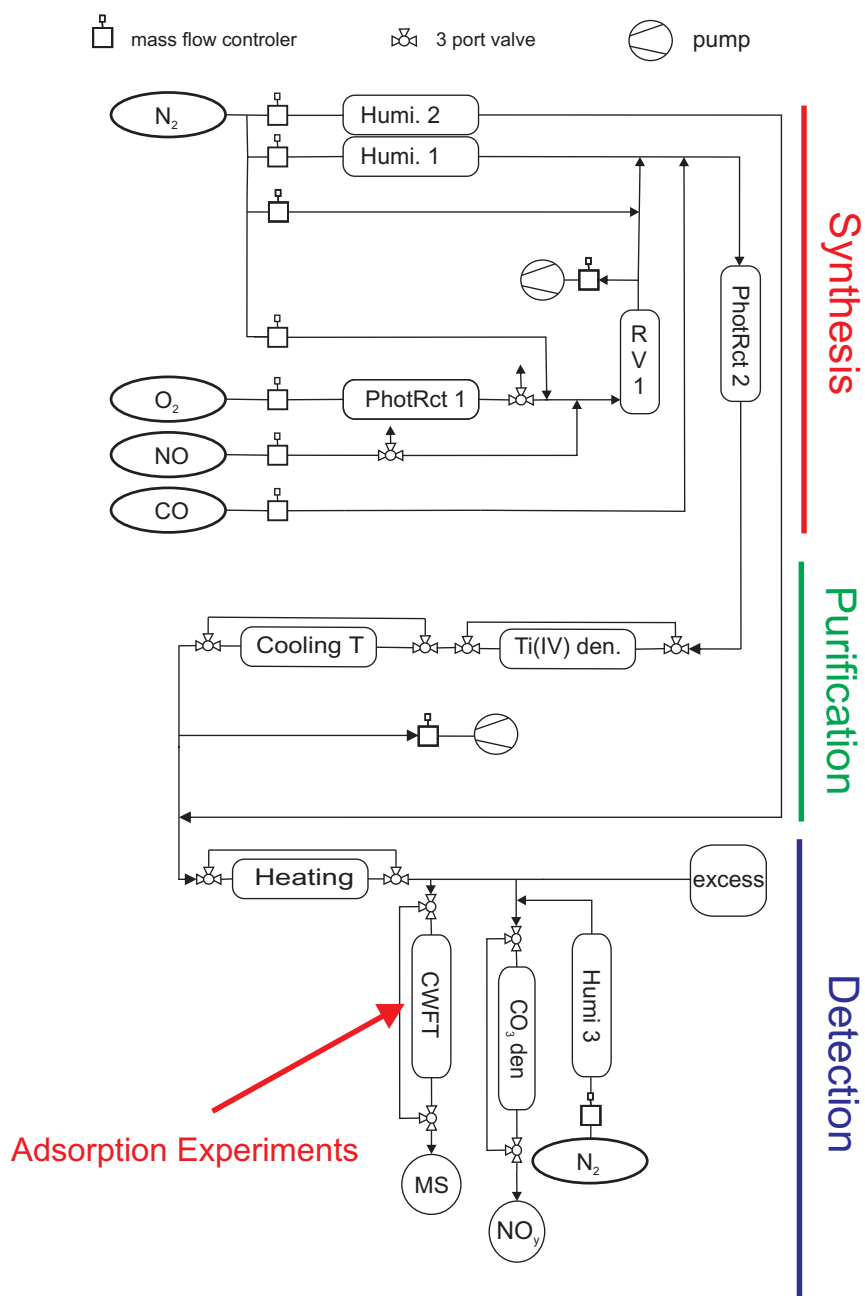
Figure 3.1: Experimental setup consisting of a gas-phase synthesis, a purification step, the adsorption experiments (CWFT), and the detection step.

of 2.5 ml min^{-1}. The residence time in the photolysis reactor was 270 ms. Relative humidity in the photolysis reactor was set to 10 %.

3.3.2 Purification of by-products

After the synthesis the gas flow was cleaned from by-products using a Ti(IV) oxysulfate denuder and a cooling trap at 243 K (see Results and Discussion). The Ti(IV) oxysulfate denuder was prepared by wetting a 49 cm long sandblasted quartz glass tube with a inner diameter of 0.7 cm with a 5 % solution of Ti(IV) oxysulfate in 30 % H_2SO_4 (Fluka 89532) and drying the solution in a flow of N_2 until a very concentrated and highly viscous solution was obtained. The cooling trap consisted of a 46 cm long, jacketed glass tube with an inner diameter of 2.4 cm, which was filled with 10 ml quartz spheres to enhance surface area.

3.3.3 Coated wall flow tube

For the uptake experiments, a gas flow of typically 560 ml min^{-1} containing HO_2NO_2 was pumped from the main gas flow and passed via an ice coated flow tube (CWFT); see Results and Discussion for details on the procedure. Reynolds numbers with an average value of 112 indicate a laminar flow regime in the CWFT. To ensure water vapor equilibrium of the gas and the ice phase, the relative humidity in the gas flow was set to match the vapor pressure of the ice in the CWFT. This was done by adding 1500 ml min^{-1} N_2 that had passed a humidifier. The concentration of HO_2NO_2 in the CWFT was kept constant for all experiments.

3.3.4 Preparation of the ice surface

A quartz tube was etched on the inside with a 5 % solution of hydrofluoric acid (HF) in water, and then rinsed with ultra pure water (MilliQ, 0.05 μS, pH: 7.3) until the pH was neutral. The pH was determined with a pH electrode optimized for and calibrated with solutions of low ionic strength (Orion 3 Star, Thermo). The quartz tube was then held vertically for exactly 60 s to let excess water flow out. An ice film was frozen at 258 K by rotating the quartz tube in a snuggly-fitting cooling jacket. This procedure results in smooth ice films so that its surface area can be calculated based on its geometry (Abbatt, 2003; Huthwelker et al., 2006). The total surface of the ice film was 110 cm^2. The ice had a thickness of 10 μm $\pm$ 2.7 μm as determined by weighing. The cooling jacket was tempered with a circulating ethanol bath. Temperatures were measured with a Pt100 thermo-element directly inside the CWFT at experimental conditions. The temperature gradient along the length of the flow tube was very small. At 253K the entrance of the CWFT was about 0.03 K warmer than temperatures at its end, and at 230 K the difference was

about 0.2 K. At any position temperatures were very stable; the standard deviation at 230 K was $\pm$ 0.05 K.

3.3.5   Detection after contact with the ice

The evolution of HO_2NO_2 in the gas-phase after contact with the ice was monitored using the CIMS (Guimbaud et al., 2003). The sample gas flow of around 560 ml min^{-1} was mixed with 5 ml min^{-1} 1 % SF_6 (Messer, UHP) in Ar (Messer, 99.999 %) and 1200 ml min^{-1} N_2 (CarbaGas, 99.999 %). SF_6^- ions were produced by passing the SF_6 in N_2 through a ^{210}Po-ionizer (NRD, p-2031). HO_2NO_2 was detected with the NO_4^-(HF) cluster at m/z 98 (Slusher et al., 2001). With this setup detection limits (3$\times$standard deviation of the background signal) for HO_2NO_2 of 2.3$\times10^8$ molecules cm^{-3} in the chemical ionization chamber were reached. This corresponds to a concentration of 5.2$\times10^{10}$ molecules cm^{-3} in the CWFT, i.e. before dilution and pressure drop.

The CIMS was further used to ensure the stability of the ice film in all experiments. We observed that the SF_6^- (H_2O) cluster at m/z of 164 responds strongly and reproducibly to changes in relative humidity between 0.2 % and 10 %. This cluster was continuously monitored to confirm the equilibrium of the water vapour in the gas with the ice and stable humidity in the gas flow, whether or not it passed the ice in the CWFT.

3.3.6   Detection of by-products before the CWFT

In a typical experiment the concentration of by-products and the performance of the two traps was monitored using the CIMS. Several clusters, which have been described earlier, have been used in this work: NO_3^-(HF) from HNO_3 at m/z 82 (Huey, 2007), NO_2^-(HF) from HONO and HO_2NO_2 at m/z 66 (Longfellow et al., 1998; Slusher et al., 2001), NO_2^- from NO_2 at m/z 46 (Huey, 2007) and $SF_4O_2^-$ from H_2O_2 at m/z 140 (Bartels-Rausch et al., 2011). The fragment with m/z 66 originates not only from HONO but also from HO_2NO_2. To derive HONO levels from the m/z 66 trace, HO_2NO_2 was thermally decomposed to establish the relative contribution of HONO and HO_2NO_2 to the m/z 66 trace.

3.3.7   Quantification

The CIMS trace of HO_2NO_2, H_2O_2 and HNO_3 was calibrated to continuously monitor their concentrations during each CWFT experiment. The concentration of the other species was determined in the gas flow after the synthesis and after the purification step, mainly to describe the performance of both steps.

In detail, the HONO concentration was quantified with a commercial HONO analyzer (LOPAP, QUMA (Heland et al., 2001; Kleffmann et al., 2002)). The H_2O_2 concentration was measured with a commercial H_2O_2 analyzer (AeroLaser AL 1002). NO, NO_2, HNO_3, and HO_2NO_2 were quantified by a commercial NO_x analyzer (Monitor Labs 9841 A). This instrument measures NO directly by chemiluminescence. In a second channel the total nitrogen oxide (NO_y) concentration is determined after conversion of those species to NO in a built-in molybdenum converter. To differentiate between the individual NO_y species, chemical traps were used (Ammann, 2001). A trap of Na_2CO_3 coated on firebricks was used to scavenge all acidic nitrogen oxides (HONO, HNO_3, and HO_2NO_2) and thus to differentiate between those and the remaining NO and NO_2 in the gas phase. Similarly, a NaCl trap was used to differentiate between HNO_3 and the other NO_y species. It consisted of a sandblasted quartz tube with a length of 49 cm and an inner diameter of 0.8 cm, that was wetted inside with a slurry of NaCl in 1/1 water/methanol and dried in a stream of N_2 (Ammann, 2001). To quantify HO_2NO_2, HO_2NO_2 was decomposed to NO_2. The Na_2CO_3 trap was then used to either scavenge HONO, HNO_3 and HO_2NO_2 or only HONO and HNO_3 (Bartels-Rausch et al., 2011). The heating unit used to decompose HO_2NO_2 was a 2 m long PFA tube (I.D.: 4 mm) heated up to 373 K with a residence time of 730 ms.

We found that the presence of CO interfered with the NO measurements. Detection of NO_y – after passage through the molybdenum converter – was not affected by CO.

3.3.8 Flow system

Gases originate from certified gas bottles of N_2 (Carbagas, 99.999 %), 20 % O_2 (Carbagas, 99.995 %) in N_2 (Carbagas, 99.999 %), 10 ppm NO (Messer, 99.8 %) in N_2 (Messer, 99.999 %) and 10 % CO (Messer, 99.997 %) in N_2 (Messer, 99.9999 %). Gas flows were controlled with calibrated mass flow controllers (Brooks 5850) or gas flow regulators (Voegtlin red-y) with better than 1 % accuracy. The flow through the CWFT was given by the size of the sampling orifice situated between the CWFT and the CIMS at low pressure. The volumetric gas flows were measured once a day with a gas flow calibrator (M-5 mini-Buck Calibrator, A.P. Buck Inc.) with 0.5 % accuracy. All flows in this work refer to standard pressure and temperature (1.013 $\times 10^5$ Pa and 273.15 K). The entire flow system consisted of perfluoroalkoxy (PFA) tubing.

3.4   Results and Discussion

3.4.1   Synthesis of HO_2NO_2

Conventionally HO_2NO_2 is synthesized in the aqueous phase by reaction of NO_2BF_4 in 90 % H_2O_2 or of $NaNO_2$ and $HClO_4$ in 30% H_2O_2, which is then delivered to a gas-flow by bubbling carrier gas through the solution (Kenley et al., 1981; Appelman and Gosztola, 1995). One advantage of the gas-phase synthesis used here is that it can continuously provide HO_2NO_2 levels over long time periods, as needed for our experiments. Also, the handling of concentrated, explosive H_2O_2 solutions is omitted. Niki et al. (1977) synthesized HO_2NO_2 in the gas-phase by photolysis of HCl and subsequent reaction of the produced HO_2 with NO_2. Here, we used a different approach where H_2O is photolyzed to yield HO_2 in order to eliminate potential interference of HCl and ClONO during the adsorption experiments. We have shown previously that HO_2NO_2 yields of up to 30 % can be achieved with this synthesis route by adding CO to the photolysis gas mixture (Bartels-Rausch et al., 2011). The presence of CO reduces OH and increases HO_2 (3.3 and 3.4) (Aschmutat et al., 2001). HO_2NO_2 is then formed by the same reaction as in the atmosphere (Niki et al., 1977):

$$HO_2 + NO_2 \xrightarrow{M} HO_2NO_2 \qquad (3.1)$$

The hydrolysis of water at 172 nm in the presence of oxygen is the source of HO and HO_2 (3.2 and 3.4).

$$HO_2 \xrightarrow{h\nu} OH + H \qquad (3.2)$$

$$CO + OH \longrightarrow CO_2 + H \qquad (3.3)$$

$$H + O_2 \xrightarrow{M} HO_2 \qquad (3.4)$$

The main problem associated with both, gas-phase and aqueous phase, synthesis routes is the presence of by-products. HONO and HNO_3 can be formed by the reaction of NO or NO_2 with OH (3.5 and 3.6).

$$NO_2 + OH \xrightarrow{M} HNO_3 \qquad (3.5)$$

$$NO + OH \xrightarrow{M} HONO \qquad (3.6)$$

In the absence of CO, (3.5) has been used previously as a gas-phase source of HNO_3 with yields of up to 70 % (Vlasenko et al., 2009). NO was not fed into the photolysis reactor. It may presumably form during the photolysis by the reaction of NO_2 with H or with O radicals.

In this photolytic HO_2NO_2 synthesis the levels of by-products are generally rather low. HNO_3 and HONO levels of 1×10^{11} molecules cm^{-3} were determined for an initial NO_2 concentration of 3.4×10^{12} molecules cm^{-3} in the photolysis chamber (Fig. 3.2, 295-330 min). This is lower than observed in our previous study (Bartels-Rausch et al., 2011). The reason for this might be a more selective and direct detection mode of HNO_3 and HONO. In the previous study both species were only indirectly determined. The low levels of by-products are supported by a comparison of the rate constants showing that OH is scavenged by CO much faster than its reaction with either NO or NO_2. The ratios of rate constants of R5/R3 and R6/R3 are 0.06 and 0.03 respectively (Atkinson et al., 2004) and the CO concentration exceeds those of NO and NO_2 by three orders of magnitude.

Due to the interference in the chemiluminescence detection, we cannot quantify NO once CO is added to the gas flow and we can also not differentiate between NO and NO_2.

Another major by-product is H_2O_2 (3.7) for which levels of up to 6×10^{13} molecules cm^{-3} have been determined in the photolysis reactor.

$$HO_2 + HO_2 \longrightarrow H_2O_2 + O_2 \tag{3.7}$$
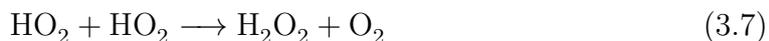
3.4.2 Purification of the synthesis from by-products

For this study, the HO_2NO_2 synthesis was significantly improved by adding a Ti(IV) denuder to remove H_2O_2 during all experiments. Figure 3.2 shows the performance of the two purification steps for a typical experimental run: Concentrations of the trace gases with time are given when the gas flow passed both the Ti(IV) denuder and the cooling trap (235-265 min), only the Ti(IV) denuder (265-295 min), and neither of the two (295-330 min). We found that the Ti(IV) denuder alone removes 96% of the H_2O_2 (Fig. 3.2, 265 - 295 min and 295 – 330 min). Ti(IV) oxysulphate forms $[Ti(O_2)(OH)_{aq}]^+$ complexes with H_2O_2. This has previously been used as an analytical method (Possanzini et al., 1988). Also HONO was reduced by 94 %, and 55 % of the HO_2NO_2 is trapped by the denuder, which lowers the overall yield of the synthesis route substantially. NO_x and HNO_3 are increased by 15 % and 240 % when the Ti(IV) denuder is used. This indicates that these species were produced by redox processes in the Ti(IV) denuder system. The subsequently installed cooling trap reduces the HNO_3 concentration by 86 % and the H_2O_2 concentration by 63 % of their respective concentration after the Ti(IV) denuder (Fig. 3.2, 235 - 265 min). The remaining HNO_3 was 8 % of the HO_2NO_2 concentration, which is comparable to or lower than that reported for the two synthesis routes in the aqueous phase (Knight et al., 2002; Jimenez et al., 2004). Knight et al. (2002) measured a HNO_3 concentration of around 10 % of the HO_2NO_2 in his sample at 273 K. Jimenez et al. (2004) measured a HNO_3 concentration of around 50 % of the HO_2NO_2
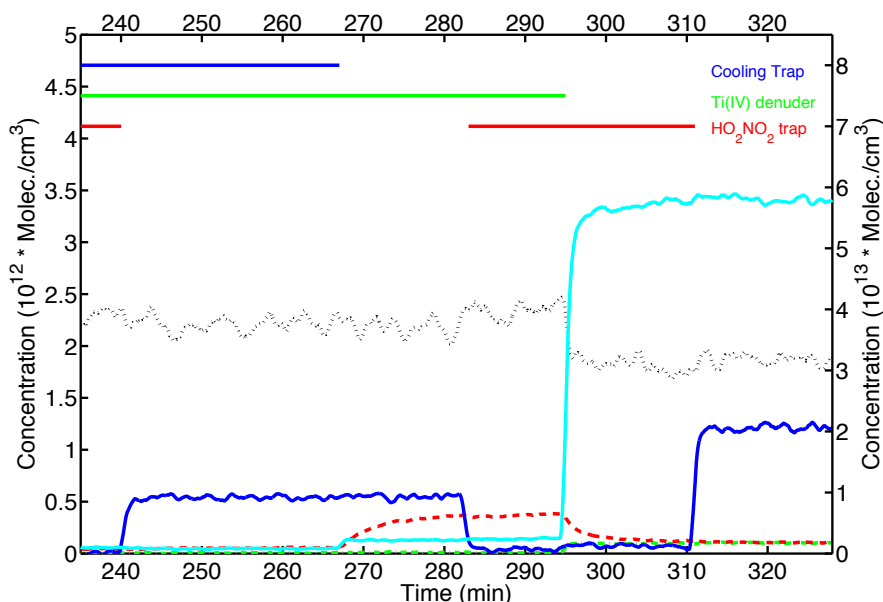
Figure 3.2: Time traces of HO_2NO_2 (blue solid line, left axis) and the by-products NO_2(black dotted line, left axis), HONO (green dash dotted line, left axis), HNO_3(red dashed line, left axis), and H_{22} (turquoise solid line, right axis). Times at which traps were active are indicated by horizontal bars: Red: HO_2NO_2 trap (heating system), green: Ti(IV) denuder, blue: Cooling trap. Concentrations are given without the dilution in front of the CWFT. The data were obtained at initial concentrations of 3.4×10^{12}molecules cm^{-3} NO_2, 5.4×10^{15} molecules cm^{-3} O_2, 1.6×10^{16} molecules cm^{-3} CO, and 2.36×10^{18} molecules cm^{-3} water vapor.

concentration behind a cold trap at 252 K. Considering H_2O_2, Knight et al. (2002) measured H_2O_2 concentrations of around 50 % and Jimenez et al. (2004) of about 10 % of the HO_2NO_2 concentration, both of which are substantially lower than achieved here, even with the very efficient Ti(IV) denuder. In our experiments the H_2O_2 concentration was similar to that of HO_2NO_2.

In summary, after dilution the typical experiment resulted in a concentration of HO_2NO_2 in the CWFT of 9.7×10^{10} molecules cm^{-3} at a CO concentration of 1.6×10^{16} molecules cm^{-3}. At these conditions, the NO_2 concentration was 4×10^{11} molecules cm^{-3}, the HONO concentration was 1×10^9 molecules cm^{-3}, the HNO_3 concentration was 9×10^9 molecules cm^{-3} and the H_2O_2 concentration was 1×10^{11} molecules cm^{-3} in the CWFT.

The concentration of HO_2NO_2, H_2O_2 and HNO_3 was monitored during each

individual CWFT experiment. For about half of the experiments the CO concentration was lowered to 0.4×10^{16} molecules cm^{-3} that – in qualitative agreement with our previous study – resulted in lower HO_2NO_2 yields, lower H_2O_2 yields and higher HNO_3 yields. The concentration of HO_2NO_2 was found to be very reproducible with $1.2 \times 10^{11} \pm 2.2 \times 10^{10}$ molecules cm^{-3} in the CWFT at a CO concentration of 1.6×10^{16} molecules cm^{-3} and with $8.2 \times 10^{10} \pm 1.7 \times 10^{10}$ molecules cm^{-3} at a CO concentration of 0.4×10^{16} molecules cm^{-3}. H_2O_2 concentration was $1.3 \times 10^{11} \pm 8.4 \times 10^{10}$ molecules cm^{-3} at high CO and $9.4 \times 10^{10} \pm 2.2 \times 10^{10}$ molecules cm^{-3} at low CO. HNO_3 concentration was $2 \times 10^{9} \pm 1.4 \times 10^{9}$ molecules cm^{-3} at high CO and $7.8 \times 10^{9} \pm 3.5 \times 10^{9}$ molecules cm^{-3} at low CO.

3.4.3 Adsorption experiments

Figure 3.3 shows typical evolutions of the HO_2NO_2 concentration with time at different temperatures as measured at the end of the CWFT. Such measurements are referred to as breakthrough curves. At time = 0 s the HO_2NO_2 in the gas flow was passed over the ice film, and its intensity drops to the background level. Then, within 200 seconds at our experimental conditions, the gas-phase concentration of HO_2NO_2 starts to recover. The onset of the recovery shows a temperature dependence with a longer lag-time at lower temperatures. The time needed to reach full recovery depends strongly on temperature as expected for an adsorption process. Full recovery means that the HO_2NO_2 traces recover to the average level when the CWFT was bypassed as determined before each single run, i.e. in the interval of 0 to -50 s.

The first result from this study is that HO_2NO_2 gas-phase concentration recovered to its initial level in all experiments. Incomplete recovery would suggest (i) chemical decomposition, (ii) slow, continuous uptake, or (iii) irreversible adsorption of HO_2NO_2. (i) Decomposition of HO_2NO_2 has been observed in water at moderate and acidic pH (Kenley et al., 1981; Lammel et al., 1990; Regimbal and Mozurkewich, 1997). HNO_3, NO_2, HONO, and H_2O_2 have been identified as products. Li et al. (1996) detected HNO_3 emissions from ice exposed to HO_2NO_2 and attributed those to impurities in the HO_2NO_2 source, and thus also concluded that HO_2NO_2 does not decompose on the ice surface. In our experimental setup, we would not expect to observe HNO_3 emissions from the ice, because of its strong tendency to stick to the ice surface. The CIMS traces of NO_2 at m/z 46 and of HONO at m/z 66 showed no increase when HO_2NO_2 was exposed to the ice surface, which further underlines our conclusion. (ii) HO_2NO_2 clearly does not show a long-term uptake as the HO_2NO_2 signal recovered completely within less than 20 minutes at our experimental conditions. Table 3.1 lists the acidity and the molecular Henry coefficients (H_{298}) for different trace gases and shows that the observed complete recovery of HO_2NO_2 fully fits into the emerging picture where acidity largely determines the tendency for long-
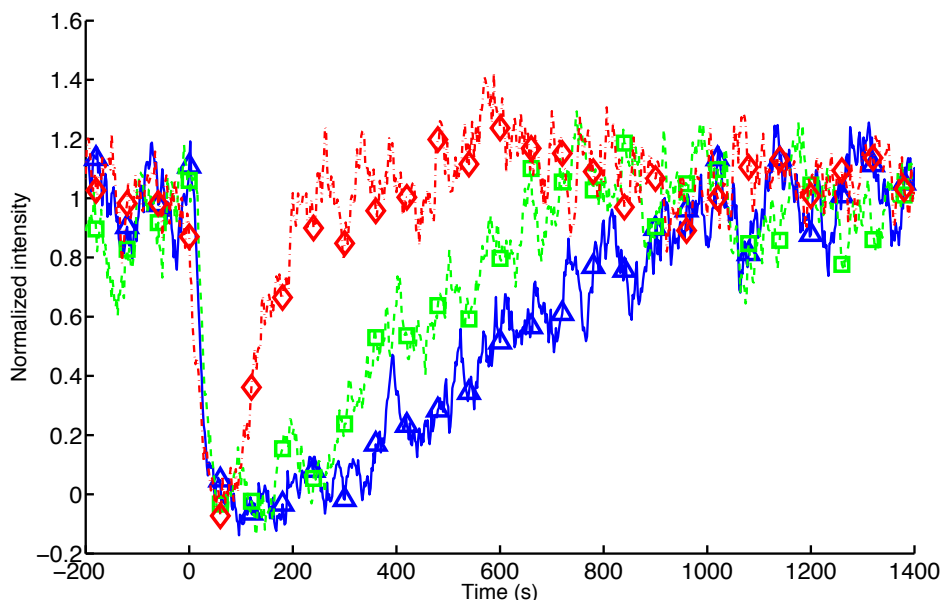
Figure 3.3: Breakthrough curves of three CWFT adsorption experiments at 236 K (blue triangles), 240 K (green squares), and 250 K (red diamonds). The gas flow is led over the CWFT at time = 0 s. The variation in intensity at 250 K (t = 400 - 1000 s) is due to instrument fluctuations.

term uptake. The observation of a strong uptake over long timescales on thin ice films is restricted to highly acidic trace gases. Typical examples are HNO_3 (Ullerstam et al., 2005), HCl (McNeill et al., 2007), and tri-fluoroacetic acid (CF_3COOH) (Symington et al., 2010). Weaker acids, such as HO_2NO_2, show a fast and complete recovery. Analogous examples are formic acid (von Hessberg et al., 2008; Symington et al., 2010), acetic acid (Picaud et al., 2005; von Hessberg et al., 2008; Kerbrat et al., 2010a; Symington et al., 2010), HONO (Chu et al., 2000), and SO_2 (Clegg and Abbatt, 2001). The non-acidic H_2O_2 shows no long term uptake (Clegg and Abbatt, 2001; Pouvesle et al., 2010). For the weak acids HONO and SO_2 a long term uptake has been observed in packed bed flow tubes that have a much larger ice volume and surface area and are thus much more sensitive to slow bulk and surface effects (Huthwelker et al., 2001; Kerbrat et al., 2010b). Molecular solubility seems not to be a strong driver for long-term uptake (Tab. 3.1). Instrumental fluctuations of $\pm$ 5 % however give the possibility that small deviations from the complete recovery remained undetected in our experiments. (iii) To test the reversibility of the uptake, the number of desorbing molecules was determined in 4 experiments at 230, 236,

Table 3.1: Solubility, acidity (pK_a), and adsorption enthalpies (ΔH_{ads}). The solubility is given as molecular Henry constant at 298 K (H_{298}).

Species	H_{298} [M/atm]				pK_a	ΔH_{ads} [kJ/mol]			
	min		max			min		max	
NO	–		–		–	-17.4	[q]	-22.6	[q]
NO$_2$	–		–		–	-21	[q]	-23	[q]
HONO	37	[a]	50	[b]	3.25	-32	[q]	-45	[r]
HNO$_3$	2.1×10^5	[c]	2.6×10^6	[d]	-1.37	-44	[q]	-68	[s]
HO$_2$NO$_2$	4×10^3	[e]	1.2×10^4	[f]	5.85	-59	[t]	–	
HCl	1.1	[g]	1.5×10^3	[f]	-7	–		–	
SO$_2$	1.1	[i]	1.4	[j]	1.77	–		–	
H$_2$O$_2$	6.9×10^4	[k]	1.4×10^5	[l]	11.6	-32	[u]	–	
HCOOH	9×10^2	[m]	1.3×10^4	[n]	3.7	-51	[v]	–	
CH$_3$COOH	8.3×10^2	[m]	1×10^4	[o]	4.67	-17.5	[w]	-55	[v]
CF$_3$COOH	8.9×10^3	[p]	–		0.3	–		–	

[a] Durham et al. (1981), [b] Becker et al. (1996), [c] Lelieveld and Crutzen (1991), [d] Chameides (1984), [e] Amels et al. (1996), [f] Regimbal and Mozurkewich (1997), [g] Marsh and McElroy (1985), [h] Chen et al. (1979), [i] Liss and Slater (1974), [j] Wilhelm et al. (1977), [k] Hwang and Dasgupta (1985), [l] Hoffmann and Jacob (1984), [m] Yaws and Yang (1992), [n] Servant et al. (1991), [o] Gaffney and Senum (1984), [p] Bowden et al. (1996), [q] Bartels et al. (2002), [r] Kerbrat et al. (2010b), [s] Thibert and Domine (1998), [t] this study, [u] Pouvesle et al. (2010), [v] von Hessberg et al. (2008), [w] Sokolov and Abbatt (2002).

238 and 244 K, respectively. This was done by exposing the ice to HO$_2$NO$_2$ until the adsorption equilibrium was reached, thermally decomposing HO$_2$NO$_2$ to NO$_2$ and HO$_2$ in the gas flow entering the CWFT, and monitoring the HO$_2$NO$_2$ release from the ice. The number of adsorbed and desorbed molecules was equal within the uncertainty of the measurements ($\pm$ 50 %) for the individual experiments below 240 K, indicating fully reversible uptake. At 244 K, the number of desorbed molecules was lower than the number of adsorbed molecules. This might in principle be due to altered surface characteristics of the ice at higher temperatures. However, since also results from the preceding adsorption experiment did lie outside the confidence interval of the data set, we concluded that this measurement is an outlier and do not consider it any further. The observation of reversible adsorption is in agreement with other data available for weak acids or non-acidic species such as H$_2$O$_2$ (Pouvesle et al., 2010), acetone (Winkler et al., 2002; Peybernes et al., 2004; Bartels-Rausch et al., 2005), formic acid (von Hessberg et al., 2008) and acetic acid (Sokolov and Abbatt, 2002; Symington et al., 2010). For the strong acids HNO$_3$ (Ullerstam et al., 2005) and HCl (McNeill et al., 2006) the peak area was significantly lower in the desorption experiments, showing that the adsorption was not reversible for these strong acids.

In summary, the uptake of HO_2NO_2 to the ice surface can be described as reversible adsorption equilibrium at temperatures from 230 K to 253 K.

3.4.4 Partition Coefficient

Surface coverage

The number of adsorbed HO_2NO_2 molecules (n_{ads}) in equilibrium is the primary observable of these experiments and is directly derived from the breakthrough curve:

$$n_{ads} = F(T) \times Int\_Area \times \frac{p_{HO_2NO_2} \times N_a}{R \times T} \tag{3.8}$$

Here, $F(T)$ is the volumetric velocity of the gas flow in $cm^3\ s^{-1}$ at T [K] - the temperature of the CWFT, Int_Area is the integrated area of the curve in s, p_{HO2NO2} is the partial pressure of HO_2NO_2 [MPa], N_a is the Avogadro constant [molecules mol^{-1}], R is the universal gas constant [J mol^{-1} K^{-1}]. The surface concentration of adsorbed HO_2NO_2 molecules at our experimental conditions ranged from $6.1\ ^{+2.8}_{-2.3} \times 10^{11}$ molecules cm^{-2} at 253 K to $7.7\ ^{+4.4}_{-2.5} \times 10^{12}$ molecules cm^{-2} HO_2NO_2 at 230 K. All uncertainties are given as 95 % confidence interval. Surface coverage is at most a few percent of a monolayer, as estimated with a maximal monolayer capacity of 3×10^{14} molecules cm^{-2} found for HONO and HNO_3 (Crowley et al., 2010). Adsorption at such a low surface coverage is most likely in the linear adsorption regime of the Langmuir adsorption isotherm.

To compare the adsorption behavior among different trace gases we express the adsorption equilibrium in terms of the partition coefficient K_{LinC} (cm), which is defined as ratio of the concentration of adsorbed molecules to the gas-phase concentration at equilibrium and which describes the initial linear part of an adsorption isotherm as defined by the Langmuir model. At equilibrium the surface concentration of adsorbates is related to the gas-phase concentration as:

$$K_{LinC} = \frac{n_{ads}/A}{n_{gas}/V} \tag{3.9}$$

where n_{gas} is the number of molecules in the gas phase [molecules], n_{ads} is the number of molecules adsorbed on the ice [molecules], V the volume of the flow tube [cm^3] and A the geometric surface area of the ice film [cm^2]. The Langmuir model has proven to describe the partitioning of a number of atmospheric trace gases well, including HNO_3 at low coverage (Ullerstam et al., 2005), HONO (Kerbrat et al., 2010b) and VOCs (Sokolov and Abbatt, 2002) and has also been adopted by IUPAC (Crowley et al., 2010).

Figure 3.4 shows the natural logarithm of K_{LinC}, plotted versus the inverse temperature in the temperature range of 230K to 253 K. K_{LinC} at 230 K is $94.4\ ^{+49}_{-32}$

cm and decreases to 5.7 $^{+3.0}_{-2.0}$ cm at 253 K. The logarithmic data follow a linear trend, clearly showing that reversible partitioning describes the interaction of HO_2NO_2 with the ice surface very well. The linear fit of $\ln(K_{LinC})$ vs. $1/T$ allows to describe the temperature dependency of K_{LinC} as $3.74 \times 10^{-12} \times e^{(7098/T)}$; the uncertainty of the exponent is $\pm$ 661 K. Such a negative Arrhenius type temperature dependency is in agreement with other trace gases that physically adsorb on ice (Huthwelker et al., 2006). Figure 3.4 also shows that K_{LinC} of HO_2NO_2 is nearly three orders of magnitude lower than the K_{LinC} of HNO_3 and lies in the same range as the K_{LinC} of HONO over the temperature range investigated. This means that at equilibrium HO_2NO_2 adsorbs less to ice than HNO_3 and about as much as HONO. The K_{LinC} values for HNO_3 and HONO were taken from the recent IUPAC compilation (Crowley et al., 2010) and are based on the following work: Abbatt et al. (1997), Chu et al. (2000), Cox et al. (2005), Hynes et al. (2002), Kerbrat et al. (2010b), and Ullerstam et al. (2005). This relative adsorption strength is in agreement with our previous study, where the migration of HO_2NO_2, HNO_3, HONO, and NO_2 was investigated in a flow tube packed with ice along which temperature decreased with distance (Bartels-Rausch et al., 2011). Those experiments showed an increasing preference for the ice phase in the sequence $NO_2 <$ HONO $= HO_2NO_2 <$ HNO_3. It is also in agreement with Li et al. (1996) who observed that HNO_3 desorbs at higher temperatures (246 K) than HO_2NO_2 (225 K) in temperature programmed desorption experiments.

Influence of solubility on the adsorption process

This relative order of K_{LinC} apparently scales with the effective solubility of the individual species in water (Tab. 3.1 and Fig. 3.5). Figure 3.5 shows the results of a multiple linear regression between the partitioning to ice, the acidity constant, and the molecular Henry constant for SO_2, HCOOH, CH_3COOH, CF_3COOH, HONO, HNO_3, HO_2NO_2, HCl and H_2O_2. The correlation is rather good when considering the large errors that might be associated with the three input parameters. Especially, the reported values of H_{298} for HO_2NO_2 might be overestimated as HO_2NO_2 easily decomposes in water, which makes reliable measurement of H_{298} difficult.

The good correlation illustrates the importance of both the acidity and the solubility on the partitioning to ice. Apparently similar molecular properties determine the tendency for uptake into water and the adsorption on ice for these acidic trace gases. This even holds for acidic organic trace gases. The relationship found is given in Eq. 3.10 and can be used to roughly estimate the partitioning of any acidic trace gas to ice.

$$\log(K_{LinC}) = 0.4977 \times \log(H_{298}) - 0.1282 \times pK_a + 1.1362 \qquad (3.10)$$
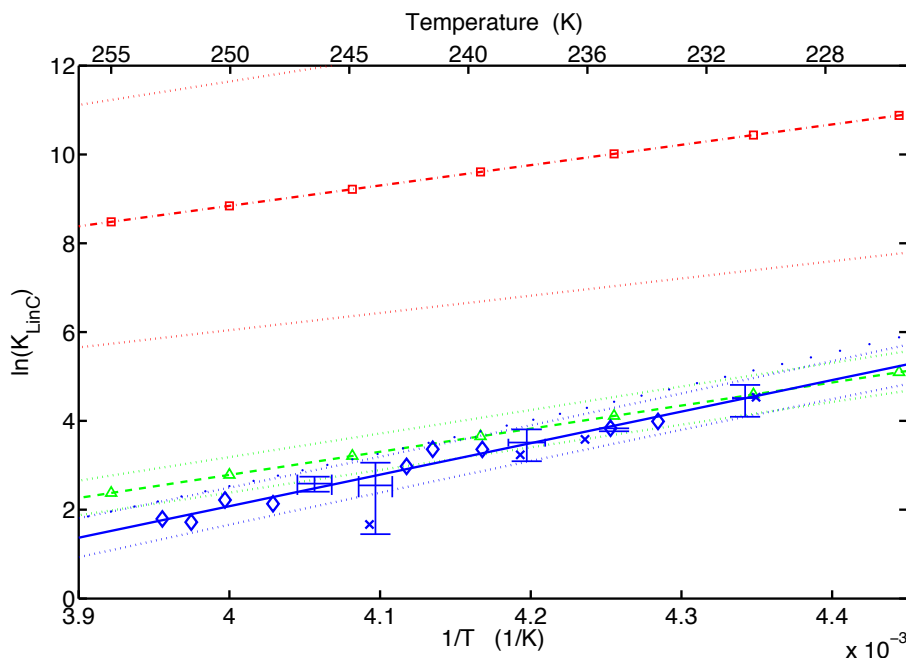
Figure 3.4: Natural logarithm of K_{LinC} versus the inverse temperature for HO_2NO_2 (blue diamonds). When several data points were available mean values are plotted with an uncertainty of two times the standard deviation. The blue, dotted lines give the 95 % confidence bounds for the linear fit (blue solid line). The thick blue dots give the maximum error with included competitive adsorption. The blue crosses indicate desorption experiments. The data are compared to the IUPAC recommendation for HONO (green, dashed line with triangles) and HNO_3 (red, dash-dotted line with squares). The dotted lines show the error for HONO and HNO_3 according to the IUPAC recommendation.

3.4.5 Enthalpy of Adsorption

The slope of the linear fits to the data in the $\ln(K_{LinC})$ versus the inverse temperature plot (Fig. 3.4) is steeper for HO_2NO_2 than for HNO_3 or HONO. This impression is confirmed by a statistical F-test, which compares the slopes of the regressions in a pairwise manner based on the standard deviation of each. The slope and standard deviation for HNO_3 and for HONO were derived from the IUPAC recommendation (Crowley et al., 2010). From the slope the standard enthalpy of adsorption (ΔH^0_{ads}) of -59.0 $\pm$ 5.5 kJ $\times$ mol^{-1} can be derived for HO_2NO_2. When comparing ΔH^0_{ads} with literature values for other nitrogen oxides as given in Tab. 3.1, one obtains the sequence NO < NO_2 < HONO = HNO_3 < HO_2NO_2. The very high enthalpy of adsorption for HNO_3 reported by Thibert and Domin (1998) of -68 $\pm$ 8.9 kJ/mol was
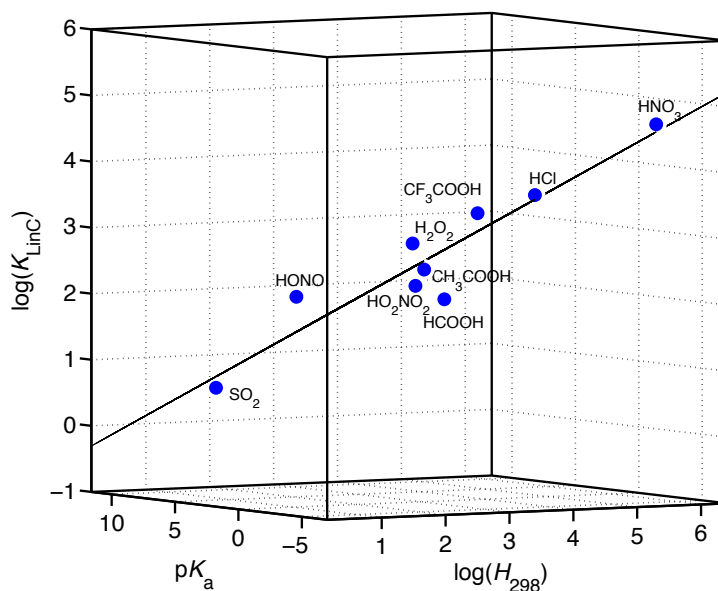
Figure 3.5: Multiple linear regression with the input parameters acid dissociation constant (pK_a) and molecular Henry constant (H_{298} [M/atm]) versus the K_{LinC} [cm^{-1}] on ice at 228 K.

not considered. The higher enthalpy of adsorption compared to the other nitrogen oxides indicates stronger HO_2NO_2 - ice interactions.

3.5   Effect of By-products

Despite careful purification steps, there is a possibility that the remaining H_2O_2, HNO_3, HONO, NO_2, and NO can interfere with the adsorption measurements of HO_2NO_2 and this is discussed below. NO and NO_2 do not interact with the ice at temperatures of our experiment (Bartels-Rausch et al., 2002), thus their presence does not influence the adsorption measurements of HO_2NO_2. Dimerization of NO_2 to N_2O_4 is unlikely at these low concentrations and is thus neglected. HONO does adsorb to the ice, but since its concentration is only 1 % of HO_2NO_2 its contribution can be neglected. HNO_3 and H_2O_2 are present at relatively high concentration and both partition to ice surfaces. We monitored their gas phase concentration after the CWFT with the CIMS during each experiment. In all experiments the HNO_3 signal remained at background level, while the onset of the recovery for the H_2O_2 signal was only visible in longer experiments (around 45 min). This observation

strongly suggests larger partitioning of either species to ice compared to HO_2NO_2. This is consistent with the work on H_2O_2 adsorption to ice by Pouvesle et al. (2010). An earlier work has shown much weaker partitioning to the ice (Clegg and Abbatt, 2001).

To estimate the impact of HNO_3 and H_2O_2 on HO_2NO_2 adsorption, the length on which they are present in the CWFT was derived. For this the surface coverage (Eq. 2) was calculated with K_{LinC} taken from Crowley et al. (2010) and Pouvesle et al. (2011) and with the measured gas phase concentration. The total area, i.e. the length, in the column where both species adsorb is then derived based on the total flux of molecules into the CWFT during the experiment and the surface coverage. HNO_3 completely adsorbs within less than 2 cm of the flow tube at any temperature and its influence on the partitioning of HO_2NO_2 to the ice in equilibrium over the whole length of the CWFT is thus neglected. H_2O_2 adsorbs along a length of up to 30 cm with a surface coverage ranging from 5 % to 10 % in the temperature range of 253 K to 238 K, and from 10 % to 18 % below 238 K. Such a high surface coverage of an additional trace gas during uptake experiments might lead to a reduction in adsorbed HO_2NO_2 molecules, because both species compete for adsorption sites on the ice. To quantify the possible influence of H_2O_2 on the adsorption of HO_2NO_2, we used the competitive Langmuir model as detailed in (Kerbrat et al., 2010a). The model showed that K_{LinC} is reduced by 20 % at 230 K, by 8 % at 238 K and by 5 % at 250 K. This is thus a potential systematic error of our results at low temperatures. However, as the deviation is well within the experimental scatter of K_{LinC}, we neglected the influence of competitive adsorption (Fig. 3.4).

All experiments were done in the ice stability regime of the HNO_3 – water phase diagram (Thibert and Domin, 1998), and the H_2O_2 – water phase diagram (Foley and Giguere, 1951). Yet, surface modification of the ice by HNO_3 could be important along the first 2 cm of the CWFT. McNeill et al. (2006) have observed increased adsorption of acetic acid to ice when another strong acid, HCl, was dosed to the surface at a concentration that induced surface premelting. McNeill et al. (2006) observed this increased adsorption at HCl concentrations near the boundary of the solid ice stability regime of the HCl-water phase diagram. For partial pressures corresponding more to the center of the ice stability regime in the phase diagram no premelting and no increased uptake of acetic acid was observed. The HNO_3 concentration in this study was rather in the middle of the solid ice stability regime of the HNO_3-water phase diagram, making it unlikely that surface modifications might have occurred which enhance the uptake of HO_2NO_2. In agreement, solid ice was still observed at the surface in presence of nitrate at concentrations similar to this study (Krepelova et al., 2010).

The presence of by-products, esp. H_2O_2, might have altered the adsorption of HO_2NO_2. However, this effect is not larger than the random fluctuations of our results. We thus do not correct our values for systematic error and think that the

results given here are a good representation of environmentally relevant conditions.

3.6 Uncertainties

The uncertainty of n_{ads}, K_{LinC}, the exponent of the Arrhenius temperature dependency, and of ΔH^0_{ads} was determined by the 95 % confidence interval of the fit through 22 data points. The reported error represents random variations between individual experiments and is expressed as 2 times the standard deviation in each direction. The 95 % confidence interval of the fit agreed well with the confidence interval of 5 repeated experiments at 230 K. A rough estimation of the individual contributions to the total uncertainty revealed that fluctuations in n_{ads}, which are 19 % of the mean value and instrumental fluctuations, which are 5 % of the mean value, contribute strongly to the uncertainty of n_{ads}. Other random fluctuations like the temperature of the CWFT or the fluctuations of the flow through the CWFT have a lower impact on the error.

Co-adsorption has been discussed as a source of systematic error in the determination of K_{LinC} of HO_2NO_2 and it was found that this negligible (4. Effect of By-products). This conclusion relies on calculations based on $n_{\text{max}}(H_2O_2)$, $n_{\text{max}}(HO_2NO_2)$, the gas phase concentration of H_2O_2, and $K_{\text{LinC}}(H_2O_2)$. Each of these parameters has an uncertainty by itself. The effect on $K_{\text{LinC}}(HO_2NO_2)$ of each is discussed in the following. An error in n_{max} of H_2O_2 and of HO_2NO_2 was found to be negligible. In the interval of n_{max} from 2×10^{14} molecules cm^{-2} to 4×10^{14} molecules cm^{-2}, K_{LinC} only changed by 7 % at 230 K. The gas phase concentration of H_2O_2, which was tested in the $\pm$ 50% interval, changed K_{LinC} by 7 % at 230 K. This is also within the experimental scatter. A change in K_{LinC} of H_2O_2 within a + 150 % - 66 % interval, leads to a change in K_{LinC} of 22 %. This effect was the greatest, but still inside the bounds of error of experimental scatter. In summary the conclusion, that co-adsorption is negligible, is valid even when considering the systematic uncertainty.

3.7 Atmospheric Implications

Ice surfaces have been proposed to represent a sink for gas phase HO_2NO_2 (Slusher et al., 2002; Kim et al., 2007), and the magnitude of the uptake of HO_2NO_2 to ice surfaces has been proposed to be similar to that of HNO_3 (Slusher et al., 2002). In this study we show that equilibrium partitioning of HO_2NO_2 to ice at low concentration is orders of magnitude lower than expected purely based on its molecular solubility. Molecular Henry constants have been used to estimate the gas phase concentration of HO_2NO_2 over ice surfaces (Abida et al., 2011). Here we discuss the

equilibrium partitioning of HO_2NO_2 to ice clouds in the upper troposphere and to surface snow-packs under environmentally relevant conditions once the adsorption equilibrium is reached.

Figure 3.6 shows the fraction of HO_2NO_2 adsorbed to the ice phase in typical cirrus clouds in the upper troposphere. Typical temperatures and surface area densities of dense cirrus clouds, 3×10^{-4} to10^{-5} cm^2 ice surface per cm^3 of free gas phase, were taken from observations (Popp et al., 2004). The temperatures for the experiments presented in this work range from 230 K to 253 K. Data is extrapolated to temperatures down to 200 K in Fig. 3.6 which potentially adds uncertainty. Taken the excellent linear fit of $\ln(K_{\text{LinC}})$ to 1/T that represents our data, we suggest that this extrapolation is reasonable for a rough estimate of the partitioning of HO_2NO_2 to ice in the upper troposphere. The fraction of the adsorbed nitrogen oxides was calculated as proposed by Pouvesle et al. (2010):

$$\alpha = \frac{K_{\text{LinC}} \times \text{SAD}}{K_{\text{LinC}} \times \text{SAD} + 1} \tag{3.11}$$

where α [-] is the adsorbed fraction, K_{LinC} [cm] the partition coefficient as a function of the temperature and SAD [cm^{-1}] is the ice surface area per volume of gas phase (surface area density). The adsorption of HO_2NO_2 to the ice particles is only significant at cold temperatures (< 210 K) and very dense cirrus clouds (3×10^{-4} cm^{-1}); then up to 70 % of the total HO_2NO_2 is trapped. Thus when very dense clouds are present the equilibrium partitioning of HO_2NO_2 to cirrus clouds could explain the discrepancy between measured and modeled data for HO_2NO_2 in the upper troposphere.

Considering the snow cover on the ground, the surface area to air-volume ratio is orders of magnitude higher than in clouds (see below) and HO_2NO_2 adsorbs almost completely to the ice phase in the interstitial air of snow even at warmer temperatures. The specific surface area ranges from 20 cm^2 g^{-1} to >1000 cm^2 g^{-1} for melt-freeze crust and fresh dentric snow, respectively. The density and solid to air volume ratio ranges from 0.1 g cm^{-3} to 0.6 g cm^{-3} for fresh and wind-packed snow, respectively (Domin et al., 2008). The resulting surface area densities are in the range of 10's to 100's cm^{-1}. This extensive partitioning to the ice phase directly influences the transport of HO_2NO_2 through a snow-pack by diffusion. The diffusivity of species with a strong tendency to stick to ice surfaces, i.e. large K_{LinC}, is attenuated by a factor $1/f$ (3.12).

$$f_{\text{HO}_2\text{NO}_2} = \frac{1}{1 + \text{SAD} \times K_{\text{LinC},\text{HO}_2\text{NO}_2}} \tag{3.12}$$

Figure 3.7 shows f versus the temperature typical for snow-covered environments for a range of surface area densities, where the high SAD value represents fresh dentric snow and the low value wind packed snow. At temperatures below 240 K
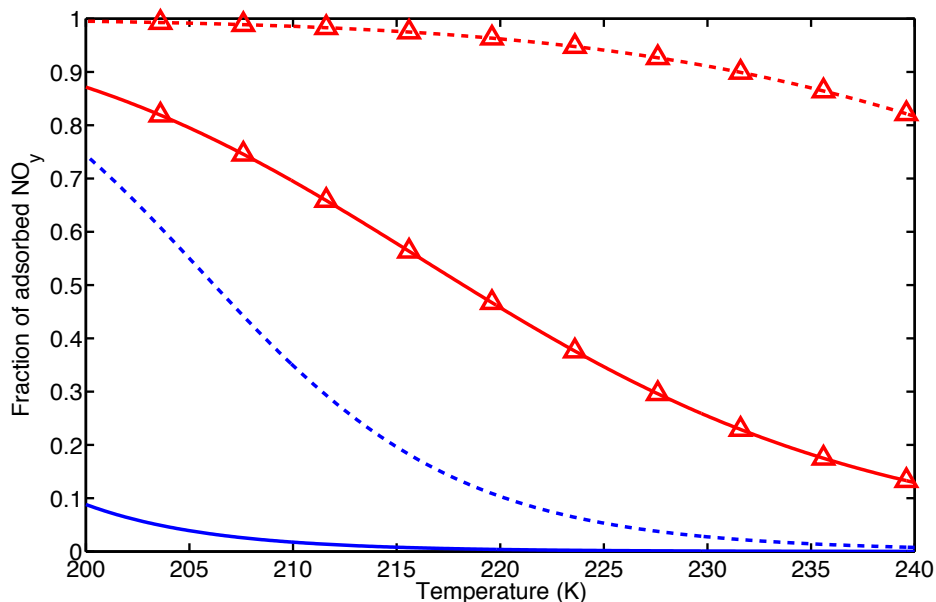
Figure 3.6: Fraction of adsorbed HO_2NO_2 (blue line) and HNO_3 (red line, triangles) to cirrus clouds at temperatures of the upper troposphere. Solid lines represent clouds with a surface area density of 10^{-5} cm^{-1}, dashed lines represent clouds with a surface area density of 3×10^{-4} cm^{-1}. Data for HNO_3 was taken from the IUPAC recommendations, the data for HO_2NO_2 is from this work.

diffusion is slowed by more than hundred times due to the interaction with the ice surface for any given snow-pack.

In summary snow and ice particles represent a sink for HO_2NO_2 in the environment. The snow pack represents a sink at any typical temperature; adsorption of HO_2NO_2 on atmospheric ice particles strongly depends on the density of the ice clouds and temperature.

3.8 Conclusions

The adsorption of HO_2NO_2 on ice and its temperature dependence has been characterized at low surface coverage. At our experimental conditions, uptake of HO_2NO_2 to ice is fully reversible and a slow, long-term loss to the ice was not observed. The partition constant K_{LinC} with a negative temperature dependence of $3.74 \times 10^{-12} \times e^{(7098/T)}$ (cm) was derived. Partitioning to ice of HO_2NO_2 is orders of magnitude smaller than values for HNO_3, and in the same range as values reported for
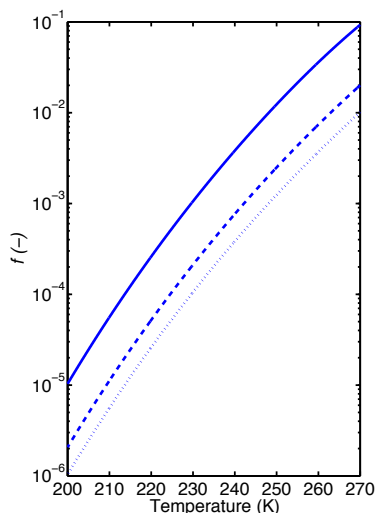
Figure 3.7: Retention factor f versus temperature for three different surface area densities of snow: Solid line = 10 cm^{-1}, dashed line: 50 cm^{-1} and dotted line: 100 cm^{-1}.

HONO. Acidity and solubility of acidic trace gases could have an important impact on the adsorption behavior. Cirrus clouds in the upper troposphere and ice and snow surfaces at South Pole and other very cold parts of the environment are a sink for gas-phase HO_2NO_2.

3.9   Acknowledgements

3.10 References

Abbatt, J. P. D.: Interaction of HNO$_3$ with water-ice surfaces at temperatures of the free troposphere, Geophysical Research Letters, 24, 1479-1482, 10.1029/97GL01403, 1997.

Abbatt, J. P. D.: Interactions of atmospheric trace gases with ice surfaces: Adsorption and reaction, Chemical Reviews, 103, 4783-4800, 10.1021/cr0206418, 2003.

Abida, O., Mielke, L. H., and Osthoff, H. D.: Observation of gas-phase peroxynitrous and peroxynitric acid during the photolysis of nitrate in acidified frozen solutions, Chemical Physics Letters, 511, 187-192, 10.1016/j.cplett.2011.06.055, 2011.

Amels, P., Elias, H., Gtz, U., Steingens, U., and Wannowius, K. J.: Chapter 3.1: Kinetic investigation of the stability of peroxonitric acid and of its reaction with sulfur(IV) in aqueous solution, edited by: Warneck, P., Springer Verlag, Berlin, 77-88 pp., 1996.

Ammann, M.: Using N-13 as tracer in heterogeneous atmospheric chemistry experiments, Radiochimica Acta, 89, 831-838, 10.1524/ract.2001.89.11-12.831, 2001.

Appelman, E. H., and Gosztola, D. J.: Aqueous peroxynitric acid (HOONO$_2$) - a novel synthesis and some chemical and spectroscopic properties, Inorganic Chemistry, 34, 787-791, 10.1021/ic00108a007, 1995.

Aschmutat, U., Hessling, M., Holland, F., and Hofzumahaus, A.: A tunable source of hydroxyl (OH) and hydroperoxy (HO$_2$) radicals: in the range between 10^6 and 10^9 cm^{-3}, Institut fr Atmosphrische Chemie, Forschungszentrum Jlich, Jlich, 811-816, 2001.

Atkinson, R., Baulch, D. L., Cox, R. A., Crowley, J. N., Hampson, R. F., Hynes, R. G., Jenkin, M. E., Rossi, M. J., and Troe, J.: Evaluated kinetic and photochemical data for atmospheric chemistry: Volume I - gas phase reactions of O$_x$, HO$_x$, NO$_x$ and SO$_x$ species, Atmospheric Chemistry and Physics, 4, 1461-1738, 2004.

Bartels-Rausch, T., Eichler, B., Zimmermann, P., Gggeler, H. W., and Ammann, M.: The adsorption enthalpy of nitrogen oxides on crystalline ice, Atmospheric Chemistry and Physics, 2, 235-247, 2002.

Bartels-Rausch, T., Huthwelker, T., Gaggeler, H. W., and Ammann, M.: Atmospheric pressure coated-wall flow-tube study of acetone adsorption on ice, Journal of Physical Chemistry A, 109, 4531-4539, 2005.

Bartels-Rausch, T., Ulrich, T., Huthwelker, T., and Ammann, M.: A novel synthesis of the radioactively labelled atmospheric trace gas peroxynitirc acid, Radiochimica Acta, 99, 1-8, 10.1524/ract.2011.1830, 2011.

Becker, K. H., Kleffmann, J., Kurtenbach, R., and Wiesen, P.: Solubility of nitrous acid (HONO) in sulfuric acid solutions, Journal of Physical Chemistry, 100, 14984-14990, 10.1021/jp961140, 1996.

Bowden, D. J., Clegg, S. L., and Brimblecombe, P.: The Henry's law constant of trifluoroacetic acid and its partitioning into liquid water in the atmosphere, Chemosphere, 32, 405-420, 10.1016/0045-6535(95)00330-4, 1996.

Chameides, W. L.: The photochemistry of a remote marine stratiform cloud, Journal of Geophysical Research-Atmospheres, 89, 4739-4755, 10.1029/JD090iD03p05865, 1984.

Chen, C. C., Britt, H. I., Boston, J. F., and Evans, L. B.: Extension and Application of the Pitzer Equation for Vapor-Liquid-Equilibrium of Aqueous-Electrolyte Systems with Molecular Solutes, Aiche Journal, 25, 820-831, 10.1002/aic.690250510, 1979.

Chu, L., Diao, G. W., and Chu, L. T.: Heterogeneous interaction and reaction of HONO on ice films between 173 and 230 K, Journal of Physical Chemistry A, 104, 3150-3158, 10.1021/jp9937151, 2000.

Clegg, S. M., and Abbatt, J. P. D.: Uptake of gas-phase SO_2 and H_2O_2 by ice surfaces: Dependence on partial pressure, temperature, and surface acidity, Journal of Physical Chemistry A, 105, 6630-6636, 10.1021/jp010062r, 2001.

Cox, R. A., Fernandez, M. A., Symington, A., Ullerstam, M., and Abbatt, J. P. D.: A kinetic model for uptake of HNO_3 and HCl on ice in a coated wall flow system, Physical Chemistry Chemical Physics, 7, 3434-3442, 10.1039/b506683b, 2005.

Crowley, J. N., Ammann, M., Cox, R. A., Hynes, R. G., Jenkin, M. E., Mellouki, A., Rossi, M. J., Troe, J., and Wallington, T. J.: Evaluated kinetic and photochemical data for atmospheric chemistry: Volume V - heterogeneous reactions on solid substrates, Atmospheric Chemistry and Physics, 10, 9059-9223, 10.5194/acp-10-9059-2010, 2010.

Davis, D. D., Seelig, J., Huey, G., Crawford, J., Chen, G., Wang, Y., Buhr, M., Helmig, D., Neff, W., Blake, D., Arimoto, R., and Eisele, F.: A reassessment of Antarctic plateau reactive nitrogen based on ANTO 2003 airborne and ground based measurements, Atmospheric Environment, 42, 2831-2848, 10.1016/j.atmosenv.2007.07.039, 2008.

Domin, F., Albert, M., Huthwelker, T., Jacobi, H. W., Kokhanovsky, A. A., Lehning, M., Picard, G., and Simpson, W. R.: Snow physics as relevant to snow photochemistry, Atmospheric Chemistry and Physics, 8, 171-208, 2008.

Durham, J. L., Overton, J. H., and Aneja, V. P.: Influence of gaseous nitric-acid on sulfate production and acidity in rain, Atmospheric Environment, 15, 1059-1068, 10.1016/0004-6981(81)90106-2, 1981.

Foley, W. T., and Giguere, P. A.: Hydrogen peroxide and its analogues. 2. Phase equilibrium in the system hydrogen peroxide water, Canadian Journal of Chemistry-Revue Canadienne De Chimie, 29, 123-132, 10.1139/v51-016, 1951.

Gaffney, J. S., and Senum, G. I.: ?, in: Gas-liquid chemistry of natural waters, edited by: Newman, L., Brookhaven National Laboratory, 5-1 - 5-7, 1984.

Gierczak, T., Jimenez, E., Riffault, V., Burkholder, J. B., and Ravishankara, A. R.: Thermal decomposition of HO_2NO_2 (peroxynitric acid, PNA): Rate coefficient and determination of the enthalpy of formation, Journal of Physical Chemistry A, 109, 586-596, 10.1021/jp046632f, 2005.

Grannas, A. M., Jones, A. E., Dibb, J., Ammann, M., Anastasio, C., Beine, H. J., Bergin, M., Bottenheim, J., Boxe, C. S., Carver, G., Chen, G., Crawford, J. H., Domine, F., Frey, M. M., Guzman, M. I., Heard, D. E., Helmig, D., Hoffmann, M. R., Honrath, R. E., Huey, L. G., Hutterli, M., Jacobi, H. W., Klan, P., Lefer, B., McConnell, J., Plane, J., Sander, R., Savarino, J., Shepson, P. B., Simpson, W. R., Sodeau, J. R., von Glasow, R., Weller, R., Wolff, E. W., and Zhu, T.: An overview of snow photochemistry: evidence, mechanisms and impacts, Atmospheric Chemistry and Physics, 7, 4329-4373, 2007.

Guimbaud, C., Bartels-Rausch, T., and Ammann, M.: An atmospheric pressure chemical ionization mass spectrometer (APCI-MS) combined with a chromatographic technique to measure the adsorption enthalpy of acetone on ice, International Journal of Mass Spectrometry, 226, 279-290, 10.1016/S1387-3806(03)00019-8, 2003.

Heland, J., Kleffmann, J., Kurtenbach, R., and Wiesen, P.: A new instrument to measure gaseous nitrous acid (HONO) in the atmosphere, Environmental Science & Technology, 35, 3207-3212, 10.1021/es000303t, 2001.

Hoffmann, M. R., and Jacob, D. J.: Kinetics and mechanisms of the catalytic oxidation of dissolved sulfur dioxide in aqueous solution: An application to nighttime fog water chemistry, in: SO_2, NO and NO_2 oxidation mechanisms: Atmospheric considerations, edited by: Calvert, J. G., Butterworth Publishers, Bosten, MA, 101-172, 1984.

Huey, L. G.: Measurement of trace atmospheric species by chemical ionization mass spectrometry: Speciation of reactive nitrogen and future directions, Mass Spectrometry Reviews, 26, 166-184, 10.1002/mas.20118, 2007.

Huthwelker, T., Lamb, D., Baker, M., Swanson, B., and Peter, T.: Uptake of SO_2 by polycrystalline water ice, Journal of Colloid and Interface Science, 238, 147-159, 10.1006/jcis.2001.7507, 2001.

Huthwelker, T., Ammann, M., and Peter, T.: The uptake of acidic gases on ice, Chemical Reviews, 106, 1375-1444, 10.1021/cr020506v, 2006.

Hwang, H., and Dasgupta, P. K.: Thermodynamics of the hydrogen-peroxide water-system, Environmental Science & Technology, 19, 255-258, 10.1021/es00133a006, 1985.

Hynes, R. G., Fernandez, M. A., and Cox, R. A.: Uptake of HNO_3 on water-ice and coadsorption of HNO_3 and HCl in the temperature range 210-235 K, Journal of Geophysical Research-Atmospheres, 107, 10.1029/2001JD001557, 2002.

Jimenez, E., Gierczak, T., Stark, H., Burkholder, J. B., and Ravishankara, A. R.: Reaction of OH with HO_2NO_2 (peroxynitric acid): Rate coefficients between 218 and 335 K and product yields at 298 K, Journal of Physical Chemistry A, 108, 1139-1149, 10.1021/jp0363489, 2004.

Kenley, R. A., Trevor, P. L., and Lan, B. Y.: Preparation and thermal-decomposition of pernitric acid ($HOONO_2$) in aqueous-media, Journal of the American Chemical Society, 103, 2203-2206, 10.1021/ja00399a012, 1981.

Kerbrat, M., Huthwelker, T., Bartels-Rausch, T., Gggeler, H. W., and Ammann, M.: Co-adsorption of acetic acid and nitrous acid on ice, Physical Chemistry Chemical Physics, 12, 7194-7202, 10.1039/b924782c, 2010a.

Kerbrat, M., Huthwelker, T., Gggeler, H. W., and Ammann, M.: Interaction of nitrous acid with polycrystalline ice: Adsorption on the surface and diffusion into the bulk, Journal of Physical Chemistry C, 114, 2208-2219, 10.1021/jp909535c, 2010b.

Kim, S., Huey, L. G., Stickel, R. E., Tanner, D. J., Crawford, J. H., Olson, J. R., Chen, G., Brune, W. H., Ren, X., Lesher, R., Wooldridge, P. J., Bertram, T. H., Perring, A., Cohen, R. C., Lefer, B. L., Shetter, R. E., Avery, M., Diskin, G., and Sokolik, I.: Measurement of HO_2NO_2 in the free troposphere during the intercontinental chemical transport experiment - North America 2004, Journal of Geophysical Research-Atmospheres, 112, 10.1029/2006JD007676, 2007.

Kleffmann, J., Heland, J., Kurtenbach, R., Lorzer, J., and Wiesen, P.: A new instrument (LOPAP) for the detection of nitrous acid (HONO), Environmental Science and Pollution Research, 48-54, 2002.

Knight, G., Ravishankara, A. R., and Burkholder, J. B.: UV absorption cross sections of HO_2NO_2 between 343 and 273 K, Physical Chemistry Chemical Physics, 4, 1432-1437, 10.1039/b108904h, 2002.

Krepelova, A., Newberg, J. T., Huthwelker, T., Bluhm, H., and Ammann, M.: The nature of nitrate at the ice surface studied by XPS and NEXAFS, Physical Chemistry Chemical Physics, 12, 8870-8880, 10.1039/c0cp00359j, 2010.

Lammel, G., Perner, D., and Warneck, P.: Decomposition of pernitric acid in aqueous-solution, Journal of Physical Chemistry, 94, 6141-6144, 10.1021/j100378a091, 1990.

Lelieveld, J., and Crutzen, P. J.: The role of clouds in tropospheric photochemistry, Journal of Atmospheric Chemistry, 12, 229-267, 10.1007/BF00048075, 1991.

Li, Z. J., Friedl, R. R., Moore, S. B., and Sander, S. P.: Interaction of peroxynitric acid with solid H_2O ice, Journal of Geophysical Research-Atmospheres, 101, 6795-6802, 10.1029/96JD00065, 1996.

Liss, P. S., and Slater, P. G.: Flux of gases across air-sea interface, Nature, 247, 181-184, 10.1038/247181a0, 1974.

Longfellow, C. A., Imamura, T., Ravishankara, A. R., and Hanson, D. R.: HONO solubility and heterogeneous reactivity on sulfuric acid surfaces, Journal of Physical Chemistry A, 102, 3323-3332, 10.1021/jp9807120, 1998.

Marsh, A. R. W., and McElroy, W. J.: The dissociation-constant and Henry law constant of HCl in aqueous-solution, Atmospheric Environment, 19, 1075-1080, 10.1016/0004-6981(85)90192-1, 1985.

McNeill, V. F., Loerting, T., Geiger, F. M., Trout, B. L., and Molina, M. J.: Hydrogen chloride-induced surface disordering on ice, Proceedings of the National Academy of Sciences of the United States of America, 103, 9422-9427, 10.1073/pnas.0-603494103, 2006.

McNeill, V. F., Geiger, F. M., Loerting, T., Trout, B. L., Molina, L. T., and Molina, M. J.: Interaction of hydrogen chloride with ice surfaces: The effects of grain size, surface roughness, and surface disorder, Journal of Physical Chemistry A, 111, 6274-6284, 10.1021/jp068914g, 2007.

Niki, H., Maker, P. D., Savage, C. M., and Breitenbach, L. P.: Fourier-transform IR spectroscopic observation of pernitric acid formed via $HOO + NO_2 -> HOONO_2$, Chemical Physics Letters, 45, 564-566, 10.1016/0009-2614(79)85027-7, 1977.

Peybernes, N., Marchand, C., Le Calve, S., and Mirabel, P.: Adsorption studies of acetone and 2,3-butanedione on ice surfaces between 193 and 223 K, Physical Chemistry Chemical Physics, 6, 1277-1284, 10.1039/b315064j, 2004.

Picaud, S., Hoang, P. N. M., Peybernes, N., Le Calve, S., and Mirabel, P.: Adsorption of acetic acid on ice: Experiments and molecular dynamics simulations, Journal of Chemical Physics, 122, 194707, 10.1063/1.1888368, 2005.

Popp, P. J., Gao, R. S., Marcy, T. P., Fahey, D. W., Hudson, P. K., Thompson, T. L., Karcher, B., Ridley, B. A., Weinheimer, A. J., Knapp, D. J., Montzka, D. D., Baumgardner, D., Garrett, T. J., Weinstock, E. M., Smith, J. B., Sayres, D. S., Pittman, J. V., Dhaniyala, S., Bui, T. P., and Mahoney, M. J.: Nitric acid uptake on subtropical cirrus cloud particles, Journal of Geophysical Research-Atmospheres, 109, 10.1029/2003JD004255, 2004.

Possanzini, M., Dipalo, V., and Liberti, A.: Annular denuder method for determination of H_2O_2 in the ambient atmosphere, Science of the Total Environment, 77, 203-214, 10.1016/0048-9697(88)90056-3, 1988.

Pouvesle, N., Kippenberger, M., Schuster, G., and Crowley, J. N.: The interaction of H_2O_2 with ice surfaces between 203 and 233 K, Physical Chemistry Chemical Physics, 12, 15544-15550, 10.1039/c0cp01656j, 2010.

Regimbal, J. M., and Mozurkewich, M.: Peroxynitric acid decay mechanisms and kinetics at low pH, Journal of Physical Chemistry A, 101, 8822-8829, 10.1021/jp971908n, 1997.

Servant, J., Kouadio, G., Cros, B., and Delmas, R.: Carboxylic monoacids in the air of mayombe forest (Congo) - Role of the forest as a source or sink, Journal of Atmospheric Chemistry, 12, 367-380, 10.1007/BF00114774, 1991.

Slusher, D. L., Pitteri, S. J., Haman, B. J., Tanner, D. J., and Huey, L. G.: A chemical ionization technique for measurement of pernitric acid in the upper troposphere and the polar boundary layer, Geophysical Research Letters, 28, 3875-3878, 10.1029/2001GL013443, 2001.

Slusher, D. L., Huey, L. G., Tanner, D. J., Chen, G., Davis, D. D., Buhr, M., Nowak, J. B., Eisele, F. L., Kosciuch, E., Mauldin, R. L., Lefer, B. L., Shetter, R. E., and Dibb, J. E.: Measurements of pernitric acid at the South Pole during ISCAT 2000, Geophysical Research Letters, 29, 10.1029/2002GL015703, 2002.

Slusher, D. L., Neff, W. D., Kim, S., Huey, L. G., Wang, Y., Zeng, T., Tanner, D. J., Blake, D. R., Beyersdorf, A., Lefer, B. L., Crawford, J. H., Eisele, F. L., Mauldin, R. L., Kosciuch, E., Buhr, M. P., Wallace, H. W., and Davis, D. D.: Atmospheric chemistry results from the ANTCI 2005 Antarctic plateau airborne study, Journal of Geophysical Research-Atmospheres, 115, 10.1029/2009JD012605, 2010.

Sokolov, O., and Abbatt, J. P. D.: Adsorption to ice of n-alcohols (ethanol to 1-hexanol), acetic acid, and hexanal, Journal of Physical Chemistry A, 106, 775-782, 10.1021/jp013291m, 2002.

Symington, A., Cox, R. A., and Fernandez, M. A.: Uptake of organic acids on ice surfaces: Evidence for surface modification and hydrate formation, Zeitschrift Fur Physikalische Chemie-International Journal of Research in Physical Chemistry & Chemical Physics, 224, 1219-1245, 10.1524/zpch.2010.6149, 2010.

Thibert, E., and Domin, F.: Thermodynamics and kinetics of the solid solution of HNO_3 in ice, Journal of Physical Chemistry B, 102, 4432-4439, 10.1021/jp980569a, 1998.

Ullerstam, M., Thornberry, T., and Abbatt, J. P. D.: Uptake of gas-phase nitric acid to ice at low partial pressures: evidence for unsaturated surface coverage, Faraday Discussions, 130, 211-226, 10.1039/b417418f, 2005.

Vlasenko, A., Huthwelker, T., Gaggeler, H. W., and Ammann, M.: Kinetics of the heterogeneous reaction of nitric acid with mineral dust particles: An aerosol flow-tube study, Physical Chemistry Chemical Physics, 11, 7921-7930, 10.1039/b904290n, 2009.

von Hessberg, P., Pouvesle, N., Winkler, A. K., Schuster, G., and Crowley, J. N.: Interaction of formic and acetic acid with ice surfaces between 187 and 227 K. Investigation of single species- and competitive adsorption, Physical Chemistry Chemical Physics, 10, 2345-2355, 10.1039/b800831k, 2008.

Wilhelm, E., Battino, R., and Wilcock, R. J.: Low-pressure solubility of gases in liquid water, Chemical Reviews, 77, 219-262, 10.1021/cr60306a003, 1977.

Winkler, A. K., Holmes, N. S., and Crowley, J. N.: Interaction of methanol, acetone and formaldehyde with ice surfaces between 198 and 223 K, Physical Chemistry Chemical Physics, 4, 5270-5275, 2002.

Yaws, C. L., and Yang, H.-C.: Henry's law constant for compound in water, Thermodynamic and Physical Property Data, edited by: Yaws, C. L., Gulf Publishing Company, Houston, Texas, 1992.

Chapter 4

The nature of the uptake of H_2O_2 to ice

T. Ulrich[1,2], M. Ammann[1] and T. Bartels-Rausch[1,0]

To be submitted to: Journal of Physical Chemistry A

---

[1]Paul Scherrer Institut, Laboratory of Radiochemistry and Environmental Chemistry, 5232 Villigen PSI, Switzerland

[2]Universität Bern, Department of Chemistry and Biochemistry, 3008 Bern, Switzerland

[0]Author for correspondence (Email: thorsten.bartels-rausch@psi.ch)

4.1   Abstract

Hydrogen peroxide (H$_2$O$_2$) is an important trace gas with oxidative properties in snow packs and links to the atmospheric HO$_X$ chemistry. The uptake of H$_2$O$_2$ to ice has been investigated in laboratory studies with regard to its importance in conditions relevant for the upper troposphere, disagreeing in terms of magnitude and timescale of uptake. In this study we analyzed the uptake of H$_2$O$_2$ to ice in coated wall flow tube experiments with a fluorescence detection method, which allows for a subsequent analysis of the molten ice film. We present results, where we could reproduce the higher partitioning towrds the ice. Also we were able to disentangle the surface adsorption mode from the bulk uptake in this study, while deriving partitioning from the gas phase to the bulk in good agreement with a previous study. A high affinity of H$_2$O$_2$ for the bulk ice is found. The environmental implications are discussed regarding snow packs as source and sink terms for H$_2$O$_2$.

4.2   Introduction

Trace gases are ubiquitously present in the atmosphere. In colder environmental regions these trace gases interact with snow and ice (Abbatt, 2003; Huthwelker et al., 2006). Hydrogen Peroxide (H$_2$O$_2$) is an important trace gas with impact on the oxidative capacity of the atmosphere due to its connection to the atmospheric HO$_X$ (= OH + HO$_2$) chemistry (Logan et al., 1981). In the upper troposphere partitioning of H$_2$O$_2$ to ice clouds and subsequent gravitational settling might impact the oxidative capacity (Lawrence and Crutzen, 1998). Its oxidation potential makes H$_2$O$_2$ important in the oxidation of sulfur-dioxide in rain droplets (Penkett et al., 1979) and ice (Clegg and Abbatt, 2001b) in the atmosphere.

Interactions of H$_2$O$_2$ with snow alter the gas phase concentrations of H$_2$O$_2$ above snow packs on the ground during day and night cycles (Jacobi et al., 2002; Jacobi et al., 2004). In addition the oxidation potential of H$_2$O$_2$ is of great importance within snow packs (Bartels-Rausch et al., 2013a). The presence of H$_2$O$_2$ in snow packs has a significant impact on light absorption, for example at Summit, Greenland 20 % of the light absorption of soluble species is due to H$_2$O$_2$ (Anastasio and Robles, 2007). Ice core studies have been executed to understand the H$_2$O$_2$ content of the atmosphere in the past (Sigg and Neftel, 1991; Sigg et al., 1992; McConnell et al., 1997a; McConnell et al., 1997b; McConnell et al., 1998; Hutterli et al., 2003). A rise of H$_2$O$_2$ of anthropogenic origin has been reported by Sigg et al. (1991).

Yet the transfer function of H$_2$O$_2$ from the atmosphere to the firn and to the ice and its reverse process, are still not fully understood (McConnell et al., 1998). Laboratory studies are a useful tool to understand the partitioning of H$_2$O$_2$ to ice and snow.

Several studies have been executed under controlled conditions relevant for two different environments: Ice clouds in the upper troposphere and snow packs and ice sheets on the ground. All studies showed an uptake of H_2O_2 by the ice.

Clegg and Abbatt (2001a) and Pouvesle et al. (2010) used ice coated wall flow tubes to investigate the uptake of H_2O_2 to ice. Their temperature range is relevant for the upper troposphere. The timescales of both their experiments were very short. Also the smooth ice surface in their experiments has a low ice area to gas volume ratio. The smooth surface of the ice in this setup resembles environmental conditions of ice crystals in clouds. In their studies, they reported only a surface adsorption process without an uptake to the bulk. Yet the studies of Clegg and Abbatt (2001a) and Pouvsele et al. (2010), which both focus on upper tropospheric conditions, disagree both in the magnitude of the uptake and its temperature dependence. The partitioning of H_2O_2 to ice measured by Pouvesle et al. (2010) was two orders of magnitude higher than the one of Clegg and Abbatt (2001a).

Conklin et al (1993) analyzed the uptake of H_2O_2 to ice in a packed bed flow tube of artificially frozen ice spheres. The experimental conditions chosen by Conklin et al. (1993) make their experiments more relevant for snow packs. The surface area and ice volume in these packed bed experiments are higher than those of Clegg and Abbatt (2001a) or Pouvesle et al. (2010), resembling the environmental conditions of snow packs. Conklin et al. (1993) reported the probable presence of a liquid phase at the necks of adjacent ice beads, which may significantly alter the uptake characteristics. Also they used much longer experimental time scales than their co-workers. In their study, they reported a diffusive long term uptake into the ice as well as a surface uptake process.

The observed long term uptake by Conklin et al. (1993) gives rise to the question in which reservoir is H_2O_2 transported. For this reservoir several options are possible. Conklin et al. (1993) proposed uptake into the disordered layer of ice and diffusion into the ice matrix. The acidic trace gases HCl and HNO_3 as well as the non-acidic formaldehyde have been reported to diffuse into the bulk of single crystalline ice in diffusion chamber experiments (Thibert and Domine, 1997, 1998; Barret et al., 2011). Grain boundaries in polycrystalline ice have also been proposed as a possible reservoir for trace gas species (Huthwelker et al., 2001). Also indirect evidence hints at a stronger mode of adsorption at these sites (McNeill et al., 2007a). Alteration of the molecular surface layers of the ice by surface disorder could enhance the magnitude of trace gas uptake (McNeill et al., 2006; McNeill et al., 2007a).

To elucidate the previous results reported for the uptake of H_2O_2 by ice, we used a coated wall flow tube (CWFT) technique with long residence times of the H_2O_2 in contact with the ice surface. By the use of long residence times in combination with a coated wall technique our experiments are both sensitive to partitioning to the surface and bulk uptake, while avoiding liquid reservoirs possibly being present in the packed bed experiments. In addition we were also able to analyze the molten

ice phase for peroxides, which gives conclusions about budgets and possible decomposition H_2O_2.

4.3   Methods

The uptake experiments on ice were executed in an ice coated flow tube (CWFT) and detected by a fluorometric method (Lazrus et al., 1985) with a commercial H_2O_2 analyzer (AL2021). H_2O_2 was dosed from the gas phase to the ice surface while its gas phase concentration was measured after the CWFT. In additional experiments the molten ice phase was analyzed for its H_2O_2 content.

4.3.1   Coated wall flow tube

The experiments were executed in an 80 cm long quartz glass tube with an inner diameter of 8 mm. The inner surface with an area of 150 cm^2 of the quartz tube was coated with ice. Additional experiments were executed in a 45 cm long quartz glass tube of the same diameter. The temperature inside the coated wall flow tube was measured at experimental conditions with a type K thermocouple.

The flow through the CWFT was controlled by the H_2O_2 analyzer and set to either 2000 ml/min STP (standard temperature and pressure: 273.15 K and 1 bar) or 500 ml/min STP, respectively. Reynolds numbers were calculated for both flow regimes and resulted in 440 for 2000 ml/min STP and 110 for 500 ml/min STP. This indicates laminar flow throughout all experiments.

The gas flow was humidified to equilibrium conditions over the ice surface. The dew point of the gas flow was compared to the dew point of the ice with a commercial dew point sensor (EdgeTech Dewmaster) before each experiment. For this the dew point of the gas flow was measured, subsequently the dew point after the CWFT was measured and compared to the temperature inside the CWFT and the dew point of the gas flow. If necessary the temperature of the CWFT was adjusted to the dew point of the water vapor in the gas flow.

4.3.2   Preparation of ice films

The ice film was prepared following a procedure described before (Ulrich et al., 2012). First, the quartz tube was etched inside with a solution of 5 % HF in water. The tube was then rinsed several times with purified water (Millipore MilliQ, 0.05 μS). Subsequently 8 ml – 10 ml of ultra pure water (HPLC grade, Fluka 14263) were pipetted into the quartz tube. Some experiments were executed with ice produced from purified water produced in our laboratory (Millipore MilliQ, 0.05 μS). The data derived from both types of ice were in excellent agreement. Excess water was

removed subsequently by holding the quartz tube in a vertical position for exactly 60 s. The water was then frozen to an ice film at 258 K while slowly rotating the flow tube. The freezing of the ice film and the experiments were executed in a snuggly fitting double mantled cooling jacket. This procedure resulted in polycrystalline ice films with a thickness of 10 μm as determined by weighing.

4.3.3 Production of gas phase H_2O_2

Gas phase H_2O_2 was dosed from a custom built permeation tube. For this a liquid solution of 30 % H_2O_2 (Perhydrol p.a., 7209 Merck) was filled in a 17.4 cm long, thin walled fluorinated ethylene propylene (FEP) tube. The tube was sealed with a hot air gun. The permeation tube was then placed in a commercial permeation oven (VICI Dynacalibrator), which was held constantly at 323 K. A flow of pure nitrogen (Carbagas 99.9995 % purity) through the permeation oven was established to transport the gas phase H_2O_2 into the experimental setup.

4.3.4 Detection

H_2O_2 was measured in the gas phase by a commercial H_2O_2 analyzer (AL2021). The instrument relies on a fluorometric method, by which H_2O_2 is stripped from the gas phase in a glass coil and then reacts with p-hydroxyphenylacetic acid and peroxidase to a fluorescence dimmer. This method detects all peroxides in the solution. The reagents used for the analyzer were: Potassium phthalate (monobasic, 96148 Fluka), EDTA (Titriplex III p.a., 1.08418 Merck), NaOH (1N, 71463 Fluka), formaldehyde (37 wt. % in water, 252549 Sigma-Aldrich), p-hydroxyphenylacetic acid (98 %, H5,000-4 Sigma-Aldrich) and peroxidase (from horseradish, P8250 Sigma-Aldrich). The reagents were dissolved in double distilled water (3478.2 Roth). The instrument was calibrated with diluted liquid solutions of H_2O_2 (Perhydrol 30 % p.a., 7209 Merck), which were titrated against a permanganate solution (Permanganate 1/500 mol 38136 Fixanal) of known concentration. It is notable that the liquid detection method of the analyzer leads to a smearing of the signal at short timescale events. Since H_2O_2 is dissolved in the solution containing the reagents, it diffuses in the liquid during its residence time (7 min) before detection in the analyzer. Our experiments were executed in time scales of hours, so the smearing effect can be neglected.

To analyze the ice phase in the CWFT, the ice was molten and eluted with 50 ml of purified water (Millipore MilliQ, 0.05 μS) while rotating the quartz tube. The sample was then connected to the liquid inlet of the H_2O_2 analyzer and measured. The background of the purified water was subtracted during data analysis.
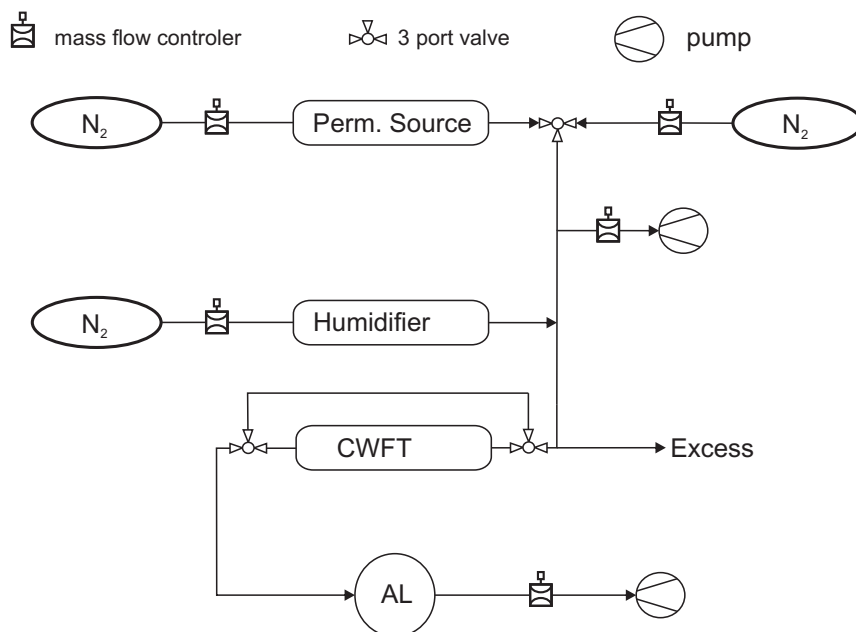
Figure 4.1: Set up of the experiments. H_2O_2 is brought into the gas flow system by introducing N_2 into a heated permeation oven. The concentration of H_2O_2 is adjusted by a pump and dilution step. The equilibrium humidity for the CWFT experiments is adjusted by the humidifier. The pump after the analyzer AL establishes a stable flow through the CWFT and the analyzer.

4.3.5   Flow system

Figure 4.1 shows the setup of the experiments. All tubing consisted of FEP and all gas flows were regulated by mass flow controllers (Brooks MFC or Kobold). Nitrogen (Carbagas 99.9995 % purity) was used as carrier gas. The flow through the permeation source was held constant at 1500 ml/min STP. A pumping and dilution step was used to adjust the concentration of H_2O_2 in the gas flow, the volumetric flow velocity after the production step was kept at 1500 ml/min STP. A flow of 500 ml/min STP of nitrogen was passed over an ice surface at a controlled temperature to humidify the gas flow to equilibrium conditions.

4.4 Results and discussion

To investigate the interaction of trace gas species with surfaces, coated wall flow tube (CWFT) experiments have proven to be a reliable instrument for the analysis of uptake of these species on a surface (e.g. Abbatt, 2003; Huthwelker et al., 2006 for ice CWFT). The uptake is thereby measured by leading a gas flow containing a known concentration of the trace gas species, here H_2O_2, through a tube coated with the medium, here ice. During the experiment the gas phase concentration of the trace gas species is monitored after the CWFT, resulting in so called breakthrough curves. The number of molecules lost from the gas phase can thereby be calculated by integration of the area of the breakthrough curve and the by-pass signal with the gas flow velocity and the gas phase concentration.

4.4.1 General discussion of the experiments

The majority of the experiments were performed with the 80 cm long quartz tubes as support for the ice film and at a volumetric flow velocity of of the carrier gas of 2000 ml/min STP.

Figure 4.2A shows the gas phase concentration of H_2O_2 versus time as measured after the CWFT at a temperature of 245 K. The blue line is a mean of six individual experiments. The concentrations were normalized to the concentration of H_2O_2 in the by-pass and ranged from 4.4×10^{10} molecules / cm^3 to 9.8×10^{10} molecules/cm^3. The grey shaded area gives the uncertainties at the $2 \times \sigma$ level. A loss from the gas phase is visible, which corresponds to the uptake of H_2O_2 by the ice. In the following we will discuss the appearance of the breakthrough curves and the implications for data evaluation.

For each experimental run, the concentration of H_2O_2 is first measured without contact to the ice sample (here-after referred to as by-pass mode). Trends in this signal, which occurred in some experiments due to interaction of H_2O_2 with the non-passivated tubing material, were fitted and corrected by a linear relationship. At time t = 0 s the by-pass is switched off and the gas-flow is led through the CWFT. Now the H_2O_2 molecules in the gas phase start to interact with the ice, which is visible by the drop in gas-phase concentration measured after the CWFT. The concentration starts to recover after the initial drop as the ice surface equilibrates with H_2O_2 with time. After t $\approx$ 2500 s, the initial fast part of recovery is completed. The data of Pouvesle et al. (2010) would suggest a recovery within around 1100 s. The initial dip in concentration indicates the gas phase molecules are lost to the ice in a fast process. After 2500 s the signal shows a long-lasting trend. At t = 5000 s the experiment was switched to by-pass mode again.

The general behavior with temperature can be seen, if we compare the concentration versus time signal at 258 K (Figure 4.2B, blue line) and 245 K (Figure 4.2A,
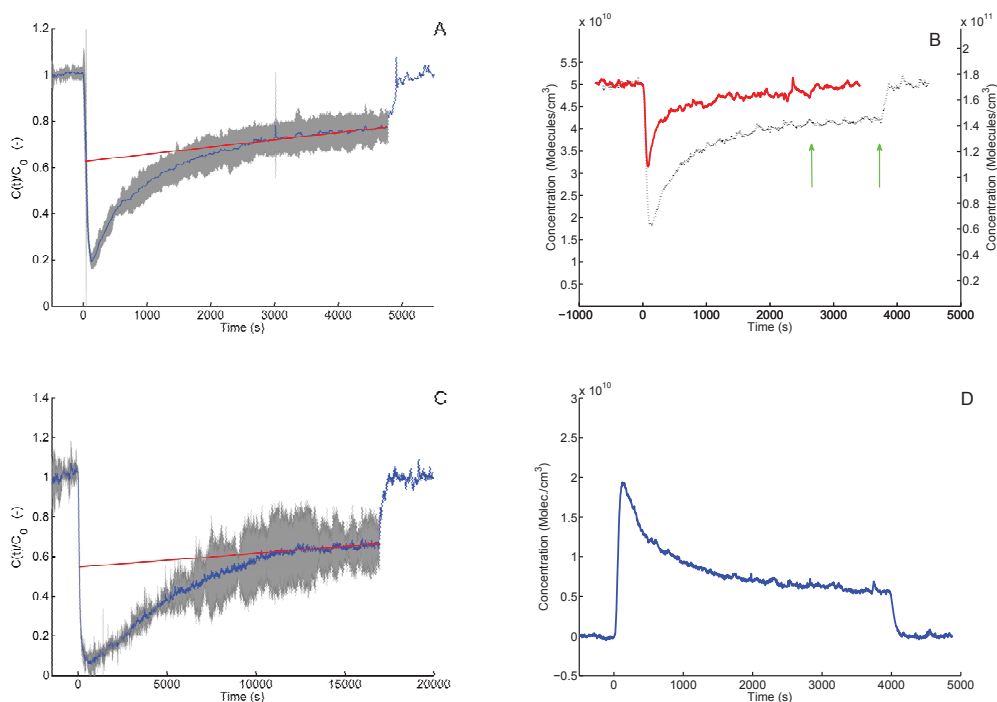
Figure 4.2: Examples for typical breakthrough curves collected in our experiments. 2A: Relative gas phase concentration of H_2O_2 is plotted versus the experimental time at a volumetric gas flow of 2000 ml/min STP and a temperature of 245 K. The blue line is the mean of six individual experiments. The grey shaded area gives the uncertainty at the $2\times\sigma$ level. The gas phase concentrations ranged from 4.4×10^{10} molecules / cm^3 to 9.8×10^{10} molecules/cm^3. A linear fit (red) is included in the plot. 2B: Absolute gas phase concentration of H_2O_2 versus time is shown at 2000 ml/min STP and a temperature of 258 K for an ice experiment (blue line, left axis). Compared to a quartz experiment at 2000 ml/min STP and 243 K (red line, right axis). The green arrows indicate when the experiments were switched to by-pass mode again (left arrow: quartz, right arrow: ice). 2C: Relative gas phase concentration of H_2O_2 versus time at a volumetric gas flow of 500 ml/min STP and a temperature of 235 K for two individual experiments. The grey shaded area gives the uncertainty at the $2\times\sigma$ level. Red line: Linear fit through the later part of the breakthrough curve. 2D: Absolute concentration versus time of a desorption experiment at 258 K and 2000 ml/min STP.

blue line). Note that the experiments at 235 K in Figure 4.2C were carried out at another flow rate and thus are not directly comparable. The initial uptake of

molecules from the gas phase is smaller at higher temperatures (1.7×10^{12} molecules / cm^2) and larger at lower temperatures (5.2×10^{12} molecules / cm^2). How the surface concentrations were derived is defined in the next section.

The slow long term trend over such timescales is somewhat unusual for CWFT experiments for non-acidic trace gas species. As the surface concentration of H_2O_2 on the ice comes into equilibrium with the gas phase concentration with no other process present, the signal in the analyzer should have returned to the stable level of the by-pass mode. Such behavior of complete recovery has been reported for many other species such as HNO_4 (Ulrich et al., 2012) or acetic acid (Kerbrat et al., 2010a) for example. A complete recovery has also been reported for H_2O_2 in fast flow experiments (Clegg and Abbatt, 2001; Pouvesle et al., 2010). Very acidic species like HNO_3 (Ullerstam et al., 2005) or HCl (McNeill et al., 2006) can instead show a long term uptake under certain experimental conditions. The long term uptake with incomplete recovery during our experimental timescale of 4 h is an interesting feature for H_2O_2.

The difference in the extend of recovery to the data by Pouvesle (2010) is explained by the different residence time in the flow tube. Since there seem to be unresolved issues with the data of Clegg and Abbatt (2001a), we focused only on the study by Pouvelse at al. (2010). The authors investigated the uptake of H_2O_2 to ice surfaces in a fast flow reactor with chemical ionization mass spectrometry (CIMS) and electron impact mass spectrometry (EIMS). They reported a recovery to 100 % of the initial concentration with their experimental uncertainties. In contrast to our experiments the authors executed their experiments at much lower pressure and higher flow, namely at 1.33 mbar and a linear velocity of 774 cm/s, whereas we worked at around 980 mbar and 64 cm/s to 15 cm/s. This results in an up to 450 times higher residence time in the CWFT during our experiments compared to Pouvesle et al. (2010). Consequently the time scale of the experiments of Pouvesle et al. (2010) was much shorter; their experiments reached a stable plateau in concentration after 50 s at 233 K. To reach a stable level our experiments took more than 12000 s at 234 K, resulting in a much longer time for the molecules to interact with the bulk. 50 s may be too short to identify a long term uptake, since for example with the maximal diffusivity we achieved in a later section the characteristic time of diffusion, which gives the time when the respective reservoir is saturated, would be more than 5 hours. Hence the molecules do not have enough time to significantly diffuse into the bulk of the ice.

Interpretation of the two modes of uptake

As mentioned above we distinguished between an initial fast uptake mode and a slower long term uptake mode. We attribute the fast initial uptake to a surface adsorption process and the slow long term trend to a bulk uptake process. Both

processes are distinguished graphically in Figure 4.2A and 4.2C by the red line, which represents a linear fit through the slow long term signal of the experiment. It has to be mentioned that this fit does not have a physical basis. Therefore it can only be used to roughly divide both processes. The area between the breakthrough curve and the red line in the beginning gives the number of molecules adsorbed on the surface. The area between the by-pass signal and the breakthrough curve gives the number of molecules taken up by the ice in total. Bulk-uptake was defined as the difference of total and surface uptake. The term bulk is there after used for the volume of polycrystalline ice, including grain boundaries and possible molecular disordered regions.

It has to be noted that the method applied here some what underestimates the adsorption part. Other methods use the whole integral to the time when two thirds of the recovery are reached (e.g. Ullerstam et al., 2005). Those methods overestimate the adsroption part.

The integration of the normalized breakthrough curves (either normalized to the by-pass signal or the linear fit) yields a term Int_Area in units of seconds. The number of molecules n taken up with each mode is given by E(4.1):

$$n = F(T) \times Int\_Area \times \frac{p_{H2O2} \times N_a}{R \times T} \tag{4.1}$$

Where $F(T)$ is the volumetric gas flow at the experimental temperature, p_{H2O2} is the partial vapor pressure of H_2O_2, N_a the Avogadro constant (molecules/mol), R the universal gas constant (J/(mol $\times$ K)) and T the experimental temperature.

We interpret the long term uptake as a diffusion process as detailed in a later section. Apart from diffsuion into the ice other reasons might induce a long term uptake signal. In the following we present data to check for different explanations for the observed long term uptake other than bulk uptake and discard these explanations.

Due to the long flow tube geometry and the high flows a temperature gradient along the first 20 cm of the flow tube existed in some experiments. This may result in cold quartz surfaces in those experiments, when the ice has sublimated over the initial 20 cm of the flow tube. Additional experiments were executed with shorter flow tubes of 45 cm and a lower flow of 500 ml/min STP. At these conditions no temperature gradient was present (see Figure 4.3). The results are presented in Figure 4.2C. The mean of two experiments at 235 K are shown, the grey shaded areas give the error at the $2\times\sigma$ level. The general appearance of the breakthrough curves is in good agreement with the experiments where the temperature gradient was present. The feature of a long term uptake was persistent. Results in terms of partitioning to the ice surface and surface coverage as well as total uptake were the same as in the experiments at higher flows and longer flow tubes.

Blank experiments on the quartz flow tube without ice film have been executed (Figure 4.2B). We carried out experiments on the quartz surface of the flow tube
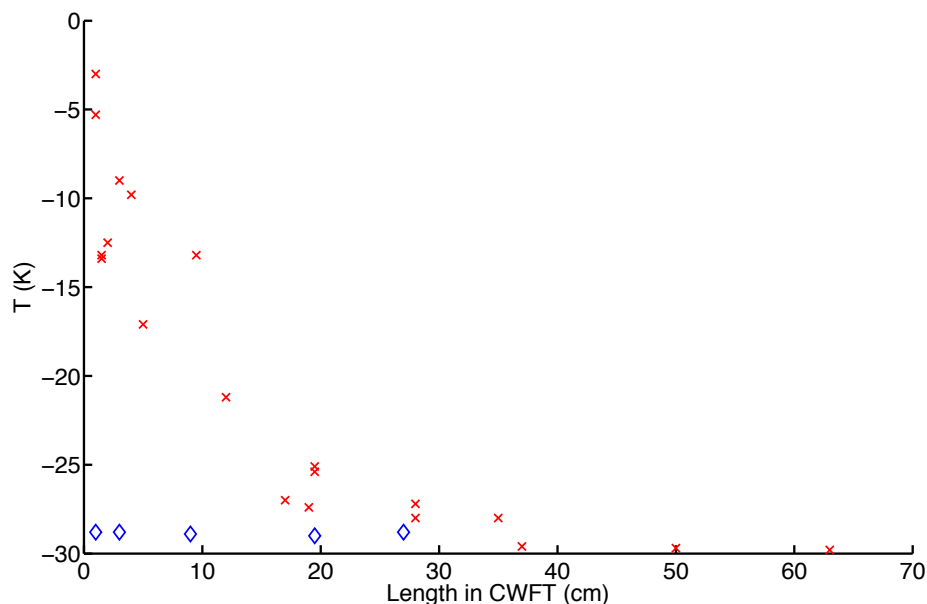
Figure 4.3: Temperature profile over the length of the CWFT. The experiments were both executed at 245 K. Red crosses: 2000 ml/min and 80 cm long flow tube. Blue diamonds: 500 ml/min and 45 cm long flow tube.

with the long flow tube geometry at a gas flow of 2000 ml/min STP. Figure 4.2B compares the resulting breakthrough curves for ice and for quartz. The temperature and H_2O_2 gas-phase concentration of the uptake experiments to the quartz tube were chosen so that the surface concentrations on quartz were similar to those on the ice surface (9.2×10^{12} molecules /cm^2 on quartz and 9.9×10^{12} molecules/cm^2 on ice). The results show that it is possible to measure a complete recovery to initial concentrations with our experimental setup, as shown by the quartz breakthrough curve giving strong indications that the observations are real and not an artifact.

In summary, the uptake of H_2O_2 to the quartz surfaces possibly present in some experiments with the long geometry can be neglected; the partitioning to quartz in the initial 20 cm is maximally only a sixth of the partitioning to the ice surface. This is well within our errors in K_{LinC}.

Molecule budgets of the adsorption experiments

We checked the molecule budgets of the molecules lost from the gas phase in total and the molecules found in the ice phase after the experiments. For this H_2O_2 was dosed to the ice surface as in the experiments shown in Figure 4.2. The total loss
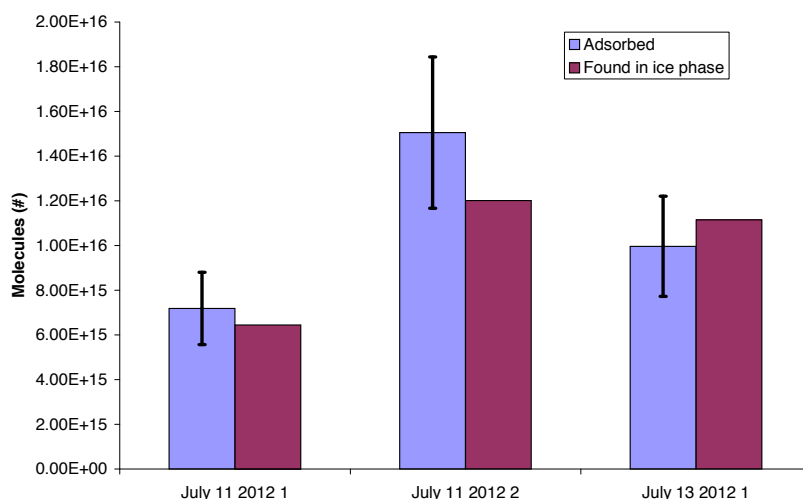
Figure 4.4: Number of molecules lost to the ice in total in comparison to number of molecules found in the molten ice phase. Errors are given on 1 ×sigma derived from K_{LinC}.

of molecules to the ice was determined by the area between the full breakthrough curve and the by-pass signal by (4.1). The CWFT was then removed from the cooling jacket and the ice was molten. The subsequent analysis of the molecule budget in the ice phase is shown in Figure 4.4. As shown, all molecules lost from the gas phase were found in the ice within error ($1 \times \sigma$ level). No H_2O_2 was lost due to the experimental set up at our experimental time scales, hinting that no decomposition of H_2O_2 takes place. It has to be noted, that the H_2O_2 analyzer does not distinguish between H_2O_2 and organic peroxides in the mode used Therefore the possibility remains that H_2O_2 forms organic peroxides with contaminants in the lab air or in the ice.

Desorption experiments

Desorption experiments were executed after some exposure experiments. The results are shown in Figure 4.2D at 258 K. The experiments were performed analogous to the uptake experiments. The timescale of the experiment is roughly the same as for the uptake experiment at 258 K. The appearance of the desorption curve is similar to that of the breakthrough curve of the adsorption with a fast initial desorption

Table 4.1: Molecules lost from the gas phase compared to molecules desorbed from the ice after equivalent times.

T(K)	molecules lost from the gas phase	molecules desorbed from the ice
245	8.0×10^{14}	2.5×10^{14}
245	2.3×10^{15}	8.6×10^{14}
245	4.2×10^{15}	1.6×10^{15}
245	9.6×10^{14}	3.8×10^{14}
245	3.7×10^{15}	1.5×10^{15}
245	1.3×10^{16}	7.5×10^{15}
258	1.5×10^{15}	9.4×10^{14}
258	1.5×10^{15}	1.3×10^{15}
258	1.5×10^{15}	7.2×10^{14}

peak and a slower long term desorption signal. Even at longer experimental times the signal does not reach the background level, hinting that the long term process is also relevant for desorption. The number of molecules desorbed from the ice surface in total was much lower than the total amount lost from the gas phase, as visible in Table 4.1. The times over which the integration was performed were chosen so, that they were equal for both the adsorption and desorption parts. The results are explained by a persisting bulk uptake. While the molecules near the surface can reenter the gas phase and create the desorption signal, a significant part of the molecules lost to the ice stays in the bulk at our experimental timescales.

4.4.2 Quantification of the surface adsorption

In the following we will focus only on the fast initial adsorption part, which we interpret as a surface adsorption process. The number of molecules adsorbed to the ice surface in the initial fast process was calculated for all experiments. We compared our results to the data of Clegg and Abbatt (2001a) and Pouvesle et al. (2010).

We were working at gas phase concentrations ranging from 8×10^9 molecules/cm^3 to 4×10^{11} molecules / cm^3. For comparison Pouvesle et al. (2010) worked in the range of 6×10^9 molecules / cm^3 to 1×10^{12} molecules / cm^3; mostly in a lower temperature range compared to our experiments. However our lowest temperature agrees with their highest temperature, namely 233 K. This lets us compare our results with their work. Pouvesle et al. (2010) observed a saturation effect on the partitioning towards the surface at around 2×10^{11} molecules/cm^3 at 233 K. In Figure 4.6 (crosses) we present the concentration dependencies for the partitioning of H_2O_2 to the ice surface for 245 K and 239 K, respectively. As shown both concentration

dependencies are well within the linear range. This is in agreement with the results of Pouvesle et al. (2010), which were also in the linear range at our gas phase concentrations.

The Langmuir model would suggest a saturation of the surface concentrations near the monolayer capacity, which is estimated to be around 2.5×10^{14} molecules/cm^2 (Pouvesle et al., 2010). With this, our surface coverage, based on the initial uptake, ranged from 0.5 % to 9 % at 245.15 K and 2 % to 20 % at 239.15 K, respectively. The surface concentrations are in the linear regime (Figure 4.6), with this E(4.2) is appropriate for our experimental conditions:

$$K_{\text{LinC}} = \frac{C_{\text{surf}}}{C_{\text{gas}}} \tag{4.2}$$

where K_{LinC} is the linear partition coefficient [cm], C_{surf} the surface concentration [molecules/cm^2] and C_{gas} the gas phase concentration [molecules/cm^3]. Figure 4.5A shows the temperature dependence for those derived values of K_{LinC}. The relationship is given as a Van't Hoff plot where the natural logarithm of K_{LinC} is plotted versus the temperature as derived from:

$$K^0 = \exp(\frac{\Delta G^0_{\text{ads}}}{R \times T}) \tag{4.3}$$

and

$$K_{\text{LinC}} = K^0 \times V^0/A^0 \tag{4.4}$$

where K^0 is the dimensionless partition coefficient at standard conditions (-), ΔG^0_{ads} (J/mol) is the standard free energy of adsorption (-), R is the universal gas constant (J/(mol × K)), T the temperature (K) and V^0/A^0 (m) is the volume to area ratio of an ideal gas at standard conditions ($\tilde{1}.7\times10^7$ cm (Kemball et al., 1948)).

The relationship is linear, with a higher partitioning towards the ice surface at lower temperatures. The temperature dependence proposed by Pouvesle et al. (2010), extrapolated to our temperatures is given by the red line. The partitioning between the surface concentration on the ice and the gas phase concentration is in very good agreement with their data and supports the data of Pouvesle et al. (2010) as opposed to the data by Clegg and Abbatt (2001a). The higher error of the Pouvesle et al. (2010) data is due to their parameter variation while our error is based on the $2\times\sigma$ level of experimental scatter at each temperature.

To estimate the thermodynamic properties of the surface adsorbed H_2O_2 we used E(4.3). We found a standard enthalpy of adsorption of -29 ± 7 kJ/mol. This is very close to the value of -32 kJ/mol reported by Pouvesle et al. (2010). The authors of that study proposed hydrogen bonding as a surface adsorption mode. This is supported by theoretical work, which proposed a standard enthalpy of adsorption
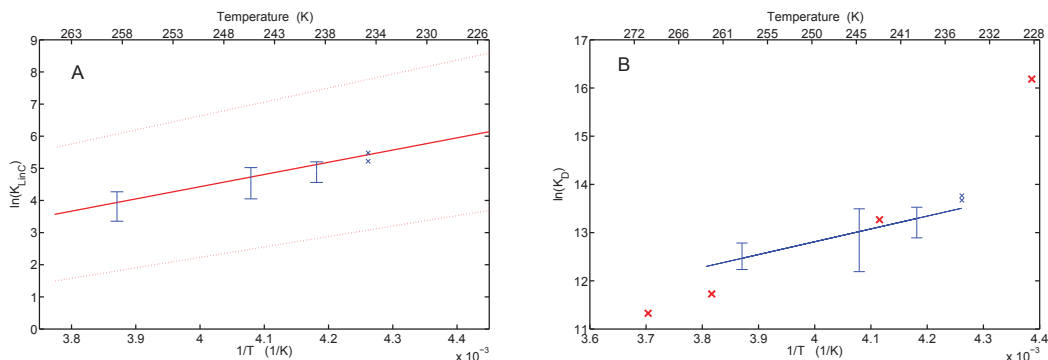
Figure 4.5: Temperature dependence of partitioning towards the ice as Van't Hoff relationship. Left side: K_{LinC} versus temperature. Red lines: Data from Pouvesle et al. (2010). Dotted lines give the errors. Blue: this study, error on $2 \times \sigma$ level. Right side: K_{D} versus temperature. Red crosses: Data from Conklin et al. (1993). Blue: This study, errors at $2 \times \sigma$ level. Solid line gives a linear fit through our data.

between 22 – 32 kJ/mol by DFT calculations, considering hydrogen bonding to the surface (Ignatov et al., 2009).

4.4.3 Quantification of the bulk uptake

In this section we will focus on the long term part of the uptake of H_2O_2 to ice. The total amount of molecules lost to the ice during our experiments was calculated from the area between the breakthrough curve and the by-pass concentrations. At the time we switched on the by-pass again, the monolayer coverage was not reached in any experiment, but in some experiments at lower temperatures surface concentrations reached 2.0×10^{14} molecules/cm^2, which is close to monolayer coverage. A monolayer coverage of 2.5×10^{14} molecules/cm^2 was predicted by Pouvesle et al. (2010) as mentioned; also values ranging from 2×10^{14} molecules/cm^2 to 3×10^{14} molecules/cm^2 were predicted for many other trace gases (Crowley et al., 2010). If we suppose that the entire loss of H_2O_2 from the gas phase is accommodated on the ice surface (i.e. there is no bulk uptake) a deviation from the linear concentration dependency would be expected. As shown in Figure 4.6 (circles) the relationship is linear even with the total uptakes. It is improbable that that many molecules can be accommodated on the surface without a saturation effect. Hence an uptake to the bulk can be expected.

If we compare the general appearance of our breakthrough curves to those of Conklin et al. (1993) it becomes obvious, that they observed a complete recovery to initial concentrations after 2 h to 11 h at 270 K and 243 K respectively. Conklin
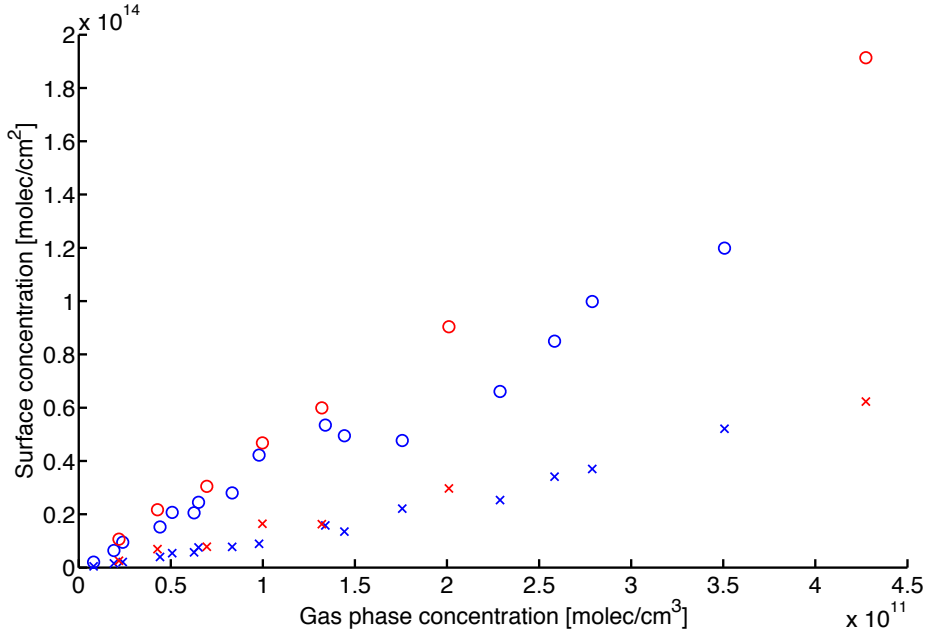
Figure 4.6: Gas phase versus surface concentration dependency. Blue markers: 245 K, red markers 239 K. Crosses: Adsorption part, Circles: Total uptake.

et al. (1993) executed their experiments in packed bed flow tube experiments with flow velocities through their flow tubes of 198 cm/s to 260 cm/s and a tube length of 2.5 cm to 5 cm. Our total ice surface was higher than theirs but in the same magnitude (80 cm^2 at the experiments of Pouvelse et al. (2010) and 151 cm^2 at our experiments). Hence, due to their much longer experimental times, they reached equilibrium conditions.

To estimate how many molecules can be taken up by our ice at equilibrium conditions, we extrapolated the fit through the long term uptake (red line, Figure 4.2A) to the by-pass concentration and used this to calculate the number of molecules at equilibrium. From this we calculated K_D values which give the partitioning of H_2O_2 from the gas phase to the ice in total. K_D is thereby defined as:

$$K_D = \frac{C_{ice}}{C_{gas}} \tag{4.5}$$

Where K_D is the partition constant (-) and C_{ice} is the concentration in the ice (molecules/cm^3). We compared our derived K_D values with the ones reported by Conklin et al. (1993) in Figure 4.5B. As shown our data is in good agreement with their results.

4.4.4 Diffusion into the bulk

We assume diffusion of H_2O_2 into the bulk of the ice as the most probable explanation for the long term uptake. Other explanations will be discussed in a later section. Abbatt (1997) suggested, that if diffusion into the bulk takes place, the later part of the breakthrough curve should be fittable to an $H \times D^{1/2}$ relationship detailed in E(4.6) as adapted from Kerbrat et al. (2010b):

$$C_{\text{gas}}(t) = C_0 \times \exp(-\frac{l_{\text{ice}}}{u_{\text{gas}}} \times \frac{a_{\text{ice}}}{c_{\text{CWFT}}} \times H \times \sqrt{\frac{D}{\pi \times t}}) \qquad (4.6)$$

where C_{gas} is the gas phase concentration [molecules/cm^3] at the time t [s], C_0 is the initial gas phase concentration, before the by-pass is deactivated, l_{ice} is the length of the flow tube [cm], u_{gas} is the linear gas flow [cm/s], a_{ice} is the ice surface [cm^2], v_{CWFT} is the volume of the flow tube [cm^3], H is the dimensionless Henry constant [-] and D is the diffusivity [cm^2/s].

We applied such fits to our data as shown in Figure 4.7. As shown, some fits match the experimental data well over the whole time scale while others only match the long term part. The fit is quite robust; if the fitted data range is doubled resulting $H \times D^{1/2}$ vary by less than 2 %. From the general look of the fits, we conclude that the entire uptake can not be explained by diffusion into the bulk. Especially the initial fast response of the signal, where a lot of molecules are lost from the gas phase over a short time scale, might be better explained by a surface adsorption process. The long term behavior however could be fitted for all experiments. The obtained $H \times D^{1/2}$ values were checked for their physical sensibility. The Henry constant and the diffusivity can not be separated by this fitting method. To derive values for the Henry constant and the diffusivity we used literature values of either constant to disentangle them.

Uptake into the ice

We used published data on the diffusivity of H_2O_2 in polycrystalline ice by Conklin et al. (1993) to derive the solubility of H_2O_2 in ice. The grain boundary content in polycrystalline ice might enhance total diffusivity significantly. Lu et al. (2009) derived higher diffusivities of water in grain boundaries of ice compared to bulk ice by three orders of magnitude. Conklin et al. (1993) reported their values clearly for polycrystalline ice in the temperature range of 270 K -228 K, but did not characterize the grain boundary content in their ice. Since the temperature dependency of diffusivities follows an Arrhenius relationship (e.g. Thibert and Domine, 1998), we extrapolated the diffusivities by Conklin et al. (1993) to our experimental temperatures. At 258 K the diffusivity given by Conklin et al. (1993) was 1.7×10^{-10} cm^2/s.
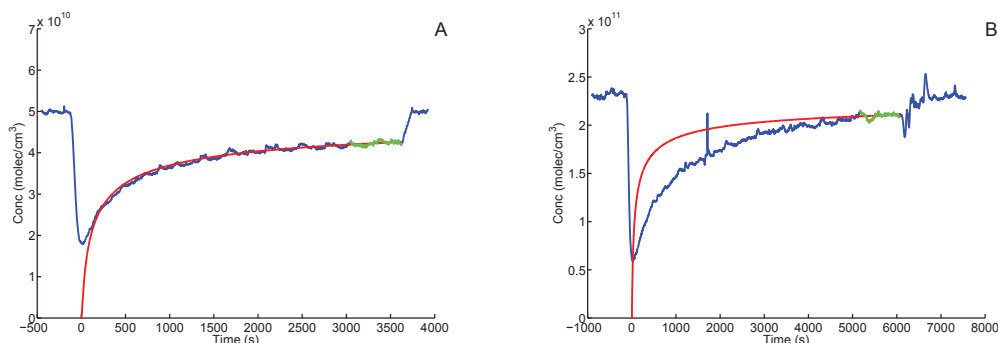
Figure 4.7: Fit according to E(4.6). The blue line gives the gas phase concentration in the experiment, the red line is the fit and the green line the range for the fit. Left side: 258 K and 2000 ml/min STP. Right side: 245 K and 2000 ml/min STP.

In comparison to the diffusivity of 1.7×10^{-10} cm^2/s at 258 K, the better defined diffusivities at the same temperature in single crystalline ice are around 1×10^{-12} cm^2/s for HCl and HCHO (Thibert and Domine, 1997; Barret et al., 2011) and 1×10^{-10} cm^2/s for HNO$_3$ (Thibert and Domine, 1998). Our extrapolated diffusivity for polycrystalline ice is within this range, but at the higher end.

Applied to our experimental time scales and temperatures the characteristic diffusion length ($= (D \times t)^{0.5}$) is around 3 μm to 7 μm, compared to our ice film thickness of 10 μm. The diffusion front does not reach the quartz-ice interface during the experimental time scales. This results in a persisting concentration gradient, driving the diffusion throughout our experimental time scales.

We used the diffusivities from Conklin et al. (1993) to derive the solubility in the ice with E(4.6). The errors for the solubilities resulting from the fit were quite high, up to 80 % of the obtained value. Nonetheless we will use the values to determine if the uptake of H_2O_2 to the bulk of the ice is a likely explanation. The highest obtained mole fraction in ice was $4.3 \times 10^{-6} \pm 1.2 \times 10^{-6}$ at 239 K and a gas phase concentration of 4.3×10^{11} molecules/cm^3.

This mole fraction in the ice can also be compared to other species in single crystalline ice. They range from 7×10^{-6} for HCl (Thibert and Domine, 1997) and 3.6×10^{-7} for HNO$_3$ (Thibert and Domine, 1998) to 1.3×10^{-7} for HCHO (Barret et al., 2011) at the same temperature and gas phase concentration of the respective species. One can see that our mole fractions in ice again are on the upper end of mole fractions in single crystalline ice. Most probably the uptake is enhanced in our polycrystalline ice by diffusion into grain boundaries.

Uptake into grain boundaries

We investigated if the observed high mole fractions of H_2O_2 in ice can be explained by grain boundaries as a major reservoir for gas phase H_2O_2 loss. Grain boundary contents in ice samples have been investigated by a cross polarizer technique (Riche et al., 2012a; Riche et al., 2012b). We adapted the basic principle of this technique, yet the cylindrical geometry of our flow tubes rendered grain boundary characterization difficult. We observed a single identifiable ice grain with a diameter of roughly 1 cm. To asses the upper limit of grain boundaries in our ice samples, we assumed an average grain diameter of 1 cm and a maximal grain boundary thickness of 10 nm resulting in a volume fraction of grain boundaries of 5×10^{-5}.

We used Fick's second law of diffusion E(4.7) to asses the time scale over which the concentration gradient in the grain boundaries would be gone and thus the diffusion process would stop.

$$\frac{\delta C}{\delta t} = D \times \frac{\delta^2 C}{\delta d^2} \tag{4.7}$$

D is the diffusivity (cm^2/s), C the concentration in the grain boundaries (molecules / cm^3), t the time of the experiment (s) and d the depth into the ice (cm). To compute the concentration versus time and depth numerically, the time E(4.8) and depth E(4.9) were rendered dimensionless with:

$$\tau = \frac{D}{T^2} \times t \tag{4.8}$$

Where τ is the dimensionless time (-) and T the thickness of the ice film (cm).

$$x = \frac{d}{T} \tag{4.9}$$

To solve the partial differential equation E(4.7) the boundary condition on the gas ice interface were set to a constant concentration defined by the solubility of H_2O_2 in liquid water at 273 K (8.3×10^{19} molecules / cm^3) as a maximal estimate and the boundary condition of the ice/quartz interface was set to a flux of zero. The diffusivity was varied from 2×10^{-9} (cm^2/s) to 7×10^{-9} (cm^2/s) based on the data of Lu et al. (2009) for self diffusion of water in grain boundaries. The results showed that the grain boundaries are saturated after maximal 400 s.

High concentrations of H_2O_2 in the grain boundaries were proposed to induce the presence of a liquid phase (Huthwelker et al., 2001). Taking into account the upper limit of grain boundary volume fraction, the total loss of molecules from the gas phase in our experiments would result in a H_2O_2 concentration in the grain boundaries two orders of magnitude higher than the equilibrium concentration of H_2O_2 in liquid water at 273.15 K (extrapolated from Hwang and Dasgupta, 1985).

Such high concentrations of H$_2$O$_2$ in grain boundaries are improbable. Following the fast saturation and the high concentration in the grain boundaries, grain boundaries as the sole reservoir for the uptake become very unlikely.

Quasi-liquid layer

The upper disordered layers of the ice, which form the so called quasi liquid layer (QLL), may enhance trace gas uptake. We checked for this possibility by calculating the volume of the QLL with an assumption of a maximal QLL thickness of 30 nm (Bartels-Rausch et al., 2013b). The total uptake of molecules from the gas phase into this volume would roughly equal the solubility of H$_2$O$_2$ in liquid water at 273 K (extrapolated from Hwang and Dasgupta, 1985). The very thin QLL should be saturated fast, but McNeill et al. (2006) argued that impurities in the QLL enhance the thickness of the QLL and could be responsible for trace gas uptake beyond monolayer coverage on long time scales. If such an extended disordered layer would reach a thickness of 100 nm the total uptake of molecules would result in only a fourth of the equilibrium with liquid water at 273 K. Hence an additional long term uptake into an enhanced disordered layer can not be neglected.

In conclusion, most probably the uptake takes place into polycrystalline ice. Furthermore a diffusive uptake into an extended disordered interface could additionally take place. The total solubility in the polycrystalline ice is thereby on the upper end of solubilites found in single crystalline ices for the other trace gases, as mentioned above.

4.4.5   Other reasons for a long term uptake to the ice

While the stated hypothesis looks at diffusion into the ice, several other reasons for a long term uptake exist. There could be burial by growing ice, resulting from the temperature gradient in some experiments (Ullerstam and Abbatt, 2005). Also hydrate formation may alter the magnitude of the uptake (McNeill et al., 2007b; Symington et al., 2010).

As mentioned above, the temperature gradient resulted in an under saturation of the water vapor in the first 20 cm of the CWFT. The experiments were adjusted to the water vapor equilibrium pressure at the later stable part of the flow tube, so the ice was too warm in the beginning part. This results in water sublimating here and condensing in the later colder part by vapor deposition.

The evaporation rate over the ice surface at the beginning of the flow tube is very high, so the amount of molecules lost from the ice film is determined only by the amount of molecules necessary to reach equilibrium in the gas phase. To give an upper limit for the water vapor transport, we estimated the time it took to completely sublimate the area of the flow tube where the temperature gradient was

present. The first 20 cm of the flow tube sublimated within the first 30 min of the experiment.

The water vapor deposition in the later part of the flow tube could lead to burial of H_2O_2 in the growing ice during the first 30 min of the experiment (Ullerstam and Abbatt, 2005). We still observed long term uptake after hours. In addition experiments without a temperature gradient also resulted in long term uptake (Figure 4.2C). Hence we conclude that the long term uptake is not induced by burial of H_2O_2 in the ice.

The formation of hydrates of H_2O_2 on the surface could significantly alter the uptake process. McNeill et al. (2007a) for example found uptake of HCl to ice exceeding surface saturation if HCl-hexahydrates were stable. Our experiments were executed above 230 K. At temperatures below 220.75 K it is possible that $H_2O_2 \times 2H_2O$ hydrates form. This suggests we were not in the stability regime of $H_2O_2 \times 2H_2O$ hydrates in our experiments. To show where our experiments took place in the phase diagramm, we used the data published by Foley and Giguere (1951) and the vapor pressure over pure H_2O_2 from Manatt and Manatt (2004) to calculate the phase diagram with Raoult's law. The results are shown in Figure 4.8. It has to be mentioned that the phase diagram of Foley and Giguere (1951) is based on measurements of frozen liquid solutions of H_2O_2 in water, while we dosed H_2O_2 from the gas phase to an already frozen ice surface. Most probably the thermodynamic stable liquid solution visible in Figure 4.8 which would suggest a liquid solution above the ice, is not formed, due to the low surface coverages in our expierments. The $H_2O_2 \times 2H_2O$-water- ice stability line is not known to this date. Yet, since our experiments were conducted far away from the borders of the stability lines, we conclude that $H_2O_2 \times 2H_2O$ hydrates were not present under our experimental conditions.

4.5   Environmental implications

The results presented in this study have a significant impact on the behavior of H_2O_2 in contact with snow packs or ice sheets. Our experiments showed a long term loss from the gas phase in agreement with Conklin et al. (1993). A long term uptake to the ice would have considerable environmental implications, since gas phase H_2O_2 above or inside a snowpack for example, would show a much larger uptake as suggested from the reversible adsorption alone.

Our data is in agreement with field measurements, where temperature dependent day and night cycles have been observed (Hutterli et al., 2001; Jacobi et al., 2002). The strong negative temperature dependence of the adsorption we observed could explain these variations. Even on longer time scales, H_2O_2 reentering the gas phase from the bulk of the ice could in summer is a net source of H_2O_2 (Hutterli et al.,
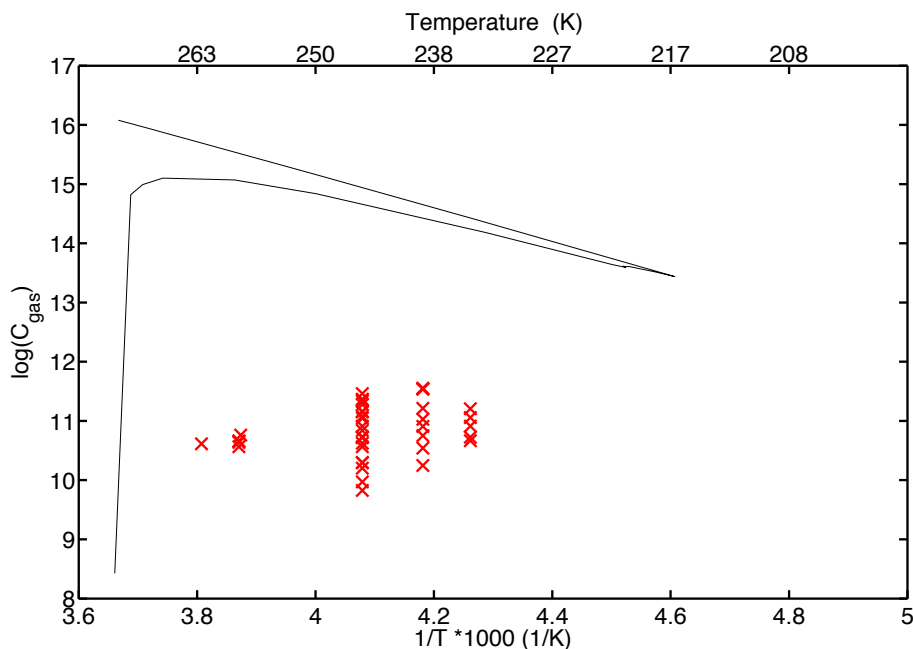
Figure 4.8: Phase diagram of H_2O_2 – water with vapor pressures. Our experimental conditions are marked with red crosses.

2001).

Considering H_2O_2 as a light absorber in snow packs (Anastasio and Robles, 2007) our study shows that a significant amount of H_2O_2 is present on the snow surface where photochemistry is feasible. H_2O_2 can be photolysed to OH, which further impacts oxidative capacity in the boundary layer.

4.6   Conclusions and Outlook

Our experiments in ice coated wall flow tube experiments with long residence times in the flow tubes showed two distinct modes of uptake of H_2O_2 to the ice: An initial fast surface adsorption process and an uptake to the bulk of the ice on much longer time scales. We separated both processes and evaluated the magnitude of the uptake in terms of partitioning from the gas phase to the respective reservoir. The temperature dependence and magnitude of both partitioning modes are in very good agreement with two earlier studies, which focused on surface adsorption (Pouvesle et al., 2010) and uptake to the bulk of the ice (Conklin et al., 1993). The results of Pouvesle et al. (2010) could be confirmed, regarding previous disagreements with another study (Clegg and Abbatt, 2001a) focusing on surface adsorption. Our

results show a high solubility of H_2O_2 in the bulk of polycrystalline ice. To further investigate uptake of H_2O_2 to environmental relevant ice, laboratory studies are needed to investigate trace gas uptake in combination with grain boundary content.

4.7   Acknowledgements

4.8   References

Abbatt, J. P. D.: Interaction of HNO$_3$ with water-ice surfaces at temperatures of the free troposphere, Geophysical Research Letters, 24, 1479-1482, 10.1029/97GL01403, 1997.

Abbatt, J. P. D.: Interactions of atmospheric trace gases with ice surfaces: Adsorption and reaction, Chemical Reviews, 103, 4783-4800, 10.1021/cr0206418, 2003.

Anastasio, C., and Robles, T.: Light absorption by soluble chemical species in Arctic and Antarctic snow, Journal of Geophysical Research-Atmospheres, 112, D24304, 10.1029/2007jd008695, 2007.

Barret, M., Houdier, S., and Domine, F.: Thermodynamics of the Formaldehyde-Water and Formaldehyde-Ice Systems for Atmospheric Applications, Journal of Physical Chemistry A, 115, 307-317, 10.1021/jp108907u, 2011.

Bartels-Rausch, T., Jacobi, H.-W., Kahan, T. F., Thomas, J. L., Thomson, E. S., Abbatt, J. P. D., Ammann, M., Blackford, J. R., Bluhm, H., Boxe, C., Domine, F., Frey, M. M., Gladich, I., Guzman, M. I., Heger, D., Huthwelker, T., Klan, P., Kuhs, W. F., Kuo, M. H., Maus, S., Moussa, S. G., McNeill, V. F., Newberg, J. T., Pettersson, J. B. C., Roeselova, M., and Sodeau, J. R.: Relationship between snow microstructure and physical and chemical processes, Atmospheric Chemistry and Physics Discussions, 12, 30409-30541, 2013a.

Bartels-Rausch, T., Wren, S., Schreiber, S., Riche, F., Schneebeli, M., and Ammann, M.: Diffusion of volatile organics through porous snow: Impact of surface adsorption and grain boundaries, submitted to Atmospheric Chemistry and Physics, 2013b.

Clegg, S. M., and Abbatt, J. P. D.: Uptake of gas-phase SO$_2$ and H$_2$O$_2$ by ice surfaces: Dependence on partial pressure, temperature, and surface acidity, Journal of Physical Chemistry A, 105, 6630-6636, 10.1021/jp010062r, 2001a.

Clegg, S. M., and Abbatt, J. P. D.: Oxidation of SO$_2$ by H$_2$O$_2$ on ice surfaces at 228 K: a sink for SO2 in ice clouds, Atmospheric Chemistry and Physics, 1, 73-78, 2001b.

Conklin, M. H., Sigg, A., Neftel, A., and Bales, R. C.: Atmosphere-Snow Transfer-Function for H$_2$O$_2$ - Microphysical Considerations, Journal of Geophysical Research-Atmospheres, 98, 18367-18376, 10.1029/93jd01194, 1993.

Crowley, J. N., Ammann, M., Cox, R. A., Hynes, R. G., Jenkin, M. E., Mellouki, A., Rossi, M. J., Troe, J., and Wallington, T. J.: Evaluated kinetic and photochemical data for atmospheric chemistry: Volume V - heterogeneous reactions on solid substrates, Atmospheric Chemistry and Physics, 10, 9059-9223, 10.5194/acp-10-9059-2010, 2010.

Foley, W. T., and Giguere, P. A.: Hydrogen Peroxide and Its Analogues .2. Phase Equilibrium in the System Hydrogen Peroxide Water, Canadian Journal of Chemistry-Revue Canadienne De Chimie, 29, 123-132, 10.1139/v51-016, 1951.

Huthwelker, T., Lamb, D., Baker, M., Swanson, B., and Peter, T.: Uptake of SO_2 by polycrystalline water ice, Journal of Colloid and Interface Science, 238, 147-159, 10.1006/jcis.2001.7507, 2001.

Huthwelker, T., Ammann, M., and Peter, T.: The uptake of acidic gases on ice, Chemical Reviews, 106, 1375-1444, 10.1021/cr020506v, 2006.

Hutterli, M. A., McConnell, J. R., Stewart, R. W., Jacobi, H. W., and Bales, R. C.: Impact of temperature-driven cycling of hydrogen peroxide (H_2O_2) between air and snow on the planetary boundary layer, Journal of Geophysical Research-Atmospheres, 106, 15395-15404, 10.1029/2001jd900102, 2001.

Hutterli, M. A., McConnell, J. R., Bales, R. C., and Stewart, R. W.: Sensitivity of hydrogen peroxide (H_2O_2) and formaldehyde (HCHO) preservation in snow to changing environmental conditions: Implications for ice core records, Journal of Geophysical Research-Atmospheres, 108, 4023, 10.1029/2002jd002528, 2003.

Hwang, H., and Dasgupta, P. K.: Thermodynamics of the Hydrogen-Peroxide Water-System, Environmental Science & Technology, 19, 255-258, 10.1021/es00133a-006, 1985.

Ignatov, S. K., Razuvaev, A. G., Sennikov, P. G., and Schrems, O.: H_2O_2 adsorption on the ice Ih surface. Theoretical study with systematic assessment of the orientation isomerism of the hydrogen bond network, Journal of Molecular Structure-Theochem, 908, 47-54, 10.1016/j.theochem.2009.05.003, 2009.

Jacobi, H. W., Frey, M. M., Hutterli, M. A., Bales, R. C., Schrems, O., Cullen, N. J., Steffen, K., and Koehler, C.: Measurements of hydrogen peroxide and formaldehyde exchange between the atmosphere and surface snow at Summit, Greenland, Atmospheric Environment, 36, 2619-2628, Pii s1352-2310(02)00106-1, 10.1016/s1352-2310(02)00106-1, 2002.

Jacobi, H. W., Bales, R. C., Honrath, R. E., Peterson, M. C., Dibb, J. E., Swanson, A. L., and Albert, M. R.: Reactive trace gases measured in the interstitial air of surface snow at Summit, Greenland, Atmospheric Environment, 38, 1687-1697, 10.1016/j.atmosenv.2004.01.004, 2004.

Kemball, C., Rideal, E. K., and Guggenheim, E. A.: Thermodynamics of Monolayers, Transactions of the Faraday Society, 44, 948-954, 10.1039/tf9484400948, 1948.

Kerbrat, M., Huthwelker, T., Bartels-Rausch, T., Gaeggeler, H. W., and Ammann, M.: Co-adsorption of acetic acid and nitrous acid on ice, Physical Chemistry Chemical Physics, 12, 7194-7202, 10.1039/b924782c, 2010a.

Kerbrat, M., Huthwelker, T., Gaeggeler, H. W., and Ammann, M.: Interaction of Nitrous Acid with Polycrystalline Ice: Adsorption on the Surface and Diffusion into the Bulk, Journal of Physical Chemistry C, 114, 2208-2219, 10.1021/jp909535c, 2010b.

Lawrence, M. G., and Crutzen, P. J.: The impact of cloud particle gravitational settling on soluble trace gas distributions, Tellus Series B-Chemical and Physical Meteorology, 50, 263-289, 10.1034/j.1600-0889.1998.t01-2-00005.x, 1998.

Lazrus, A. L., Kok, G. L., Gitlin, S. N., Lind, J. A., and McLaren, S. E.: Automated Fluorometric Method for Hydrogen-Peroxide in Atmospheric Precipitation, Analytical Chemistry, 57, 917-922, 10.1021/ac00281a031, 1985.

Logan, J. A., Prather, M. J., Wofsy, S. C., and McElroy, M. B.: Tropospheric Chemistry - a Global Perspective, Journal of Geophysical Research-Oceans and Atmospheres, 86, 7210-7254, 10.1029/JC086iC08p07210, 1981.

Lu, H., McCartney, S. A., and Sadtchenko, V.: H/D exchange kinetics in pure and HCl doped polycrystalline ice at temperatures near its melting point: Structure, chemical transport, and phase transitions at grain boundaries, Journal of Chemical Physics, 130, 054501, 10.1063/1.3039077, 2009.

Manatt, S. L., and Manatt, M. R. R.: On the analyses of mixture vapor pressure data: The hydrogen peroxide/water system and its excess thermodynamic functions, Chemistry-A European Journal, 10, 6540-6557, 10.1002/chem.200400104, 2004.

McConnell, J. R., Bales, R. C., Winterle, J. R., Kuhns, H., and Stearns, C. R.: A lumped parameter model for the atmosphere-to-snow transfer function for hydrogen peroxide, Journal of Geophysical Research-Oceans, 102, 26809-26818, 10.1029/96jc02-194, 1997a.

McConnell, J. R., Winterle, J. R., Bales, R. C., Thompson, A. M., and Stewart, R. W.: Physically based inversion of surface snow concentrations of H_2O_2 to atmospheric concentrations at South Pole, Geophysical Research Letters, 24, 441-444, 10.1029/97gl00183, 1997b.

McConnell, J. R., Bales, R. C., Stewart, R. W., Thompson, A. M., Albert, M. R., and Ramos, R.: Physically based modelling of atmosphere-to-snow-to-firn transfer of H2O2 at South Pole, Journal of Geophysical Research-Atmospheres, 103, 10561-10570, 10.1029/98jd00460, 1998.

McNeill, V. F., Loerting, T., Geiger, F. M., Trout, B. L., and Molina, M. J.: Hydrogen chloride-induced surface disordering on ice, Proceedings of the National Academy of Sciences of the United States of America, 103, 9422-9427, 10.1073/pnas.0-603494103, 2006.

McNeill, V. F., Geiger, F. M., Loerting, T., Trout, B. L., Molina, L. T., and Molina, M. J.: Interaction of hydrogen chloride with ice surfaces: The effects of grain size, surface roughness, and surface disorder, Journal of Physical Chemistry A, 111, 6274-6284, 10.1021/jp068914g, 2007a.

Penkett, S. A., Jones, B. M. R., Brice, K. A., and Eggleton, A. E. J.: Importance of Atmospheric Ozone and Hydrogen-Peroxide in Oxidizing Sulfur-Dioxide in Cloud and Rainwater, Atmospheric Environment, 13, 123-137, 10.1016/0004-6981(79)90251-8, 1979.

Pouvesle, N., Kippenberger, M., Schuster, G., and Crowley, J. N.: The interaction of H2O2 with ice surfaces between 203 and 233 K, Physical Chemistry Chemical Physics, 12, 15544-15550, 10.1039/c0cp01656j, 2010.

Riche, F., Bartels-Rausch, T., Schreiber, S., Ammann, M., and Schneebeli, M.: Temporal evolution of surface and grain boundary area in artificial ice beads and implications for snow chemistry, Journal of Glaciology, 58, 815-817, 10.3189/2012JoG12-J058, 2012a.

Riche, F., Schneebeli, M., and Tschanz, S. A.: Design-based stereology to quantify structural properties of artificial and natural snow using thin sections, Cold Regions Science and Technology, 79-80, 67-74, 10.1016/j.coldregions.2012.03.008, 2012b.

Sigg, A., and Neftel, A.: Evidence for a 50-Percent Increase in H_2O_2 over the Past 200 Years from a Greenland Ice Core, Nature, 351, 557-559, 10.1038/351557a0, 1991.

Sigg, A., Staffelbach, T., and Neftel, A.: Gas-Phase Measurements of Hydrogen-Peroxide in Greenland and Their Meaning for the Interpretation of H2o2 Records in Ice Cores, Journal of Atmospheric Chemistry, 14, 223-232, 10.1007/bf00115235, 1992.

Symington, A., Cox, R. A., and Fernandez, M. A.: Uptake of organic acids on ice surfaces: Evidence for surface modification and hydrate formation, Z. Phys. Chem., 224, 1219-1245, 10.1524/zpch.2010.6149, 2010.

Thibert, E., and Domine, F.: Thermodynamics and kinetics of the solid solution of HCl in ice, Journal of Physical Chemistry B, 101, 3554-3565, 10.1021/jp962115o, 1997.

Thibert, E., and Domine, F.: Thermodynamics and kinetics of the solid solution of HNO_3 in ice, Journal of Physical Chemistry B, 102, 4432-4439, 10.1021/jp980569a, 1998.

Ullerstam, M., and Abbatt, J. P. D.: Burial of gas-phase HNO_3 by growing ice surfaces under tropospheric conditions, Physical Chemistry Chemical Physics, 7, 3596-3600, 10.1039/b507797d, 2005.

Ullerstam, M., Thornberry, T., and Abbatt, J. P. D.: Uptake of gas-phase nitric acid to ice at low partial pressures: evidence for unsaturated surface coverage, Faraday Discussions, 130, 211-226, 10.1039/b417418f, 2005.

Ulrich, T., Ammann, M., Leutwyler, S., and Bartels-Rausch, T.: The adsorption of peroxynitric acid on ice between 230 K and 253 K, Atmospheric Chemistry and Physics, 12, 1833-1845, 10.5194/acp-12-1833-2012, 2012.

Chapter 5

A new reactor to investigate grain boundary dependent uptake of trace gases to ice

T. Ulrich[1,2], M. Ammann[1] and T. Bartels-Rausch[1,0]

---

[1]Paul Scherrer Institut, Laboratory of Radiochemistry and Environmental Chemistry, 5232 Villigen PSI, Switzerland

[2]Universität Bern, Department of Chemistry and Biochemistry, 3008 Bern, Switzerland

[0]Author for correspondence (Email: thorsten.bartels-rausch@psi.ch)

5.1   Abstract

The uptake of trace gases to the grain boundaries of ice has long been discussed as an important environmental contribution to total trace gas uptake on ice. Yet up till now there has not been a study which clearly distinguishes grain boundary uptake from other modes of uptake. Here we present the design of a new flow through reactor for trace gas uptake to ice. By zone refining, the grain boundary content of the ice can be controlled. In a subsequent step trace gases can be dosed to the ice surface in the same reactor. The planar geometry of the reactor allows analysis of the grain boundary content by light microscopy. The results of zone refined ices produced with this reactor show a grain boundary content increase of a factor of five.

5.2   Introduction

Snow and ice surfaces cover great parts of the Earth. Chemical exchange with these surfaces has been shown to significantly impact the composition of the overlaying air masses (Domine and Shepson, 2002). A lot of work has been done in the field (e.g. Jacobi et al., 2002; Eisele et al., 2008; Slusher et al., 2010), with physical models (e.g. McConnell et al., 1998) and in laboratory studies (Abbatt, 2003; Huthwelker et al., 2006) to understand the uptake of such trace gases by snow and ice. The picture of snow and ice as a chemical reactor becomes even more relevant, when the microstructure of snow packs and bulk ice are considered. Snow and ice matrices are sites, where chemical reactions and physical processes take place. Sites of special interest are the grain boundaries between ice grains because of their different physical characteristics as compared to the bulk of the entire ice (Bartels-Rausch et al., 2013a).

5.2.1   What are grain boundaries

Water does not necessarily freeze at 0 °C. To initialize the freezing process, crystallization nuclei are necessary. If a great number of crystallization nuclei are present, ice crystals or grains will grow around each of them. As the bulk of the liquid freezes, those grains will grow toward each other, forming interface areas between them. These interfaces, termed grain boundaries, act like defects in the crystal structure providing different physical characteristics as compared to the bulk of the ice. Self diffusion of water for example is enhanced in grain boundaries by three orders of magnitude as compared to the bulk (Lu et al., 2009). Triple junctions where three grain boundaries meet are called veins. The interfacial curvatures with their inverse Kelvin effect may provide liquid or liquid like channels through the

pure ice matrix near the melting point of ice (Mader, 1992; Wettlaufer, 1999).

While grain boundaries relevant for example in ice core studies are intrinsically present in solid ice sheets, in the snow pack they form by snow metamorphism where individual snow crystals are in contact with each other. Their characteristics may be crucial for the interaction of ice with trace gas species.

Enhanced uptake of HCl on the ice surface has been observed in grain richer ices compared to ice with lower grain content. The grooves of grain boundaries on top of the ice surface could be responsible for this enhanced uptake (McNeill et al., 2007). As the diffusivities in grain boundaries are higher than in the bulk of the ice (Domine et al., 1994; Lu et al., 2009), it could be possible for species accommodated there to be transported into the ice along grain boundaries (Huthwelker et al., 2001). Diffusion into the bulk of polycrystalline ice could represent an important long term reservoir in the environment i.e. they are not captured by surface adsorption processes alone. Yet not all species have been shown to be sensitive to grain boundary uptake. For example methanol and acetone did not show a different uptake in comparison to ices with different grain contents (Bartels-Rausch et al., 2013b).

The fate of trace gases previously adsorbed on the surface and then diffusing along grain boundaries into the bulk, is also determined by the characteristics of these special environments. The concentrations of impurities can be enhanced in grain boundaries or veins. After freezing of liquid solutions in a laboratory study (Wolff et al., 1989), HCl for example , was found in much higher concentrations in the veins than in the bulk. Also in an Antarctic ice core sample it has been proposed that H_2SO_4 resides mostly in the ice veins (Mulvaney et al., 1988). High concentrations of acidic impurities like HCl or H_2SO_4 at these sites might very well induce pre-melting of the ice at the veins (McNeill et al., 2006). Chemical reactions may also be enhanced on the disordered surface layer. McNeill et al. (2006) for example found the chlorine activation of HCl with $ClONO_2$ was enhanced by surface disordered ice.

5.2.2 Investigation of Grain boundaries

Ice crystals are optically anisotropic and birefringent i.e. are a double refractive medium with a birefingance of 0.004 (-). Their refractive indices depend on the polarization and propagation directions in respect to the optical axis of the crystal. Polarized light shining through an ice crystal splits into two rays polarized in a 90 ° angle with regard to each other and rotated in respect to the angle of the original polarized light entering the crystal. Both have different indices of refraction and hence two different velocities in the medium resulting in retardation of the slower light ray. By placing an ice sample between a cross polarizer, only light polarized parallel to the second polarization filter passes through. The different velocities in
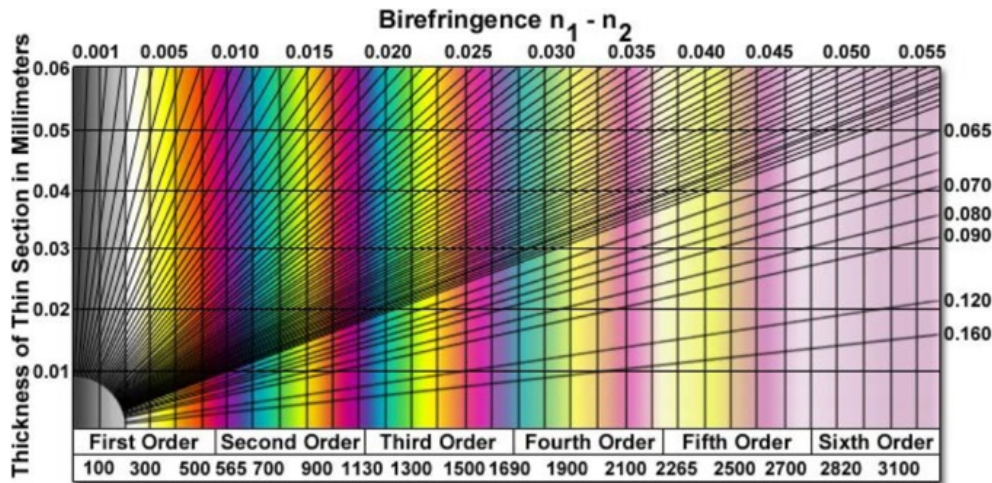
Figure 5.1: Michel-Levy chart for analysis of birefringent crystals (taken (permission pending) from Olympus Japan Corporation (1995) (Copyright 1995, Olympus Japan Corporation)). Lower X-axis: Retardation (nm), Top X-axis and angular lines: Birefingence (-). Y-axis: Thickness (mm). Birefringence of ice: 0.004.

the birefringent medium result in a color spectrum caused by interference of the light rays. An example for colors obtained by such analysis is given in Figure 5.1. Resulting colors are shown as a function of retardation (nm), thickness of the sample (mm) and maximal difference between the two refractive indices (= birefringence (-)) for thin sections.

With this type of analysis the individual ice grains become visible in different colors depending on the angle between the optical axis and the light source. The grain boundaries are the lines between those grains.

This method was used in an earlier study to investigate artificial and natural snow grain boundary interface areas by a stereoscopic method (Riche et al., 2012a; Riche et al., 2012b).

A number of methods exist, which allow the control of the grain boundary content of an ice sample These methods include controlling the freezing temperature, controlling the density of crystallization nuclei or controlling the growth rate of the ice crystal. In this study we rely on a zone refining method similar to McNeill et al. (2006). By zone refining a small melting zone is moved through the ice sample in one direction. As the molten zone within the ice is moved along, the ice begins to re-crystallize behind after this zone. As a result of the slow refreezing big grains start to form. The slower the movement of the heating unit, the lower is the content of grains in the ice. Even single crystals of ice can be produced with this method (Bilgram et al., 1973).

Studies of trace gas uptake on ice with emphasis on grain boundary charac-

teristics are only sparsely available. In coated wall flow tube studies, which are a traditional tool for the investigation of trace gas uptake by ice, it is difficult to analyze the grain boundary content because of the cylindrical geometries of the tubes. Knudsen cells would provide ice surfaces with planar geometry, but only few grain boundary dependent trace gas uptake studies have been executed.

Pratte et al. (2006) investigated condensation and evaporation rates of water on poly- and single crystalline ices in a Knudsen cell. They found both higher condensation and evaporation rates with the presence of grain boundaries.

In another Knudsen cell study with poly- and single crystalline ices Aguzzi et al. (2003) found higher diffusivities in the surface layer for HCl and HBr in the polycrystalline ice.

McNeill et al. (2007) studied the uptake of HCl by two ices differing in grain boundary content as confirmed with a cross polarization. Hollow ice cylinders were zone refined by heating to produce ice low in grain boundaries compared to more polycrystalline ice. The authors presented indirect evidence for two modes of adsorption, a strong one and a weaker one. This could hint at for a stronger interaction with HCl at the grain boundary grooves in comparison to the crystal faces.

Bartels-Rausch et al. (2004) compared acetone uptake in artificially frozen ice beads of high grain boundary content with single crystals and natural snow of lower grain boundary content. They found no dependence between acetone uptake and the grain boundary content. In two later studies (Kerbrat et al., 2010; Pinzer et al., 2010) a grain boundary dependent uptake for nitrous acid (HONO) was proposed. The authors compared artificial snow of low grain boundary content (Pinzer et al., 2010) with artificially frozen ice beads of high grain boundary content (Kerbrat et al., 2010) and argued that the bulk uptake was significantly higher in the case with higher grain boundary content (Pinzer et al., 2010). Note that in these studies the grain boundary content had not been directly characterized. In a more recent study (Bartels-Rausch et al., 2013b) the grain boundary content has been characterized for artificial snow and ice beads, but no dependence of grain boundary uptake for methanol or acetone was observed.

5.2.3 This study

To investigate trace gas uptake to grain boundaries of ice we developed a new reactor, which can produce ice samples with different amounts of grains, to which in a subsequent step trace gases can be dosed. The ice samples can be removed from the reactor, so that their grain boundary content can be analyzed by light microscopy. We thereby used a direct length measurement of the grain boundary grooves on the ice surface. This suface groove length may be more appropriate than the interface area between the grains; since they are the site directly interacting with the gas phase. The reactor is designed as a flow through system; data can be collected anal-

ogous to flow tube experiments with ice (Abbatt, 2003; Huthwelker et al., 2006). We investigated HONO and H_2O_2 for their feasibility of grain boundary uptake in our reactor.

5.3   Methods

5.3.1   The reactor

A flow through reactor was designed for the investigation of trace gas uptake by ice grain boundaries. Central to this reactor is its planar geometry. This allows direct analysis of the ice grain boundary content by an optical light microscopy method. For the first time ice sheets available for optical analysis after each experiment can be produced varying in grain boundary content. Also the content of grain boundaries in the ice can be analyzed in dimensions relevant to trace gas uptake from the gas phase. The reactor thereby works in two experimental modes: Zone refining - and trace gas uptake mode.

Figure 5.2 shows the working principle of the reactor in trace gas uptake- and zone refining mode. In the trace gas uptake mode a trace gas of known concentration is passed over the ice surface. In the zone refining mode a heater is slowly moved over the ice surface, while a humidified gas flow of nitrogen guarantees water vapor equilibrium above the ice surface. The gas channel above the ice has a width of 32 mm and a height of 4.5 mm on a length of 400 mm. The ice surface area has the dimensions 27.5 mm × 398 mm. The thickness of the ice can ve varried between 0.8 - 1.5 mm. The initial and end parts of the gas channel are used to avoid turbulence and establish laminar flow. The characteristic length L regarding the Reynolds number according to (5.1) in such a geometry is twice the height of the gas channel (Fox et al., 2004).

$$Re = \frac{v \times L}{\nu} \tag{5.1}$$

Where Re is the Reynolds number (-), v the linear velocity (m/s), L the characteristic length and ν the kinematic viscosity (m^2/s). Reynolds numbers of 233 indicate laminar flow in the gas channel above the ice at a volumetric gas flow of 2000 ml/min.

Figure 5.3 shows the individual modules of the reactor. The reactor consists of three modules made out of aluminum blocks. The base plate (1): The inside of the base plate contains flow channels for a cooling liquid (e.g. ethanol), by which it can be cooled down to experimental conditions. The top plate: The top plate consists of an aluminum block analogous to the base plate with channels for a cooling liquid. Below the top plate the inlet for the trace gases is located (2). It consists
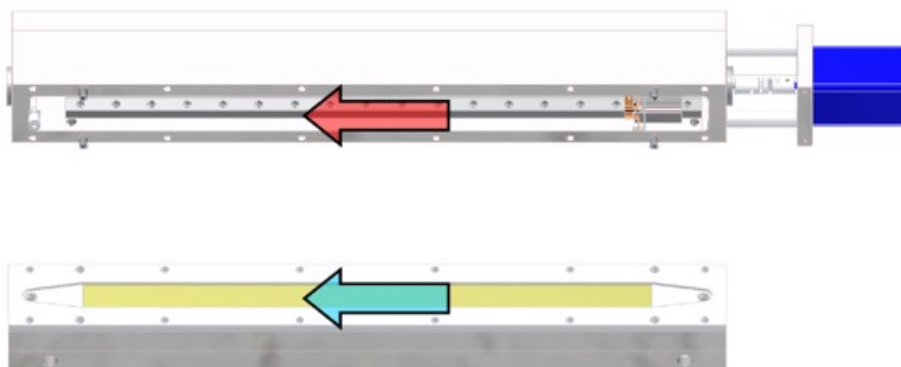
Figure 5.2: Planar flow reactor at uptake mode (below) and zone refining mode (top). Blue arrow indicates gas flow direction, red arrow indicates movement of the heating.

of a block of PTFE Teflon with a long inlet line to pre-cool the gas flow. The gas flow can than be directed vertically onto the ice by PVDF valves. Between the aluminum blocks of the reactor the experimental chamber (3) is located. It consists of a sandwich construction of PTFE Teflon plates. The lowest plate is used to house the borosilicate glass plate on which the ice is frozen. The custom made glass plate contains a basin to hold the water / ice sheet. The next very thin plate (not shown) covers the glass border on top of the glass plate, so that the trace gases only have contact with the ice and the PTFE. The next plate is used to establish the gas flow channel. During uptake mode the gas flow inlet is mounted on top, so the trace gas species has contact only with ice or PTFE parts. The zone refining unit (4): The zone refining unit consists of an aluminum block with a small copper sheet heating unit and a step motor. The step motor moves the heating unit slowly over the ice, melting the ice beneath it. By the slow melting and refreezing process ice with lower grain boundary content can be produced. The zone refining unit is cooled in the same way as the base plate. The whole reactor is housed in an isolating Styrofoam jacket.

5.3.2 Preparation of the ice sample

The borosilicate glass plate is etched with a solution of 5 % HF in water to establish a homogeneous water film and then rinsed with purified water (Millipore, 0.05 μS). The reverse of the glass plate and the outer border are dried with paper towels. The glass plate is then filled with 5-8 ml of the same purified water. The ice sheet is
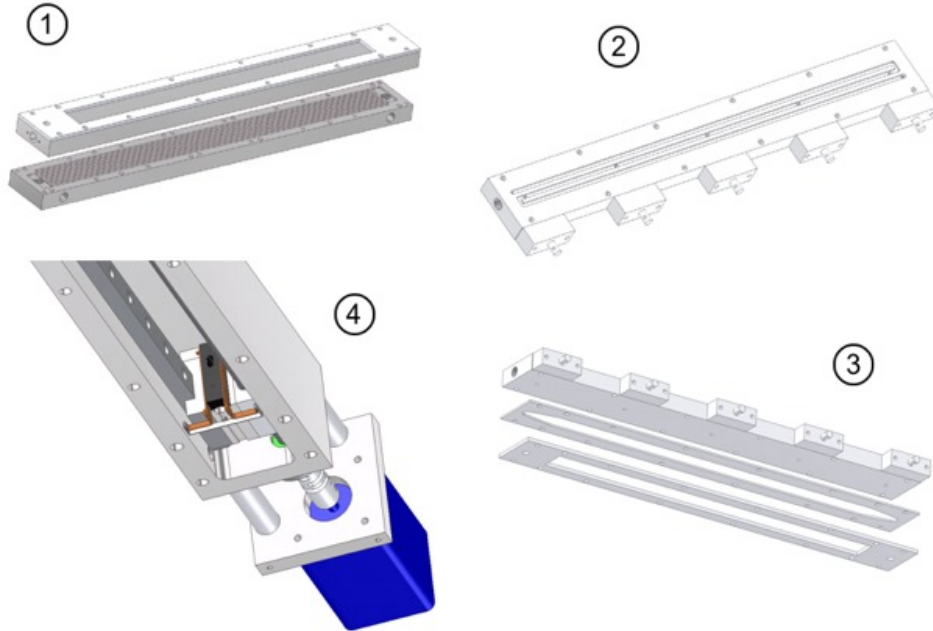
Figure 5.3: Drawings of the reactor. Top left (1): Base plate with channels for cooling liquid and the first Teflon plate, which houses the glass plate. Top right (2): Top view of the gas flow inlet with cooling channels to pre per-cool the gas flow, valves to direct the gas flow to the ice and inlet for the gas flow. The cooling unit is equivalent to the bottom plate and is therefore not shown. Teflon foil between cooling unit and gas flow inlet is also not shown. Bottom right (3): Bottom view of the gas flow inlet, with two Teflon plates. The top plate represents the gas flow channel, The bottom plate is again the glass plate holder as seen in (1). Bottom left (4): Heating system with copper plate and step motor. Cooling unit not shown.

always frozen at 263 K while an equilibrium humidified gas flow of N_2 is passed over the glass plate.

5.3.3   Grain boundary analysis of ice samples

The glass plate with the ice is removed after a freezing or freezing and zone refining step. The glass plate is placed under a commercial USB light microscope. The cross polarizer is adjusted until the ice grains become clearly visible. The ice plate is then pushed horizontally under the lens of the microscope to analyze the ice grains along the length of the glass plate.
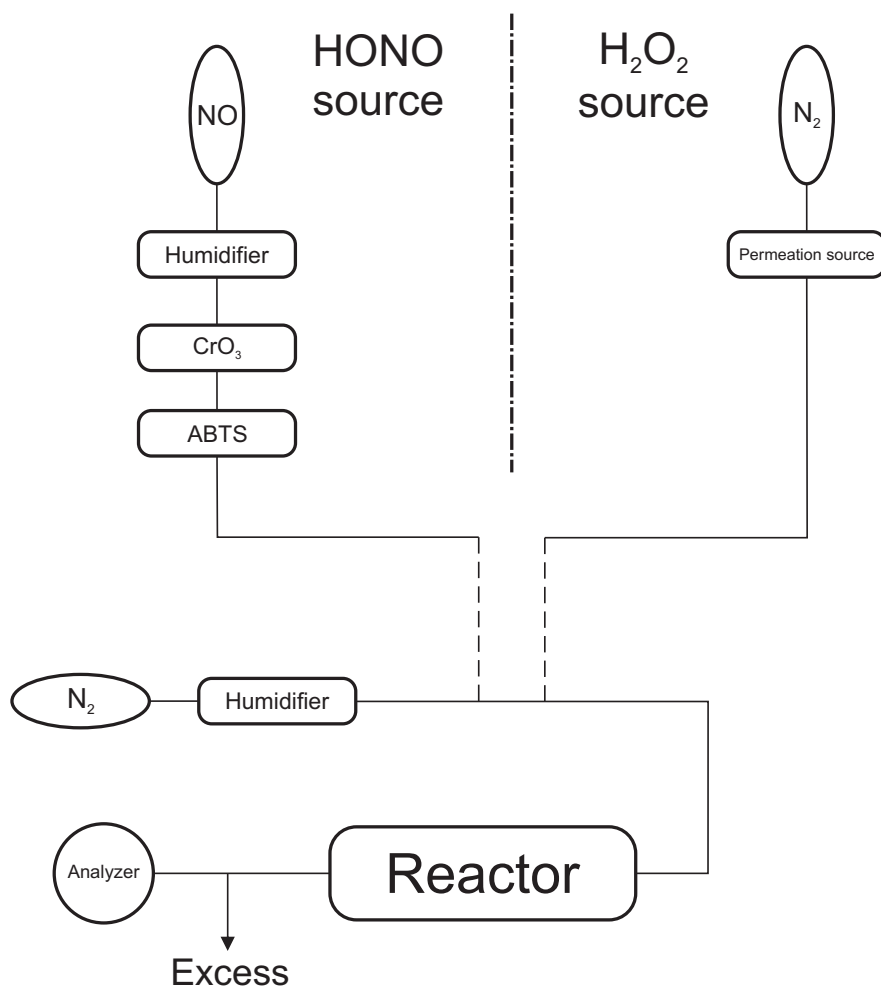
Figure 5.4: Setup for the trace gas experiments.

5.3.4   Uptake experiments

To investigate the uptake of trace gases to the ice or to the walls of the reactor, a gas flow of known velocity and trace gas concentration is directed over the ice. All tubing consists of fluorinated ethylene propylene (FEP). All gas flows were maintained using mass flow controllers (Brooks 5850 or Kobold). The concentration after the reactor is measured in by-pass mode (either only FEP tubes at room temperature or Teflon parts of the inlet at experimental temperature) or experimental mode (Teflon part and ice surface at low temperatures). The tested trace gases were HONO and H_2O_2. The set up for both kinds of experiments is shown in Figure 5.4.

HONO

Uptake experiments with HONO were carried out. HONO was produced by oxidizing humidified NO (Carba Gas 10.03 ppm NO 99.8 % pure in N_2 99.995 % pure) to NO_2 over a CrO_3 catalyst. In a subsequent step HONO was produced from NO_2 over 2,2-azino-bis(3-ethylbenzothiazoline-6-sulfonic acid) diammonium salt (ABTS). This synthesis was previously used by Kerbrat et al. (2010). The gas flow containing HONO was mixed with a gas flow of pure N_2 (Carba Gas 99.9995 % pure) and humidified to the equilibrium water vapor partial pressure of the individual experiment. The gas flow was then delivered to either the reactor with the cooled PTFE inlet system or to the reactor directly. Gas phase HONO concentrations were around 3×10^{11} molecules/cm^3. HONO was measured by a commercial NO analyzer (eco physics) after the reactor. To measure HONO, all NO_Y was reduced to NO by a molybdenum converter. HONO levels were obtained with a CO_3^{2-} denuder, by scavenging HONO. HONO levels were determined by the loss of acidic NO_Y (Ulrich et al., 2011).

H_2O_2

Uptake experiments with H_2O_2 were carried out. H_2O_2 was introduced from a permeation source consisting of a thin FEP tube in a commercial permeation oven (Dynacal) with pure N_2 (Carba Gas, 99.9995 % pure) flowing through it. The gas flow containing H_2O_2 was then diluted and humidified to equilibrium conditions by a second gas flow of N_2 (Carba Gas, 99.9995 % pure) and water vapor. The gas mixture was led to the reactor either directly or through the cooled PTFE inlet system. H_2O_2 was measured in the gas phase after the reactor with a commercial H_2O_2 analyzer (AeroLaser AL 2021). The principle of the detection method is explained elsewhere (Ulrich et al., 2013). Gas phase H_2O_2 concentrations were around 4×10^{11} molecules/cm^3.

5.4   Results

Here we present our results of the optical analysis of the grain boundaries, the zone refining process, quantification of the grain boundaries and preliminary uptake experiments with H_2O_2 and HONO. All temperatures given here refer to the temperature of the cryostats cooling the reactor. Temperature measurements inside the reactor have not yet been performed.
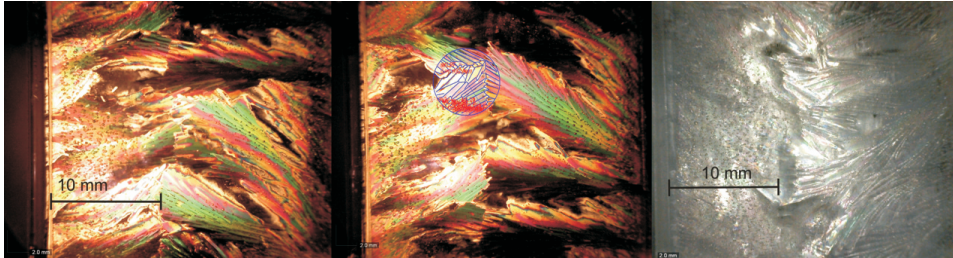
Figure 5.5: Untreated ice sample on the glass plate. Frozen at 263 K. Middle panel shows the data evaluation. Right panel shows the ice surface without cross polarizer.

5.4.1 General optical analysis

The general optical analysis of the ice grains is explained with the help of Figures 5.5-5.9. The ice grains become distinguishable from each other by their color as discussed above.

Untreated ice

Figure 5.5 shows an untreated ice sample. The ice was frozen at 263 K. The individual ice grains are hardly distinguishable from each other here, for the following reasons: First of all, the individual ice grains are very small and formed like needles. Secondly the rainbow like spectrum across big agglomerates of grains hampers the analysis further.

To understand the rainbow like spectrum, we will first look at the growth characteristics of the ice. The ice starts to grow on the left and right borders of the glass plate as shown in Figure 5.5. These sites are energetically more favorable compared to the plain glass face in the middle, since they provide a lower temperature and have more surface for the to ice crystals to grow on.

Secondly we have to look at the underlying glass substrate of the ice. To produce a glass plate which is completely clear, a slight positive curvature of the basin base with a height of approximately 0.1 mm - 0.3 mm is produced.

As the crystals grow from the sides toward the middle, the grain surfaces in contact with the super-cooled water provide new crystallization nuclei for new ice grains. As they grow, the underlying curvature of the glass substrate shifts the optical axes of the grains by small angles. This induces the rainbow like spectrum of the agglomerates.

To verify the conclusion that the small needle like structures are indeed single ice grains we can have a look at the ice surface without the cross polarizer as shown in Figure 5.5 (right panel). The individual needles are clearly visible in a three dimensional structure on top of the ice surface.
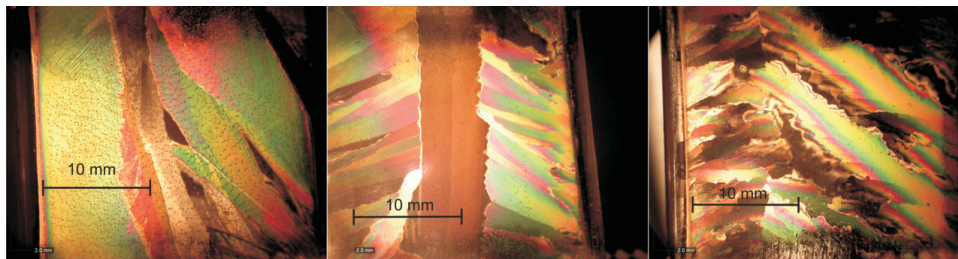
Figure 5.6: General effect of zone refining. Left: 100 mm/h, middle: 400 mm/h, right: 800 mm/h. Heating temperature 363 K. Ice frozen at 263 K.

Also visible are small gas bubbles as small dots or circles, especially at the left and right border of the glass plate in Figure 5.5 (left and middle panel). In an attempt to avoid those gas bubbles, the water was degassed with up to six freeze, pump, thaw cycles. The results were unsatisfying; during application of the water to the glass plate and the freezing process enough air was able to enter the liquid to from new gas bubbles.

In conclusion it becomes evident that untreated ice surfaces are not ideal for uptake experiments. This is due to the difficulty of distinguishing between grain boundaries in these samples, gas bubbles within the ice matrix and the rough surface.

General effect of zone refining

To optimize the zone refining for useful grain boundary properties, different temperatures of the heating and heating unit velocities were tested. At heating temperatures below 393 K the ice did not melt entirely. With 393 K the ice sheet was molten and refrozen throughout. For the following experiments the heating was set to 393 K and the cooling of the reactor to 263 K.

Figure 5.6 shows the impact of different heating unit velocities. In the left panel the velocity was 100 mm/h. It can be seen, that the small ice grains were refined to bigger areas, significantly lowering the grain boundary density. The middle panel shows the results with 400 mm/h. The refined ice crystals are smaller than those at 100 mm/h, and the general structure of the ice sheet shown in Figure 5.5 is still visible. In the middle, where the heating is the hottest, a big ice grain is visible. The right panel shows results with 800 mm/h. Here the individual ice crystals and their structures almost remain the same as in Figure 5.5 and let us conclude that velocities should be adjusted to below 800 mm/h. While these results clearly show the general characteristics of the refining process, we further increased the temperature and lowered the velocity of the heating unit to produce ice with fewer grains.
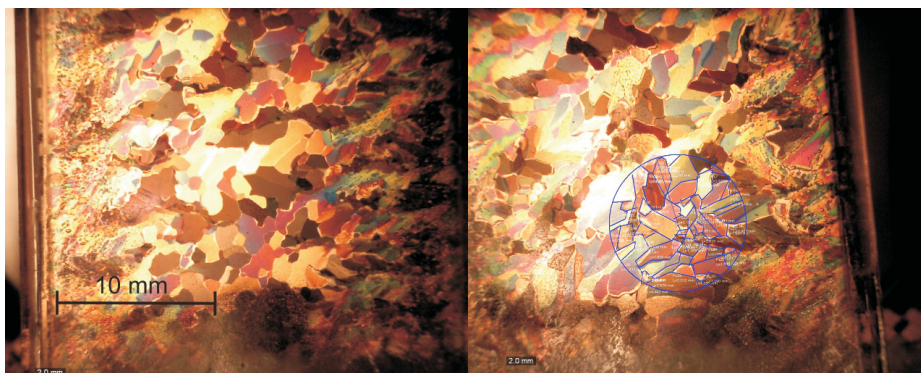
Figure 5.7: Zone refining at a velocity of 100 mm/h. Heating temperature: 433 K. Ice frozen at 263 K. Right panel shows the data evaluation.

Zone refined with high velocity

The temperature of the heating unit was set to 433 K and the velocity was set to 100 mm/h. In Figure 5.7 we see the results of such a zone refining process. The individual ice grains can now be distinguished better as the rainbow like spectra vanish and the roundish ice grains are now visible with a distinctive color.

Under these experimental conditions, the ice grains start to grow randomly on the entire face of the glass plate. Note that the optical axis of the ice grains is not necessarily perpendicular to the glass plate; the optical axis is more or less randomly developed as the grains grow. The angle of the optical axis to the incident light is responsible for the different colors.

The result is comparable to classical experiments executed on thin sections of natural snow (see Figure 5.8, (Riche et al., 2012b)).

The undefined structures at the borders of the glass plate can most probably be avoided by a better insulation or a higher heating temperature as seen for example in the experiments in Figure 5.9.

The surface of the ice in contact with the gas phase is now very smooth, the rough structures have disappeared. Also the gas bubbles were greatly reduced in the ice sample as a result of the melting and refreezing process.

In conclusion a sample produced like this could well be used for a trace gas uptake experiment with a high amount of grain boundaries.

Zone refined with low velocity

The following experiments were executed at 453 K and a velocity of 50 mm/h. The results are presented in Figure 5.9. The ice has been zone refined to very long rectangular grain shapes. Note that even at the beginning of the glass plate and

Figure 5.8: Grain boundaries of natural snow made visible with the cross polarizer technique from Riche et al. (2012b).

at the borders no smaller grains remain. The coloring of the ice grains has nearly entirely disappeared. Considering Figure 5.1 we are now in a regime with very low light retardation. Most probably the optical axis is almost perpendicular to the glass plate, this leads to a minimal retardation of the incident light. The grains can still be distinguished by the brightness of the light shining through them. At this step it is important to rotate the polarization filter back and forth below the sample during the analysis of the grain boundaries, since in the darker part several individual grains may be hidden.

Analogous to the results shown in Figure 5.9, the surface to the gas phase is very smooth and low in gas bubble content. In conclusion ice samples produced like this are highly applicable for uptake experiments with a low amount of grain boundaries.

5.4.2　Quantitative analysis of the zone refining process

The length of the grain boundary grooves was measured directly on the ice surface by optical light microscopy.

Figure 5.10 shows the grain boundary content for untreated ice and the grain boundary contents for zone refined ice at 433 K and 100 mm/h and at 453 K and 50 mm/h. The untreated ice has a grain boundary length to surface area ratio of 28 ± 2.5 cm/cm^2. With the fast heating velocity roundish grains with a grain boundary length to surface area ratio of 17 ± 1.2 cm/cm^2 were produced. With the slow
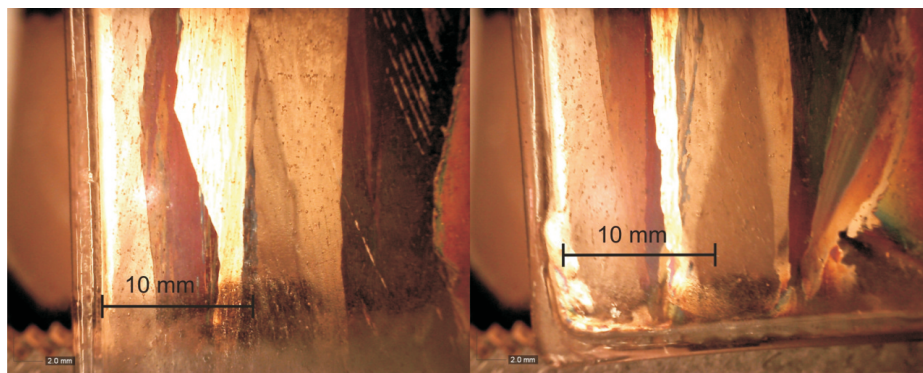
Figure 5.9: Zone refining with a velocity of 50 mm/h. Heating temperature 453 K. Ice frozen at 263 K.
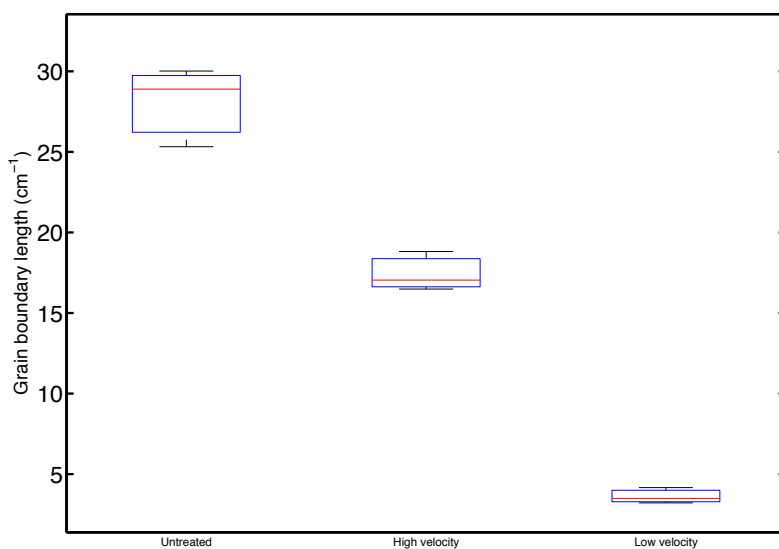

Figure 5.10: Results of the zone refining process in grain boundary length on the ice surface (cm-1). High velocity: T = 433 K and v = 100 mm/h. Low velocity: T = 453 K and v = 50 mm/h.

heating velocity resulting in big rectangular grain shapes the grain boundary length to ice surface area ratio was 3.6 ± 0.49 cm/cm^2.

The error on the untreated ice sample was derived from three individual experi-

ments; the error on the zone refined ices was estimated with data at different lengths of the glass plate in a single experiment.

Our results can be compared to previous studies, which varied the grain boundary content in trace gas uptake experiments. McNeill et al. (2006) used hollow ice cylinders which were zone refined for some experiments. From their picture in this study it is hard to estimate the difference in grain boundary content. They reported ice grains in the zone refined ice in the order of several millimeters. They did not give a number for the non-zone refined ice, but we estimate the difference by a factor of three based on their pictures of the ice. Bartels-Rausch et al. (2013b) compared artificial snow to artificially frozen ice beads in their experiments. They reported a grain boundary area to ice volume ratio of 1.5 mm^2/mm^3 in the artificial snow compared to 10 mm^2/mm^3 in the artificial ice beads. The results obtained with our reactor provided similar ratios of grain boundary content compared to Bartels-Rausch et al. (2013b).

5.5   Outlook

To investigate the uptake of different trace gases to either ice or the reactor material, the trace gases were introduced into the reactor with a carrier gas flow. The loss from the gas phase to ice and reactor material was measured.

5.5.1   NO and NO$_2$

To test the tightness of the reactor, test runs with NO and NO$_2$ were carried out. These experiments showed no loss of either species in the sample inlet or in the main reactor. When exposed to ice no uptake was visible down to temperatures of 253 K. This is in agreement with previously published data on the adsorption of nitrogen oxides to ice, which does not show uptake to ice at such high temperatures (Bartels-Rausch et al., 2002). It also proved that the reactor is gas tight.

5.5.2   H$_2$O$_2$

To ensure feasibility of the experiments, all non ice parts of the reactor must be inert for the chosen trace gas. For H$_2$O$_2$ an uptake to the PTFE material of the sample inlet is already visible at room temperature. The uptake is higher at lower temperatures down to 253 K, but the gas phase signal reaches its initial value after around 20 minutes at 500 ml/min volumetric flow velocity. Repeated uptake experiments with previously exposed reactor material showed a passivation effect; the uptake was smaller by a second exposure, but was always present. These results already show the difficulty with H$_2$O$_2$ experiments in this reactor. The wall uptake is large

and easily visible and thus influences the ice uptake experiment. Nonetheless ice uptake experiments were carried out. For this the entire base plate was filled with water and frozen, since the glass plate sample holders were not yet available. These experiments showed a complete loss of signal after the reactor. We think that the experiment failed, because the the glass plate was not available and the reactor thus was not entirely tight due to water in the sandwich structure. In conclusion experiments with H_2O_2 are not feasible due to the high uptake on the walls as experiments in the gas inlet have shown.

5.5.3 HONO

For HONO the same kinds of experiments were carried out. The sample inlet also showed an uptake of HONO, but orders of magnitude lower than for H_2O_2. Also those experiments resulted in a recovery of the signal to 100 % of the initial signal, which was not the case for H_2O_2.

An experiment for HONO with untreated ice in the main reactor volume was carried out. The results are presented in Figure 5.11. A stable known concentration of HONO was directed through the reactor with the ice surface at t = 0 s. As HONO starts to interact with the ice at this time, the gas phase signal as measured after the reactor shows a loss of molecules. As the ice surface comes into equilibrium with the HONO-gas phase the signal shows a recovery, resulting in a so called breakthrough curve. An incomplete recovery is visible within the time scale of our experiment. This could hint for a longt term uptake of HONO to the ice beyond surface adsoprtion.

From the loss of gas phase molecules the uptake to the surface can be calculated by integrating the area of the breakthrough curve. From the surface concentration and the known gas phase concentration a partition coefficient can be derived. This partition coefficient K_{LinC} is defined as:

$$K_{\text{LinC}} = \frac{C_{\text{ice}}}{C_{\text{gas}}} \tag{5.2}$$

Where C_{ice} is the surface concentration (molecules/cm^2) and C_{gas} is the gas phase concentration (molecules/cm^3).

We assumed that at the end of our experiment, where only a small rise in concentration is visible, the ice surface was already in equilibrium with the gas phase.

Analysis of K_{LinC} with this assumption shows that the derived K_{LinC} on ice, which is 62 cm in our experiment at 248 K, is similar to that recommended by IUPAC (Crowley et al., 2010) of 53 cm at 248 K. Hence measurement of gas-ice partitioning seems principally feasible with our reactor.

To clearly identify a long term upatek behaviour, which could be grain boundary dependent, blank experiments of the reactor volume are necessary. Blank experi-
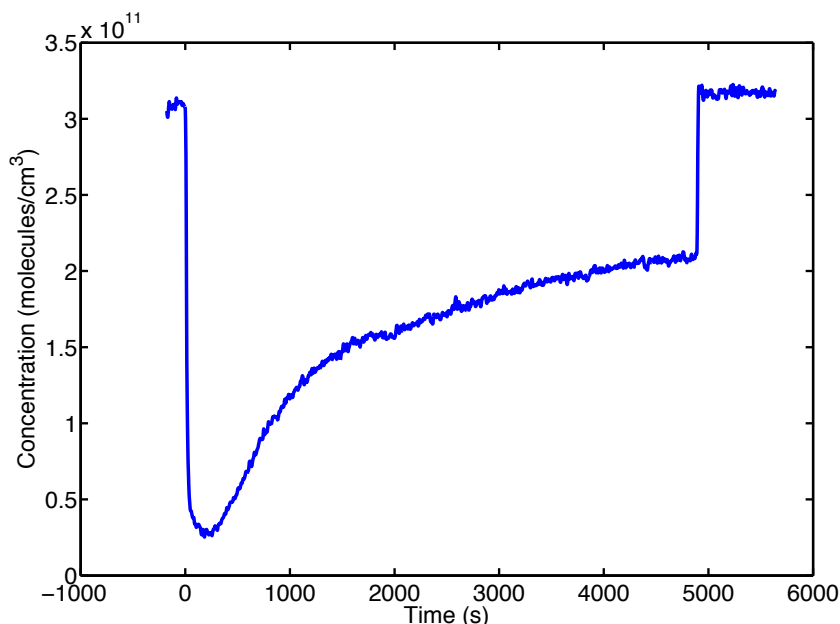
Figure 5.11: Breakthrough curve for HONO at 248 K over the ice in the reactor.

ments with a PTFE foil on the bottom of the reactor, showed higher uptake than on the ice and also much higher than the uptake in the PTFE sample inlet. This may be due to the quality of the PTFE foil used for the blank experiment, which was different to the PTFE material of the reactor. With clean new PTFE foils blank experiments could be possible.

Desorption experiments after the exposure did show, that HONO was released from the PTFE wall of the reactor. When the material was heated to temperatures above 273.15 K all HONO lost to the material could be retrieved. This shows that HONO does not decompose or react on the reactor walls. In conclusion HONO may be a species of interest for investigation in our reactor, as soon as a blank can be carried out.

5.6   Conclusions

In this study we presented the design of a new flow through reactor for grain boundary dependent uptake of trace gases to ice. Results for two zone refined ices are presented which differ in grain boundary content by a factor of five. HONO is proposed as a possible trace gas species for grain boundary dependent uptake experiments in this reactor.

5.7 References

Abbatt, J. P. D.: Interactions of atmospheric trace gases with ice surfaces: Adsorption and reaction, Chemical Reviews, 103, 4783-4800, 10.1021/cr0206418, 2003.

Bartels-Rausch, T., Eichler, B., Zimmermann, P., Gäggeler, H. W., and Ammann, M.: The adsorption enthalpy of nitrogen oxides on crystalline ice, Atmospheric Chemistry and Physics, 2, 235-247, 2002.

Bartels-Rausch, T., Guimbaud, C., Gaggeler, H. W., and Ammann, M.: The partitioning of acetone to different types of ice and snow between 198 and 223 K, Geophysical Research Letters, 31, L16110, 10.1029/2004gl020070, 2004.

Bartels-Rausch, T., Jacobi, H.-W., Kahan, T. F., Thomas, J. L., Thomson, E. S., Abbatt, J. P. D., Ammann, M., Blackford, J. R., Bluhm, H., Boxe, C., Domine, F., Frey, M. M., Gladich, I., Guzman, M. I., Heger, D., Huthwelker, T., Klan, P., Kuhs, W. F., Kuo, M. H., Maus, S., Moussa, S. G., McNeill, V. F., Newberg, J. T., Pettersson, J. B. C., Roeselova, M., and Sodeau, J. R.: Relationship between snow microstructure and physical and chemical processes, Atmospheric Chemistry and Physics Discussions, 12, 30409-30541, 2013a.

Bartels-Rausch, T., Wren, S., Schreiber, S., Riche, F., Schneebeli, M., and Ammann, M.: Diffusion of volatile organics through porous snow: Impact of surface adsorption and grain boundaries, submitted to Atmospheric Chemistry and Physics, 2013b.

Bilgram, J., Wenzl, H., and Mair, G.: Perfection of Zone Refined Ice Single-Crystals, Journal of Crystal Growth, 20, 319-321, 10.1016/0022-0248(73)90100-0, 1973.

Crowley, J. N., Ammann, M., Cox, R. A., Hynes, R. G., Jenkin, M. E., Mellouki, A., Rossi, M. J., Troe, J., and Wallington, T. J.: Evaluated kinetic and photochemical data for atmospheric chemistry: Volume V - heterogeneous reactions on solid substrates, Atmospheric Chemistry and Physics, 10, 9059-9223, 10.5194/acp-10-9059-2010, 2010.

Domine, F., Thibert, E., Vanlandeghem, F., Silvente, E., and Wagnon, P.: Diffusion and Solubility of HCl in Ice - Preliminary-Results, Geophysical Research Letters, 21, 601-604, 10.1029/94gl00512, 1994.

Domine, F., and Shepson, P. B.: Air-snow interactions and atmospheric chemistry, Science, 297, 1506-1510, 10.1126/science.1074610, 2002.

Eisele, F., Davis, D. D., Helmig, D., Oltmans, S. J., Neff, W., Huey, G., Tanner, D., Chen, G., Crawford, J., Arimoto, R., Buhr, M., Mauldin, L., Hutterli, M., Dibb, J., Blake, D., Brooks, S. B., Johnson, B., Roberts, J. M., Wang, Y., Tan,

D., and Flocke, F.: Antarctic Tropospheric Chemistry Investigation (ANTCI) 2003 overview, Atmospheric Environment, 42, 2749-2761, 10.1016/j.atmosenv.2007.04.013, 2008.

Fox, R. W., McDondald, A. T., and Pritchard, P. J.: Introduction to Fluid Mechanics John Wiley and Sons, Hoboken, 2004.

Huthwelker, T., Lamb, D., Baker, M., Swanson, B., and Peter, T.: Uptake of SO_2 by polycrystalline water ice, Journal of Colloid and Interface Science, 238, 147-159, 10.1006/jcis.2001.7507, 2001.

Huthwelker, T., Ammann, M., and Peter, T.: The uptake of acidic gases on ice, Chemical Reviews, 106, 1375-1444, 10.1021/cr020506v, 2006.

Jacobi, H. W., Frey, M. M., Hutterli, M. A., Bales, R. C., Schrems, O., Cullen, N. J., Steffen, K., and Koehler, C.: Measurements of hydrogen peroxide and formaldehyde exchange between the atmosphere and surface snow at Summit, Greenland, Atmospheric Environment, 36, 2619-2628, Pii s1352-2310(02)00106-1, 10.1016/s1352-2310(02)00106-1, 2002.

Kerbrat, M., Huthwelker, T., Gaeggeler, H. W., and Ammann, M.: Interaction of Nitrous Acid with Polycrystalline Ice: Adsorption on the Surface and Diffusion into the Bulk, Journal of Physical Chemistry C, 114, 2208-2219, 10.1021/jp909535c, 2010.

Lu, H., McCartney, S. A., and Sadtchenko, V.: H/D exchange kinetics in pure and HCl doped polycrystalline ice at temperatures near its melting point: Structure, chemical transport, and phase transitions at grain boundaries, Journal of Chemical Physics, 130, , 10.1063/1.3039077, 2009.

Mader, H. M.: Observations of the Water-Vein System in Polycrystalline Ice, Journal of Glaciology, 38, 333-347, 1992.

McConnell, J. R., Bales, R. C., Stewart, R. W., Thompson, A. M., Albert, M. R., and Ramos, R.: Physically based modelling of atmosphere-to-snow-to-firn transfer of H_2O_2 at South Pole, Journal of Geophysical Research-Atmospheres, 103, 10561-10570, 10.1029/98jd00460, 1998.

McNeill, V. F., Loerting, T., Geiger, F. M., Trout, B. L., and Molina, M. J.: Hydrogen chloride-induced surface disordering on ice, Proceedings of the National Academy of Sciences of the United States of America, 103, 9422-9427, 10.1073/pnas.06-03494103, 2006.

McNeill, V. F., Geiger, F. M., Loerting, T., Trout, B. L., Molina, L. T., and Molina, M. J.: Interaction of hydrogen chloride with ice surfaces: The effects of grain size, surface roughness, and surface disorder, Journal of Physical Chemistry A, 111, 6274-6284, 10.1021/jp068914g, 2007.

Mulvaney, R., Wolff, E. W., and Oates, K.: Sulfuric-Acid at Grain-Boundaries in Antarctic Ice, Nature, 331, 247-249, 10.1038/331247a0, 1988.

Pinzer, B. R., Kerbrat, M., Huthwelker, T., Gaeggeler, H. W., Schneebeli, M., and Ammann, M.: Diffusion of NO_X and HONO in snow: A laboratory study, Journal of Geophysical Research-Atmospheres, 115, D03304, 10.1029/2009jd012459, 2010.

Riche, F., Bartels-Rausch, T., Schreiber, S., Ammann, M., and Schneebeli, M.: Temporal evolution of surface and grain boundary area in artificial ice beads and implications for snow chemistry, Journal of Glaciology, 58, 815-817, 10.3189/2012JoG12-J058, 2012a.

Riche, F., Schneebeli, M., and Tschanz, S. A.: Design-based stereology to quantify structural properties of artificial and natural snow using thin sections, Cold Regions Science and Technology, 79-80, 67-74, 10.1016/j.coldregions.2012.03.008, 2012b.

Slusher, D. L., Neff, W. D., Kim, S., Huey, L. G., Wang, Y., Zeng, T., Tanner, D. J., Blake, D. R., Beyersdorf, A., Lefer, B. L., Crawford, J. H., Eisele, F. L., Mauldin, R. L., Kosciuch, E., Buhr, M. P., Wallace, H. W., and Davis, D. D.: Atmospheric chemistry results from the ANTCI 2005 Antarctic plateau airborne study, Journal of Geophysical Research-Atmospheres, 115, D07304, 10.1029/2009jd012605, 2010.

Ulrich, T., Ammann, M., Leutwyler, S., and Bartels-Rausch, T.: The adsorption of peroxynitric acid on ice between 230 K and 253 K, Atmospheric Chemistry and Physics, 12, 1833-1845, 10.5194/acp-12-1833-2012, 2011.

Ulrich, T., Ammann, M., Leutwyler, S., and Bartels-Rausch, T.: The nature of the uptake of H_2O_2 to ice to be submitted to Journal of Physical Chemistry A, 2013.

Wettlaufer, J. S.: Ice surfaces: macroscopic effects of microscopic structure, Philosophical Transactions of the Royal Society a-Mathematical Physical and Engineering Sciences, 357, 3403-3425, 10.1098/rsta.1999.0500, 1999.

Wolff, E. W., Mulvaney, R., and Oates, K.: Diffusion and Location of Hydrochloric-Acid in Ice - Implications for Polar Stratospheric Clouds and Ozone Depletion, Geophysical Research Letters, 16, 487-490, 10.1029/GL016i006p00487, 1989.

Chapter 6

Conclusions and Outlook

Trace gas interactions with ice surfaces impact tropospheric chemistry with high environmental relevance. In this study a gas phase sysnthesis of HNO_4 was established with which we investigated the uptake of HNO_4 to ice in laboratory experiments. For the first time the partitioning of HNO_4 to ice without interfering impurities has been measured. The temperature dependent partition constant is orders of magnitude lower than thought previously. It can now be implemented in atmospheric chemistry transport models, as well as models of the polar boundary layers. The environmental implications will be discussed below.

Also we investigated the uptake of H_2O_2 to ice. Data measured in laboratory experiments considering H_2O_2 partitioning to the ice surface differed in the magnitude as well as temperature dependence. In this study the data set suggesting a higher partitioning towards the ice with strong temperature dependence could be reproduced. The higher adsorption on the ice impacts environmental processes and will be discussed below.

A third topic of this work was to investigate the nature of the long term uptake beyond mono layer coverage. This study compares a medium acidic species, HNO_4 and an almost non-acidic species H_2O_2. As discussed in the previous sections of this thesis long term long term uptake has been reported for acidic species like HCl and HNO_3 or HONO. In this study it is shown that the medium acidic species HNO_4 does not show a long term uptake characteristic, while the almost non-acidic species H_2O_2 showed a distinctive long term uptake, most probably by diffusion into the ice. The long term uptake of H_2O_2 observed here could reproduce an earlier study in terms of magnitude of the uptake. Implications of the long term uptake of a non-acidic species are discussed below.

Grain boundaries in the ice have been proposed to be one reservoir for long term uptake as discussed in the previous sections. In this thesis the progress in production of ice surfaces differing in grain boundary content is presented. In the outlook experiments to further investigate uptake to grain boundaries are discussed.

6.1 Ice uptake experiments

6.1.1 HNO$_4$

A gas phase synthesis for HNO$_4$ including a purification system for by-products was successfully developed and tested in packed bed flow tube experiments. The partitioning towards the ice was in the order HNO$_3$ > HNO$_4$ = HNO$_2$ > NO$_2$ in those experiments.

An earlier study investigating the uptake of HNO$_4$ to ice was hampered by high concentrations of HNO$_3$ in the gas phase above the ice. As discussed in earlier sections of this thesis, strong acids like HNO$_3$ alter the ice surface and can even lead to a melting of the ice. This renders the interpretation of the mentioned study difficult. In the experiments presented here it was shown the concentration of impurities was negligible, resulting in reliable partition constants for HNO$_4$. The temperature dependence was found to be $3.74 \times 10^{-12} \times e^{(7098/T)}$ [cm] regarding the partition constant K_{LinC} in the coated wall flow tube experiments. It was found, that the adsorption can be parameterized taking into account both the solubility of HNO$_4$ in liquid water and the acidity of HNO$_4$ by a comparison with other trace gases. This relation ship can be used to give a rough estimate of the partitioning towards the ice surface for other trace gases.

By applying the gas phase ice partitioning of HNO$_4$ to the ice in environmental relevant problems, the magnitude of the partitioning has often been compared to that of HNO$_3$ previously. Here it was shown that the magnitude of partitioning of HNO$_4$ ice much lower than that of HNO$_3$. In conditions relevant for the upper troposphere the partitioning of HNO$_4$ towards ice in cirrus clouds is hence overestimated. According to the results presented here a larger part of HNO$_4$ would be present in the gas phase and impact especially O$_3$ chemistry. Implementation of the newly derived temperature dependence of partitioning into chemistry transport models could give valuable information about atmospheric NO$_X$, HO$_X$ and O$_3$ chemistry.

In Antarctica HNO$_4$ has been proposed to be an important species in the NO$_X$ recycling above the Antarctic plateau. The results presented here suggest that the snow pack is an efficient sink for HNO$_4$ due to its high specific ice surface area. HNO$_4$ adsorbed on the ice surface in the photic zone of the snow can be photolysed. Experimental studies investigating photolysis of HNO$_4$ on ice surfaces would be useful to elucidate the impact of this process.

6.1.2 H$_2$O$_2$

The uptake of H$_2$O$_2$ to ice was found to consist of a surface adsorption mode and a bulk uptake mode by diffusion. The possibility of diffusion in a disordered layer, extended by the presence of H$_2$O$_2$ on the ice surface, could not be neglected. The

temperature dependence of the adsorption part was in excellent agreement with an earlier study focusing on surface adsorption and could solve differences in existing data sets. Also the temperature dependence of the bulk uptake was found to be in good agreement with an earlier study focusing on bulk processes at longer time scales.

The results presented here show that H_2O_2 is present on the ice surface as well as the bulk of the ice. This has implications for light absorption by snow packs. As the H_2O_2 on the surface is better accessible for the incident light, it may be the more important fraction of H_2O_2 as compared to the fraction taken up by the bulk of the ice. The results presented here suggest that also the composition of the snow pack, for example regarding the amount of grain boundaries in the snow pack, should be considered when light absorption is studied. The observed long term uptake and loss to and from the ice is in agreement with processes observed in the environment, for example snow packs oversaturated with respect to adsorbed H_2O_2 as source of gas phase H_2O_2 and the smearing of the annual cycles in ice core studies.

6.2   New information about long term uptake

By-comparison of the two chemical species investigated in this study, interesting conclusions considering long term uptake by the ice can be drawn. It could be expected that HNO_4 has a higher affinity for a long term uptake than H_2O_2, due to its higher acidity. Yet the results presented here have shown no long term uptake for HNO_4 and a distinctive long term uptake for H_2O_2. It is not clear if H_2O_2 diffuses into the polycrystalline ice or if it induces a disordered interface on the ice, or both. If H_2O_2 induces disordered regions, the thickness of the generated layers must be of a significant thickness to explain the long term uptake over timescales of hours in the experiments presented here. At least the thickness has to extend the thickness of the disordered layer on pure ice, regarding the time scale of the long term uptake. Inducement of a disordered interface by H_2O_2 would also mean that the acidity of the chemical species is not the only driver resulting in disordered interfaces.

6.3   Production of ice differing in grain boundary content

Recent observations in laboratory experiments, including this study, have shown that an uptake to the grain boundaries of natural ice (i.e. polycrystalline ice) could be a significant loss process from the gas phase and long term reservoir. In this study the design of a flow through reactor is presented, by which ice surfaces can be produced, differing in a grain boundary content by a factor of five. In combination

with direct analysis of the grain boundaries by light microscopy, this uptake mode could be elucidated. Yet further development of the reactor is needed, especially identification of a trace gas with a high affinity for grain boundaries and low uptake on the reactor wall. Preliminary uptake experiments of nitrous acid (HONO) to ice have been executed with the reactor. Yet blank experiments were not possible with the material used, due to bad quality. By using a FEP (fluorinated ethylene propylene) foil for blank experiments, the uptake to the reactor without ice can be investigated. Subsequent uptake experiments of HONO to ice differing in grain boundary content could give new information about the role of grain boundaries in trace gas uptake.

Chapter 7

Acknowledgements

Working on a Ph.D. Thesis involves a lot of people, not only the writer himself. Without scientific as well as social support in the up and downs between fully working experiments and troubleshooting of details, this work would not have been completed. Therefore I want to thank:

Samuel Leutwyler for accepting me as a PhD student and fruitful inputs to this thesis

Markus Ammann for giving me the opportunity to work on this project at the Surface Chemistry Group at PSI, his driving inputs and questions considering experiments as well as data evaluation on which this work is built and of course also for supporting a healthy and open climate at work

Thorsten Bartels-Rausch not only for doing a great job in competently supervising my work, but also for providing me a more intuitive approach to atmospheric chemistry and all the important basics for working as a scientist and his optimistic attitude, as well for acquiring the funding for this project (Swiss National Science Foundation, grant number 200021_121857 and 200020_140400) and giving me the opportunity to visit international conferences

Martin Schneebeli and Fabienne Riche for their collaboration with us considering microphysical properties of snow and their help making grain boundaries visible

Andreas Türler and John Crowley for accepting to be part of the thesis committee

Off course a big thanks goes to all my colleagues at the Laboratory of Radiochemistry and Environmental Chemistry. Especially I want to thank Sarah Steimer for her great work of cheering me up in combination with scientific discussion, which involved sometimes more cheering up and sometimes more discussion; Sepp Schreiber